Dynamic Stress Behaviour of Bonded Pipes and Umbilicals

Chunyu Li

# Dynamic Stress Behaviour of Bonded Pipes and Umbilicals

Chunyu Li

Master thesis

30 June 2015

Supervisor: Svein Sævik, IMT

Co-supervisor: Naiquan Ye, Marintek

Norwegian University of Science and Technology

Department of Marine Technology

Thesis work scope

MASTER THESIS SPRING 2015

for

Stud. tech. Chunyu Li

Dynamic Stress Behaviour of Bonded Pipes and Umbilicals

Dynamisk spenningsoppførsel av bundne rør og kabler

As opposed to non-bonded flexible pipes, loading hoses are normally made as a vulcanized structure where the armor tendons are embedded in rubber. In umbilicals, it is common procedure to protect the armor layers by application of bitumen which is a strongly temperature and loading rate dependent material. In both cases, the dynamic stresses due to bending will be governed by the shear deformations and mechanical properties of the surrounding material rather than the friction between the layers as for non-bonded pipes.The flexible riser represent a vital part of many oil and gas production systems. Failure in the riser purpose of the master thesis is to investigate the stress behaviour under these circumstances both with respect to fatigue and extreme stress calculations. The work shall be carried out as follows:

1. Literature study related to bonded/non-bonded flexible pipe and umbilical technologies including the mechanical characteristics and dynamic behaviour of vulcanized rubber and bitumen. This is also to include methods for global and local response analysis focusing on the issue of calculating the stresses in flexible pipes and familiarization with the Bflex software.

2. Establish necessary input for to perform parametric studies of one bonded hose and one bitumen protected umbilical cross-section. For the bonded hose case, also establish a non-bonded model to be used as a reference (Question: at the same pressure class, what has favourable performance?). The input includes geometric and mechanical characteristic and a dynamic load scatter diagram.

3. Establish Bflex models for the above cross-sections using the new full FE (eltype

HSHEAR353, HCONT453, HCONT463 and HSHEAR463) assumptions.

4. Perform fatigue stress analysis in Bflex using the above models and compare the results in terms of stress history plots showing the results from the different models in the same plot. The plots should include the axial stress, normal curvature stress and transverse curvature stress components (the components of longitudinal stress) as well as the sum of these and the fatigue damage for a typical SN curve.

5. Conclusions and recommendations for further work

The work scope may prove to be larger than initially anticipated. Subject to approval from the supervisors, topics may be deleted from the list above or reduced in extent.

In the thesis the candidate shall present his personal contribution to the resolution of problems within the scope of the thesis work

Theories and conclusions should be based on mathematical derivations and/or logic reasoning identifying the various steps in the deduction.

The candidate should utilise the existing possibilities for obtaining relevant literature.

Thesis format

The thesis should be organised in a rational manner to give a clear exposition of results, assessments, and conclusions. The text should be brief and to the point, with a clear language. Telegraphic language should be avoided.

The thesis shall contain the following elements: A text defining the scope, preface, list of contents, summary, main body of thesis, conclusions with recommendations for further work, list of symbols and acronyms, references and (optional) appendices. All figures, tables and equations shall be numerated.

All plots shall be separately stored electronically in jpg format using self explaining filenames. It is also preferred that the thesis is written in Latex (not mandatory) and all files are to be delivered together with the report.

The supervisors may require that the candidate, in an early stage of the work, presents a written plan for the completion of the work.

The original contribution of the candidate and material taken from other sources shall be clearly defined. Work from other sources shall be properly referenced using an acknowledged referencing system.

The report shall be submitted in two copies:

- Signed by the candidate

- The text defining the scope included

- In bound volume(s)

- Drawings and/or computer prints which cannot be bound should be organised in a separate folder.

Ownership

NTNU has according to the present rules the ownership of the thesis. Any use of the thesis has to be approved by NTNU (or external partner when this applies). The department has the right to use the thesis as if the work was carried out by a NTNU employee, if nothing else has been agreed in advance.

Thesis supervisors

Prof. Svein Sævik, NTNU.

Dr. Naiquan Ye, Marintek

Trondheim,   January, 2015

Svein Sævik

Preface

This master thesis has been carried out during the spring semester of 2015 at the Department of Marine Technology, NTNU, under supervision of Prof. Svein Sævik from NTNU and Dr. Naiquan Ye from Marintek.

The thesis work includes comprehensive studies on the current flexible pipe technology. Several models have been established to have an insight into the properties of different types of flexible pipes, i.e. umbilical pipes, non-bonded and bonded flexible pipes.

I would especially like to thank Prof. Svein Sævik from NTNU for his great help and guidance during the master thesis work. Sincere thanks also give to the Dr. Naiquan Ye from MARINTEK. His patient assistance on both analytical and software study helps me perform better of the thesis. I would also like to thank Ph.D candidate Tianjiao Dai for her great help on the software studies and the analysis methods.

Last but not least, thanks for my families and all my friends for their company during this spring time of 2015.

Trondheim, Norway

June 2015

Chunyu Li

Summary

The main objective of this thesis is to study the characteristics of different types of flexible pipes and summarize the existing analytical methods, and to establish the models in order to simulate dynamic stress behavior in bending.

Comprehensive works have been reviewed before modelling. It is found that as opposed to non-bonded flexible pipes, bonded flexible pipes normally use vulcanized rubber as contact layer where the armor tendons are embedded, while in umbilicals, the armor layers are protected by filling of bitumen. In both cases, the dynamic stresses due to bending will be governed by the shear deformations and mechanical properties of the surrounding material rather than the friction between the layers as for non-bonded pipes.

Assuming no slip behavior in the bonded flexible pipes, the strain-stress relationship in the material model can be described as linear elastic. As for the umbilicals, stick-slip behavior also applies, but different from the non-bonded flexible pipe, the shear stiffness will be independent from the radial compression

When reviewing the analytical methods concerning the effect of internal pressure load, the concept *Anti-deflection moment M_p* is introduced to account for the increase of bending stiffness. In case of ovalization of pipe cross-section, the pressure force F_p and the difference-induced pressure force F_v are not in balance, and the resultant acts as a moment to resist against the bending. This may be the main reason to account the increase of EI but shall be verified in further work.

In chapter 3 the analytical methods in the analysis of the stress behavior due to axisymmetric loading and bending have been summarized so as to find the analytical solution as the evaluation of the numerical results.

The analysis starts from the non-bonded case, where a typical non-bonded flexible pipe model has been established and its stick-slip behavior is simply presented. Before modelling of bonded case, the Pag-o-flex experimental test has been review to have the basis for the bonded model.

Based on the basic components of the non-bonded model and the test sample pipe, the bonded model is established with two helical armor layers and a core pipe. As for the model using PIPE31 3D beam element as the core pipe, the results indicate that the

radial expansion can not be properly picked up. This is improved by application of HSHEAR363 3D shell element. From the analysis of the numerical results, the bonded flexible pipe model demonstrates a linear moment-curvature relationship. The bending stiffness keeps constant and resembles the test sample pipe. Parameter study is implemented to see the influence of the contact material on the bending stiffness.

Umbilical model is established later on. The helical tendons have small lay angel in order to gain tensile strength but at the expense of the radial strength. The numerical results indicate an extremely large initial bending stiffness corresponding to the stick phase. As the slip behavior gradually occurs until full-slip, the tangential bending stiffness decreases sharply to small quantity but stays stably around 10 kNm^2.

The parameter study shows that the shear stiffness influences the initial bending stiffness, while the stick limit only affects the durations of the stick or slip hevavior and the transition between.

Conclusions and further work are proposed in the end, indicating that the general properties of the bonded flexible pipes and the umbilical have been properly simulated, while more detailed structures shall be modelled and compared with the analytical solutions. In addition, the concept Anti-deflection moment shall be reviewed and verified. If needed, this effect shall be added into equilibrium iteration to get more accuracy.

Content

List of figures

List of tables

Nomenclature

b Thickness of tendon cross section

E Young's modulus of elasticity

G Shear modulus

$\boldsymbol{I_I}$ Base vectors directed along curve principal torsion-flexure axes.

I_t Cross section torsion constant

I_3 Inertia moment about X^3 axis

M_I Moment stress resultant acting about the local coordinate axes

Q_I Force stress resultants acting along the local coordinate axes

q_I Distributed loads acting along the local coordinate axes

q_t Distributed tangential reaction

R Radius from pipe centre line to tendon centre line

u_i Component form of displacement field

w Surface coordinates.

W_i Internal virtual work contribution from beam element.

X^I	Local curvilinear coordinates
α	Tendon lay angle.
ϵ_1	Axial strain of rod.
θ_i	Rotation about the local curvilinear axis
κ	Principal curvature along curve
κ_1	Total accumulated torsion of tendon centre line
κ_2	Total accumulated transverse curvature of the tendon centre
κ_3	Total accumulated normal curvature of tendon centre line
ρ	Curvature radius of pipe surface at neutral axis
σ^{ij}	Tensor and component form of the Cauchy stress tensor in the local Cartesian coordinate system.
τ	Torsion along curve
ω	Angle between surface normal and curve normal
ω_1	Torsion deformation
ω_2	Transverse curvature deformation
ω_3	Normal curvature deformation

$\Delta\pi$ Incremental potential

1. Introduction

1.1 Background

Flexible pipe systems are widely used in the current floating production and subsea systems in oil&gas industries. Compared with rigid pipe solutions, they not only allow for permanent connection between a floating support vessels with large motions and subsea installation, but also make the transport and installation significantly simplified due to the possibility for prefabrication in long lengths stored on limited sized reel ad ease of handling.

Bonded flexible pipes with rubber compound contact layer play the role in the production and injection hoses, offshore loading and exploration drilling. It shows its great advantages where short lengths are required, or the space to accommodate the line is tight. The bonded pipe has small bend radius due to inherent flexibility of rubber.

Umbilical is used to supply necessary control, energy and chemicals to subsea oil and gas wells, subsea manifolds and any subsea system requiring remote control.

In the case of extreme loading or harsh environment, the flexible pipe system are the severe component.

1.2 Objective

The main objective of this thesis work it to study the general mechanical properties of the bonded flexible pipe and the umbilical. In advance, the detailed review on the flexible pipe technology should be implemented. The methodology on the design and analysis of the flexible pipe should also be reviewed. As for the bonded flexible pipe, main differences from the non-bonded pipe shall be studied. This is the basis for the modelling.

Material properties' influence on the strength of the flexible pipe is an important issue. This will be followed by relevant parameter studies.

1.3 Literature review

Comprehensive works and researched have been carried out in the design and analysis of flexible pipe technology.

MARINTEK, NTNU and 4Subsea have carried out series of projects and have proposed the general design and operation of flexible pipes. [1] American Petroleum Institute also published relevant recommended practice on the design and analsysis of this technoogy. [2] Based on comprehensiove researches, Sevin Sevik proposed the theoretical and experimental studies of the axisymmetric behaviour of complex umbilical cross-sections [3]. Andrea Catinaccio studied the behavior of pipes under internal pressure and bending [4] More information can refer to the references.

1.4 Thesis structure

Chapter 1 provides the basic information on the topic and main issues of this thesis work.

Chapter 2 gives a comprehensive overview on the flexible pipe systems, with respect to the main applications, functions and components. Non-bonded and bonded flexible pipes as well as the umbilical are separately studied on their structure components, mechanical properties, and the material behaviors.

Chapter 3 is the methodology on the design and analysis of the flexible pipes. Analytical methods and numerical methods are both reviewed.

Chapter 4 starts the analysis from the modelling of a non-bonded pipe. Alternative models are established to model the bonded flexible pipes.

Chapter 5 describes the general concerns of the modelling and analysis of the umbilicals.

Chapter 6 concludes the main finding of the thesis work, while chapter proposes the further word to improve the reliability and accuracy of the analysis.

2. Flexible Pipe Technology

2.1 Introduction

This chapter gives a comprehensive overview on the flexible pipe system. This is followed by the detailed insight into the different types of flexible pipe, i.e. non-bonded and bonded flexible pipes, and umbilicals, with respect to their main characteristics.

2.2 Overview of Flexible Pipe System

2.2.1 Main components

Generally a flexible pipe system consists of three main components [1], i.e.

1) Riser: used to connect subsea installation with top side facilities to transport fluid, that is primarily subject to dynamic loads;

2) Flowline: pipe transporting fluid over large distances, that is primarily subject to static loads;

3) Jumper: Short length of flexible pipe transporting fluid subsea or topside.

Besides, there is another flexible pipe structure, umbilical, to supply necessary control, energy and chemicals to subsea oil and gas wells, subsea manifolds and any subsea system requiring remote control.
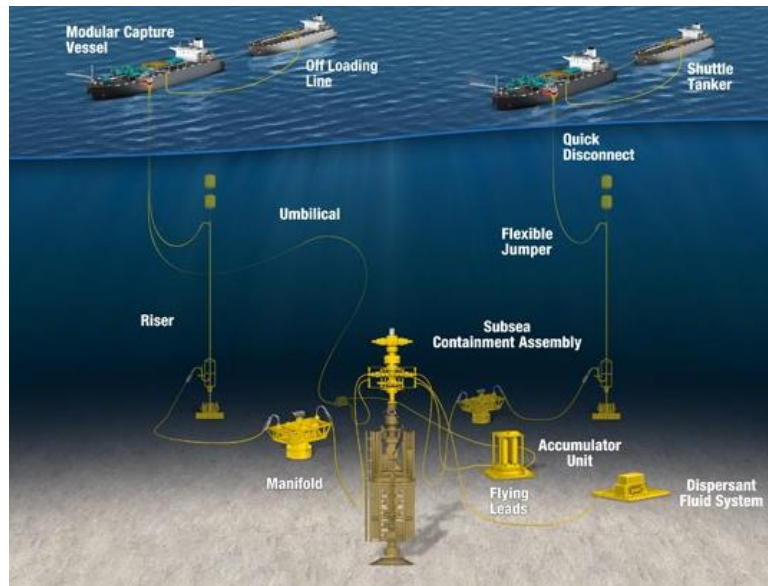
Figure 2-1 A typical flexible pipe system, Image: MWCC

2.2.2 Structure characteristics

A flexible pipe is constructed using a polymeric sealing material that contains the bore fluid, multiple helical armoring layers that provide the required strength, and a polymer outer sheath that prevents seawater from interacting with the armor wires. The construction enables design of pipes with a lower allowable bending radius compared to homogeneous pipes with the same pressure capacity. [2]

There are lots of advantages using flexible pipe systems instead of the rigid pipe system. Because the flexible pipe systems not only allow for permanent connection between a floating support vessels with large motions and subsea installation, but also make the transport and installation significantly simplified due to the possibility for prefabrication in long lengths stored on limited sized reel ad ease of handling.

2.2.3 Typical applications

Flexible pipes for offshore and onshore applications are grouped into either a static or dynamic category, [2]

1) Static Applications (SAs): primarily include flowline and fixed jacket riser service;

2) Dynamic Applications (DAs): usually involve an offshore floating production

facility or terminal connected to another floating facility, fixed structure, or fixed base.

The static and dynamic categories place different physical demands on the pipe. Both of them require mechanical strength, internal and external damage resistance, minimal maintenance and long service life, while dynamic service pipes, i.e. flexible riser, also require pliancy and adequate fatigue capacity. [2]

2.2.4 Main structural layers

The bending stiffness with high axial tensile stiffness is achieved by a composite pipe wall construction. The two basic components are helical reinforcement layers and polymer sealing layers to provide basic strength and to ensure the flow integrity. More typical structural layers are specifically described in Table 2-1, each layer of which has a specific design function.

Table 2-1 Common flexible pipe structural layers [1]

Layer	Function
Carcass	Provides Internal Pressure Sheath with collapse resistance.
Internal Pressure Sheath	Contains process fluid within pipe bore.
Pressure Armor Wire	Provides radial compression resistance. Partially supports internal sheath and contains internal pressure loads.
Intermediate sheath	Provides Internal Pressure Sheath with collapse resistance in case of outer sheath breach for smoothbore pipes.
Tensile Armor Wires	Provides tensile strength and contain end-cap loads.

	Partially supports containment of internal pressure loads.
Anti-friction layers	Tape or thin extruded polymer that prevents metal-metal contact.
Anti-buckling layer	High strength fiber composite that prevents radial or lateral buckling.
Insulation	Provides thermal insulation for bore fluid if necessary.
Outer Sheath	Prevents ingress of seawater and oxygen to the annulus.

More specific structure description is discussed in the following sections, with respect to different types of flexible pipe.

2.2.5 Category

Furthermore, the flexible pipes are categorized into bonded and non-bonded according to different component properties of the cross-section: [1]

1) Non-bonded structures, where each component makes up a cylindrical layer that is able to slide relative to the other layers. They are widely used in most applications.

2) Bonded structures, where the armor elements and the pressure containing components are molded into a single structure. All components are glued together as an elastic composite material, primarily used for short length jumpers in high dynamic applications.

The main differences and mechanical properties are discussed in later sections.

2.2.6 Failure modes and design criteria

There are various kinds of failure modes, but generally can be divided into two main types, leakage and reduction of the internal cross section. According to the [1] it can be further classified into more branches shown by the chart below.
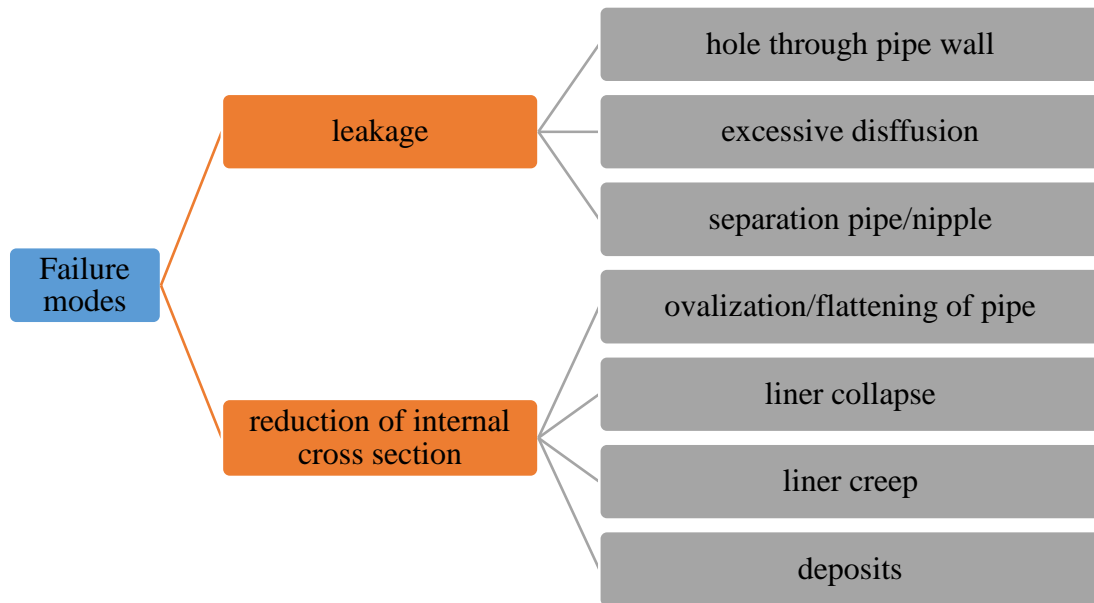
Figure 2-2 Failure modes of flexible pipes

The design criteria for non-bonded or bonded flexible pipes are based on the failure modes in terms of strain, stress, collapse and service life factors etc. Details refer to the API-17-b. [2]

2.3 Non-bonded flexible pipe

2.3.1 Structure specification

According to the definition, the most distinguishing feature of a non-bonded pipe is that each component makes up a cylindrical layer that is able to slide relative to the other layers. This is the distinguishing characteristic compared to the bonded. As for the structure layers, because of this friction resistance damage, non-bonded flexible risers are designed to be fatigue resistant by use of anti-friction tape layers and fatigue resistant materials. The general cross-section is illustrated in Figure 2-3. [2]
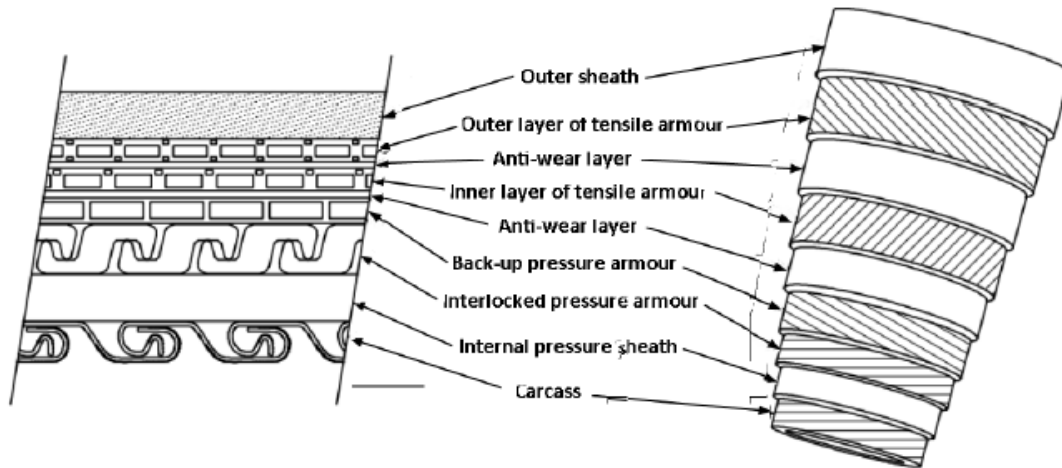
Figure 2-3 Typical non-bonded flexible pipe cross-section

Each layer has a specific function and is interacting with the other layers. Starting from the inner side, the carcass is the innermost layer of a pipe, and the only metallic component that is in direct contact with the fluid in the bore. The second steel layer is the pressure armour, whose primary function is to back up the liner and to provide the resistance against the hoop stress induced by internal pressure load. The pressure armour is also a strength component with respect to external forces.

The tensile armour is comprised of armour wires. It provides strength against axial force caused by internal pressure and by external loads. The layers are counter-wound to avoid torsion when axial loading is applied. The lay angle in most cases is 30° to 35°. [1]

2.3.2 Layer materials

The wall of a flexible pipe including ancillary components is a composite structure where a wide range of material is used, including polymer material, steel, synthetic fibres and foam, etc.

Among all the types of materials, the polymer is the most used material between the steel layers and is the main source of friction.

Some typical polymer materials for non-bonded pipe are tabulated as follows.

Table 2-2 typical polymer materials for non-bonded flexible pipes

Layer	Material Type	Elastic moduls (MPa)
Internal pressure sheath	High density polyethylene (HDPE), crosslinked polyethylene (XLPE), polyamide (PA), polyvinylidene fluoride (PVDF)	690-1800
Intermediate (anticollapse) sheaths	HDPE, XLPE, PA, PVDF, TPE	500-1600
Antiwear Layers	PA, PVDF, HDPE	690-1800
Outer sheath	HDPE, PA, TPE	500-1600
HDPE, PA, TPE	Polypropylene, polyvinyl chloride, polyurethane	2-12

In addition to the range of elastic properties the materials also differ widely in terms of strength, ductility, wear, creep, thermal expansion and other characteristics. The combination of materials that are used for a given flexible pipe design depends on the specific application. [2]

2.3.3 Bending behavior

As for non-bonded flexible pipes, the bending behavior is dominated by the steel reinforcement layer but is significantly affected by the friction and the slip behaviour. This results in a non-linear moment-curvature relationship, which is shown in the Figure 2-4.
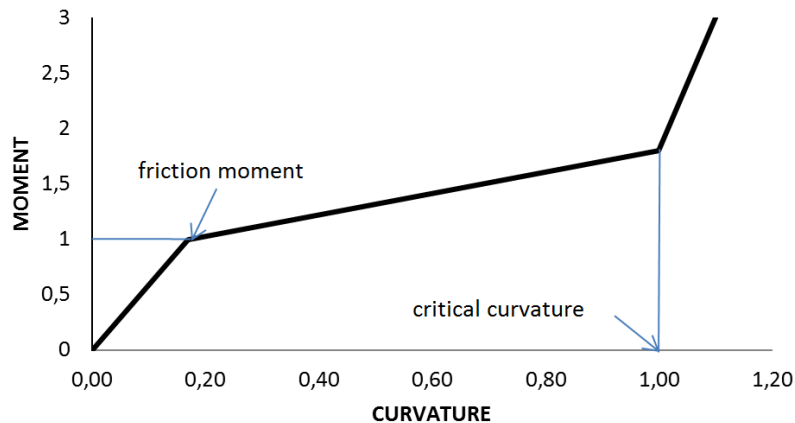
Figure 2-4 Bending behavior of non-bonded pipes [3]

According to the Svein Sævik, this load history can be divided into three steps. During step 1, no slip exists between tendons and supporting structure, and the pipe bends with a similar stiffness as a steel pipe with same cross section.

In step 2, slip occurs when the moment overcomes friction limit. The tangential stiffness drops significantly.

Later in step 3, this phase begins when the gap between each tendon is closed. In his phase, no sliding is allowed anymore. This is termed as critical radius and should be avoided in any operations. [3]

When considering the internal pressure load, the interlayer contact force is dependent of the internal pressure load. Therefore, for a given friction coefficient the stick/slip threshold increases together with the internal pressure load. [1]

2.3   Bonded flexible pipe

2.4.1 General

Bonded flexible pipes are widely used as production and injection hoses, offshore loading and exploration drilling.

It shows its great advantages where short lengths are required, or the space to accommodate the line is tight. The bonded pipe has small bend radius due to inherent flexibility of rubber.

However, the disadvantages lie in limited length per segment, long lengths will require joints. Generally it has lower crush resistance and lower axial pulling force capability than non-bonded flexibles. [6]

2.4.2 Structural specification

A typical bonded flexible pipe consists of several layers of elastomer either wrapped or extruded individually and then bonded together through the use of adhesives or by applying heat or pressure to fuse the layers into a single construction. [2]

Another way to combine those individual layers is vulcanization, by which the polymer material such as rubber is vulcanized to make the layers bonded into one unit.

1. Stainless steel interlock stipwound tube
2. Elastomeric polymer lining
3. Textile plies
4. Stiffening spiral (not shown in the figure)
5. Elastomeric cushion plies
6. High strength steel cable reinforcements
7. Elastomeric cover
8. Outer stainless steel stipwound protection

Figure 2-5 High pressure bonded hose, image:ContiTech

The reinforcement layer typically comprises helically wound steel cables in an embedding elastomer compound used to sustain tensile and internal pressure load on the pipe. The steel cables are typically laid at an angle of 55° to obtain a torsionally balanced pipe in addition to equivalent hoop and longitudinal forces in the layer due to pressure. However, this angle may increase or decrease depending on the required strength characteristics of the pipe. For example, a higher angle may be used if increased strength in the hoop direction is required at the expense of tensile capacity and axial stiffness of the pipe.

The function of elastomeric cushion plies is to ensure adhesive bonding and interaction between different plies

2.4.3 Layer materials

Elastomer materials are widely used in bonded flexible pipes. Some typically used material are listed in the table 2-3.

Table 2-3typical polymer materials for bonded pipes [2]

Layer	Material Type
liner	Nitrile butadiene rubber, hydrogenated nitrile rubber, polychloroprene, natural rubber, ethylene propylene diene monomer rubber
cover	Polychloroprene, chlorinated polyethylene
Filler	Various
Insulation	Polyvinyl chloride, polyethylene, closed cell foam, glass fiber

These elastomer materials constitute approximately 40 % to 65 % of the final compound mix, with carbon black, antioxidants, activators, plasticizers, and curing agents making up the remainder amongst other ingredients. [2]

The focus is the material of the elastomeric material of the contact layers between the steel cable reinforcements. As each rubber compound material is made up of an elastomer material and several other materials the properties will therefore vary with mix type. The final properties of the rubber compound are dependent on the final mix of all ingredients.

Typical properties of the elastomer (rubber) material used in bonded pipes is presented in the table attached in appendix. The most widely used are natural rubber, EPDM, HNBR and SBR and so on. Most of them have specific resistance to high temperature, chemicals and ozone, etc. The Young's modulus ranges from 0.5 to 50 because of

various ingredients mix.

2.4.4 Mechanical properties of vulcanized rubber

Vulcanized rubber is a solid, three-dimensional network. The more crosslinks there are in the network the greater is the resistance to deformation when a force is applied. Certain fillers, notably the reinforcing blacks, create a structure within the rubber which further resists deformation.

The load-deflection curves for rubber in tension and compression are approximately linear for strains of the order of a few per cent, and values of Young's modulus E_0 can be obtained from these linear regions. As the curves are continuous through the origin the values of Young's modulus in tension and compression are approximately equal.

However, the average design limit is 15% compression and 50% shear. Beyond this region, the linearity is no longer accurate enough.
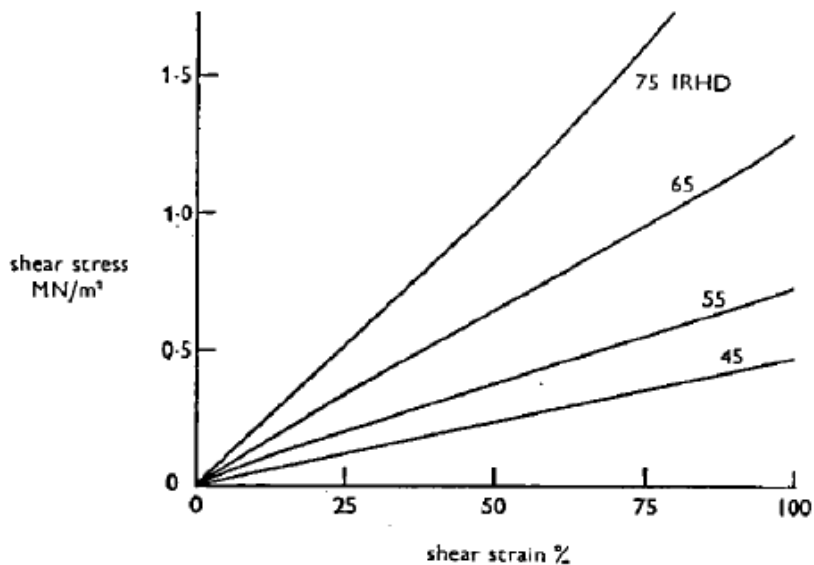
Figure 2-6 The strain-stress curves of rubber in shear deformation

For example, the rubber hardly changes in volume even under high loads. For most of the deformation there must be space into which the rubber can deform. The more restriction that is made on its freedom to deform the stiffer it will become.

As for the rubber in compression, when a long strip of rubber is compressed the strain

in the direction of its length will be negligible. As seen in the compression stress-strain plot in Figure 2-7, it loses its linearity when the strain is large.
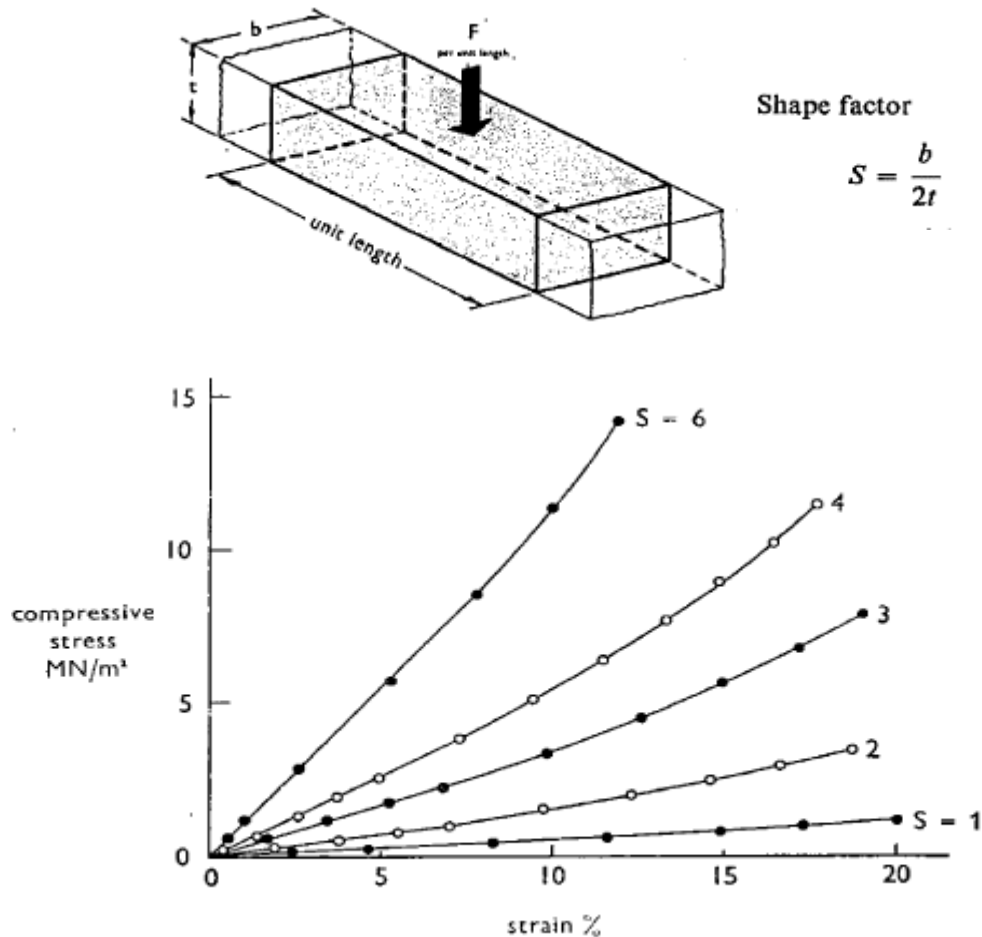
Figure 2-7 Typical compression stress-strain curve for strip rubber

To set up the inputs for the bonded flexible pipe model in Bflex2010, it is assumed the displacement is small and the stress-strain still lies within the linear region. Some discussions will be addressed later.

Friction model

The coefficient of friction against most dry surfaces is generally about unity, but for design purposes it is usually assumed that slip due to a shear force will not occur if the ratio of maximum shear force to minimum compressive force is less than rubber-steel 0.2. This has been approved sufficient.

2.4 Umbilical

2.5.1 General

Fluid conduit functional components for hydraulic control, annulus bleed or transmission of chemical injection and gas lift fluids are available in the form of steel tubes or thermoplastic hoses. These two types of functional componnets are very diverse in physical characteristics, but when combined in an umbilical can result in an improved development solution.

By combination of elements like hydraulic tubes, electrical and optical signal cables and electrical power cables, umbilicals provide remote control of subsea oil and gas wells. For extra tensile strength and outer protection the umbilicals may be armoured by galvanized steel wires. Dynamic umbilicals are terminated at offshore platforms or vessels. They are exposed to tension and bending variations caused by waves and vessel motions. As such a project specific analysis is normally required to verify that a given dynamic umbilical design with all its elements is able to withstand a service life of typically 20-30 years. [4]
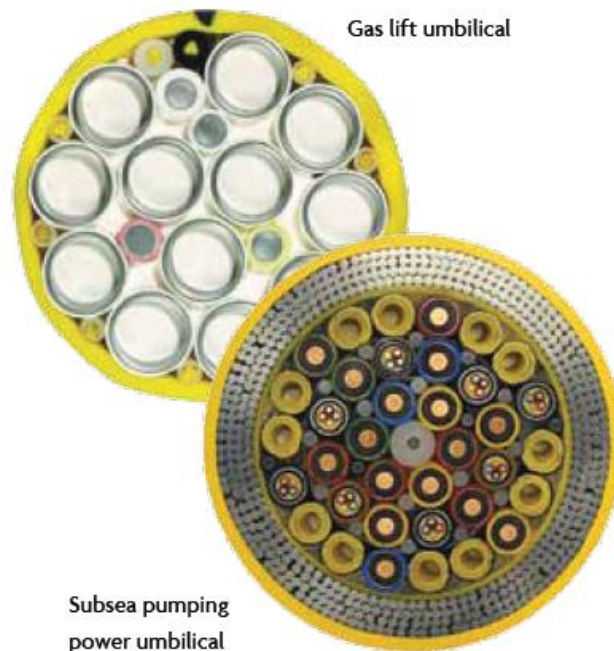
Figure 2-8 Gas lift umbilical and subsea pumping power umbilcal

2.5.2 Structure specification

The typical power umbilical cross-section is illustrated in Figure 2-10.
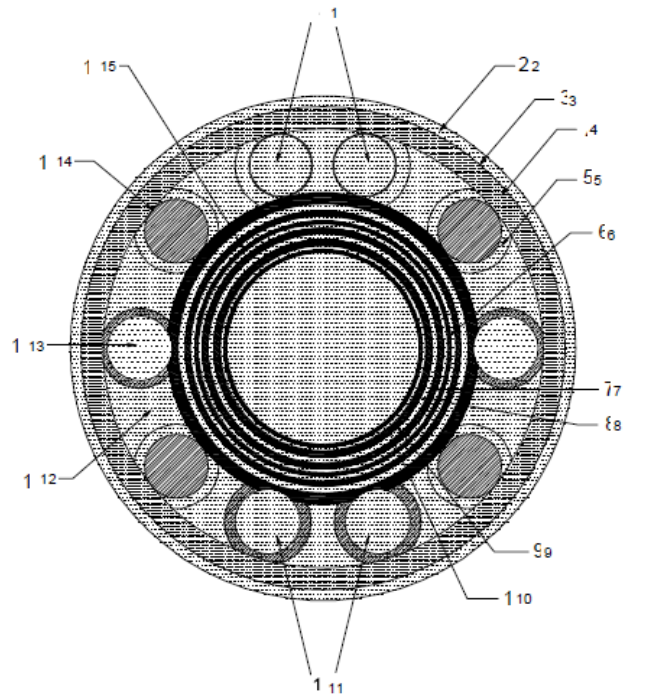
Key

1	Electric power cable	9	Internal pressure sheath
2	Outer sheath	10	Carcass
3	Tape	11	Electrical signal cable
4	Pipe outer sheath	12	Filler material
5	Tape	13	Fiber optical cable
6	Tensile armor layer	14	Hydraulic hose
7	Internal tensile armor layer	15	Antiwear tape
8	Pressure armor layer		

Figure 2-9 Typical configuration of umbilical pipe

Both helical armours and helical multi-function tubulars are used to resist tension and torque. For dynamic steel tube umbilical used in deep water and ultra-deep water, it is subjected to large tensions and cyclic bending loads during operation. [5] In this case the lay angle of the tendons is smaller mainly to gain tensile strength, e.g. 10° to 20°.

The main consideration for the steel tubes in umbilical services are tensile strength, corrosion resistance both to internal and external, and operating temperature. Materials available for umbilical construction include a range of material from carbon steel to

superduplex.

2.5.3 Filling material - bitumen

For the steel wire armour which is corrosion protected by bitumen, the friction factors may not be valid. The force transmission between the steel wires may not be governed by friction but by the viscoelastic properties of bitumen. In such a case the transition force is not only a function of contact pressure but also of sliding velocity and dimensions. [6]

When the solid elements are soaked in a viscoelastic material, such as for steel wires corrosion protected by bitumen, the stress distribution may be governed by shear forces, not friction.

Therefore the slip threshold model of the contact layer can be estimated by a shear deformation before slip, and a constant contact force afterwards. This is illustrated by Figure 2-10.
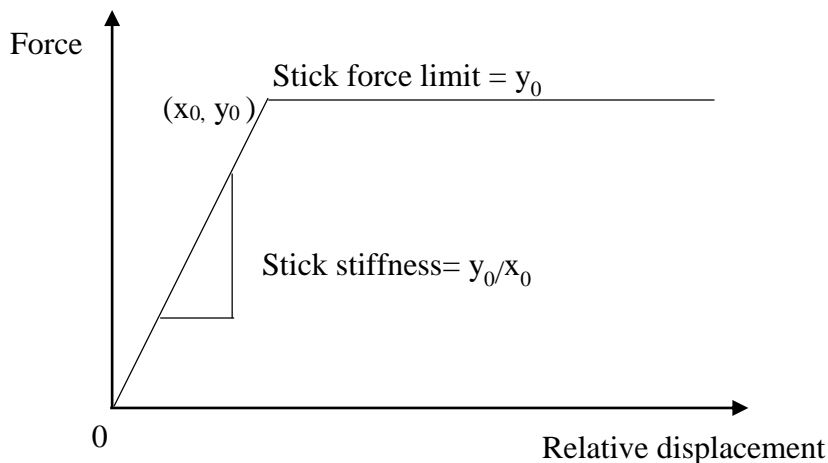
Figure 2-10 Slip threshold model of bitumen contact layer

This model is employed in the analysis of the umbilical pipe in the later chapter.

Lemflex N is a polymer modified bitumen used as corrosion protection of the armour. It contains bitumen with additions of EVA added as cement.

There is a widely used method of umbilical filling invented by Sjur, Halden (NO) and Stian, Halden (NO). The filling facility is illustrated below. [7]
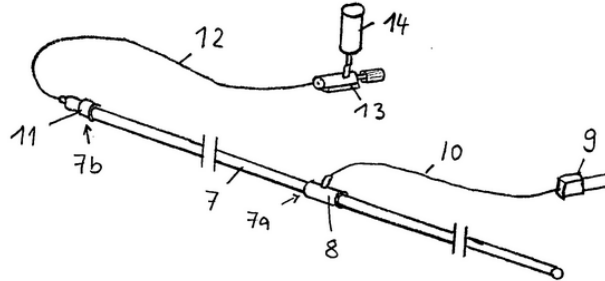
Figure 2-11 Umbilical filling facility

The common sheath are filled with a fluid filling material, e.g. bitumen, which tempers to a higher viscosity after complete filling and adheres to the outer surface of the elements and the inner surface of the common sheath. [7]

3. Methodology for design and analysis of flexible pipes

3.1 Introduction

This chapter main describes the analytical methods and numerical methods in nowadays design and analysis of the flexible pipe technology.

The analytical method mainly focus on the stress behavior of the flexible pipe due to typical loading like internal pressure load, axisymmetric loading and bending.

The numerical methods here describe the principle of virtual displacement, solution algorithms and the introduction to the Bflex2010.

3.2 Analytical method

3.2.1 Basic assumptions and governing stress components

The stress behavior of flexible pipes is complicated. The analysis is based on the assumptions proposed by Custodio and Vaz. Together with the assumptions in the model developed by S. Sævik, they are repeated here using their definitions as follows. [8] [9]

1. **Regularity of initial geometry:** (a) the homogenous layers are long and uniform cylinders; (b) the wires are wound on a perfectly cylindrical helix; (c) the wires are equally spaced; (d) the wires of an armour are numerous hence the forces they exert on the adjacent layers may be replaced by uniform pressure; (e) the structure is straight.

2. **Reduction to simple plane analysis:** (f) there are no field loads such as self-weight; (g) end effects may be neglected; (h) the material points from any layer have the same longitudinal displacement and twist; (i) all wires of an armour present the same stress state; (j) the wires maintain a helicoidal configuration when strained; (k) the angle between the wire cross-section principal inertia axis and a radial vector linking the centre of structure's cross-section and the centre of wire's cross-section is constant; (l) there is no over-penetration or gap spanning.

3. **The effects of shear and internal friction are neglected:** (m) the wires are so slender that the movements of the material points are governed only by their tangent strain and not by the change in curvature.

The fourth assumption of linearity of the response is not involved here. In addition the assumptions (c), (d), (l) are avoided in order to enable contact to be handled on individual body level. Further, the finite element approach has been selected as it allows contact interaction effects to be handled on component level, allowing local tube deformation effects to be taken into account.

As for the stresses components, in general case, 3 normal stress components σ_{11}, σ_{22}, σ_{33} and 3 shear stress components σ_{12}, σ_{23}, σ_{13} are considered. They are illustrated in the figure below.
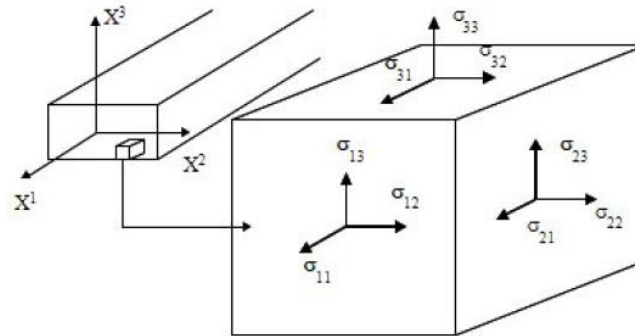
Figure 3-1 General components of stress

Since the steel layers are stress governing components with respect to structural strength and these basically consist of long slender curved beams, the primary load carrying effect will be by membrane action. Hence, the axial stresses resulting from the axial load in each wire are the primary stress components to be included in strength calculations.

Curved beam theory is used to describe the structural behavior. The stresses resultants are defined in the following figure and can be divided into two main loads. [1]

1. **Axisymmetric loads,** that only change the length and diameter of the straight pipe cylinder and with small relative deformations between wires. This includes tension, torsion, internal and external pressure loads, the latter assuming that no local buckling or collapse effects occur.

2. **Bending loads,** where the straight pipe cylinder is bent into a torus and where

significant relative deformations will occur between the wires.

The significant stress components are shown in the following figure. This includes axial force components, torsion moment and bi-directional bending stress components. Different from the previous, the stress components σ_{12}, σ_{13}, related to the local shear forces Q_2 and Q_3 are small and are neglected here.
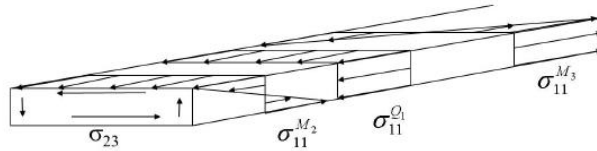
Figure 3-2 Significant stress components of tensile tendon

Polar coordinates referred to a right-hand Cartesian coordinate system are used, shown in the figure 3-3.
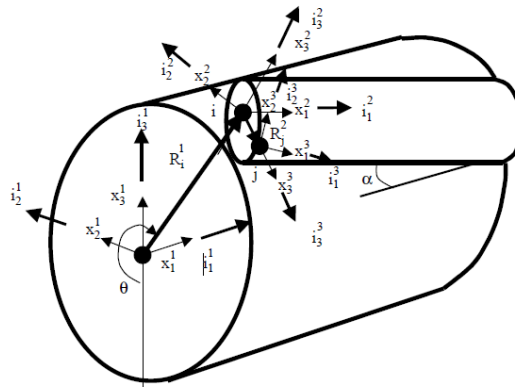
Figure 3-3 Coordinate system [9]

Detail refers to theory manual of Bflex2010 [10]and the handbook [1]

3.3.2 Stress behavior due to internal pressure loads

The flexible pipe mechanical properties regarding the strength under high internal pressure is of significance in the later analysis. In chapter 5, the bonded pipe is set to have an internal pressure load of 200 bar.

3.3.2.1 Pressure load distribution

Herein the general stress behavior is described. The following figure shows how the internal pressure load is transformed throughout the typical flexible pipe cross section.

Maximum pressure :   175.00 [bar]
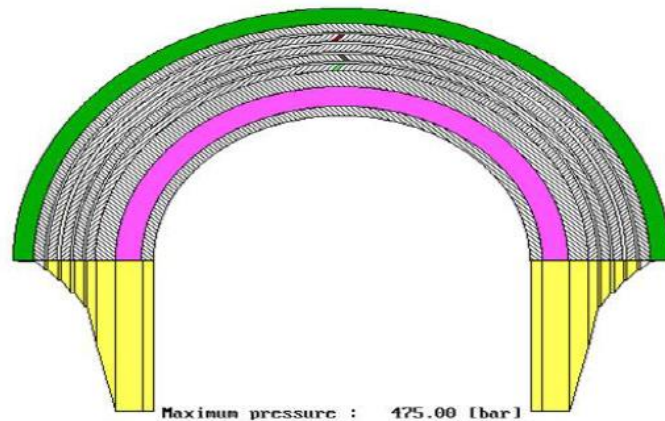
Figure 3-4 Pressure distribution in a typical flexible pipe exposed to internal pressure [1]

Starting from the insides, it is seen the carcass does not carry the pressure. This is directly transformed to the pressure spiral layer by pressure sheath. In this case the plastic pressure sheath behaves hydrostatic.

The pressure load is further transformed to tensile layers. This contact pressure from the spiral wire layer onto the tensile layer results from the end-cap effect, by which the pipe end force is balanced by the tension of the tensile armour. This contact pressure acts as a support of the pressure spiral layers, reducing the associated differential that need to be taken by the pressure spiral wires. As discussed previously on the bonded pipe, the steel cables are typically laid at an angle of 55° to obtain a torsionally balanced pipe in addition to equivalent hoop and longitudinal forces in the layer due to pressure.

Therefore, it is seen that the pressure load is primarily taken by the pressure armour and partly taken by the tensile armour. The plastic layers act as pressure transition and they influence how the load is shared between the layers.

Therefore, in the later analysis, it is assumed that the tensile layers undertake part of the pressure load. The stress components of the tendons and the contact layers will be affected by the pressure to some extent.

3.3.2.2 Contact stiffness

The shear behavior of contact layer is to some extent affected by the compressibility of material, by two main assumptions:

1) The condensation of contact material

It is assumed that the compressive load results in the condensation of material, leading to both the increase of shear stiffness and increase of compression stiffness.

This refers back to Section 2.4.4.

2) The embedding of components

This can be illustrated by the figure below.
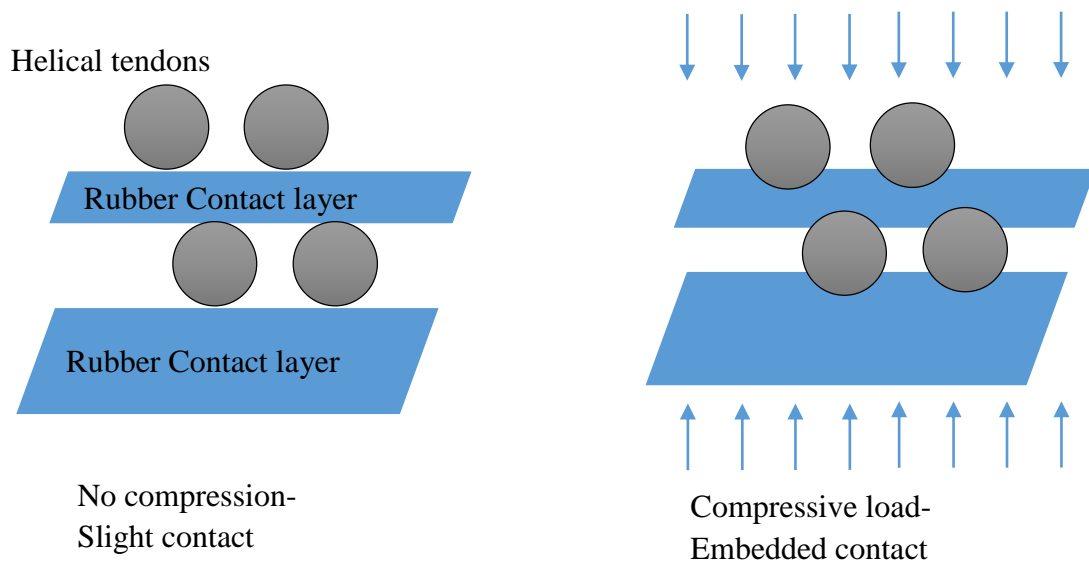
Figure 3-5 Compression model for rubber contact layers

As illustrated above, for the bonded pipe at high internal pressure load, the compression on the rubber contact layers would make relative displacement difficult, leading to relative larger shear stiffness.

3.3.2.3 Anti-deflection moment M_p against ovalization

1) In case of no ovalization:

If assuming the cross section keeps circular and no ovalization occurs,
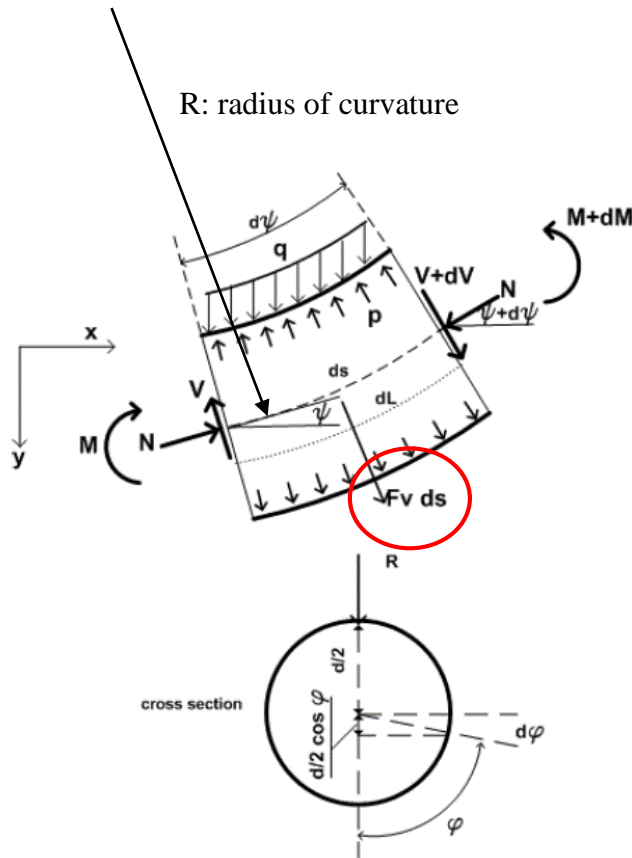
Figure 3-6 Equilibrium of an infinitesimal pipe segment, assuming constant circular cross section [11]

Figure 3-6 shows a segment dL of a slightly deflected pipe and its cross section. The length along the pipe inner surface varies from Rdy at the inner inside of the curve to $(R + d)dy$ at the outside, being R the radius of curvature and d the inner pipe diameter.

$$dL = Rd\psi + \frac{d}{2}cos\varphi \, d\psi \qquad (3\text{-}1)$$

Considering an infinitesimal strip area of the inner pipe wall,

$$dA = dL \cdot \frac{\mathrm{d}}{2} \mathrm{d}\varphi = \frac{\mathrm{d}}{2} \cdot \left(R + \frac{d}{2} cos\varphi \right) d\psi \, d\varphi \qquad (3\text{-}2)$$

The component of the force generated by the pressure on dA in the outward lateral direction is

$$dF_v = pdA \, cos\varphi \qquad (3\text{-}3)$$

Integrating this over the entire circumference leads to the net outward lateral force:

$$F_v \, ds = 2 \cdot \int_0^\pi p \frac{d}{2} \cdot (R + \frac{d}{2} cos\varphi) cos\psi \, d\psi \, d\varphi \qquad (3\text{-}4)$$

Which, for small deflections, using the relation:

$$\frac{d\psi}{ds} = \frac{1}{R} = -\frac{d^2 y}{dx^2} = \kappa \qquad (3\text{-}5)$$

The total force Fv by unit length, generated at any cross section of the pipe element by internal pressure on the pipe wall:

$$F_v = -\frac{\pi}{4} d^2 p\kappa \qquad (3\text{-}6)$$

There is another force induced by pressure on the end-cap, F_p,

$$F_p = \frac{\pi}{4} d^2 p = Cross \; section \; area * Pressure \qquad (3\text{-}7)$$

The force F_v is balanced by the pressure force F_p on the end-cap,

$$F_v ds + F_p d\psi = -\frac{\pi}{4}d^2 p\kappa \, ds + \frac{\pi}{4}d^2 p \, d\psi = 0 \qquad (3\text{-}8)$$

This balance is simply illustrated in Figure 3-7, with F_v pointing lateral outward, and F_p pointing outward perpendicular to the cross section.
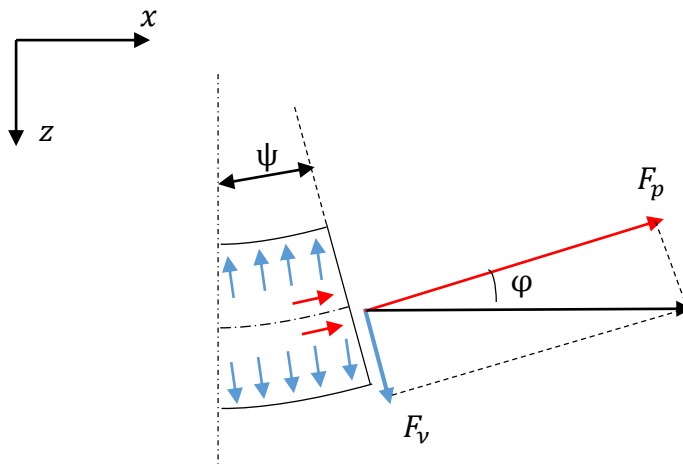
Figure 3-7 Equilibrium of the forces F_v and F_p, under assumption of no ovalization

1) In case of ovalization:

However, in case of ovalization, both the area of the pipe cross section and the structural radius change.
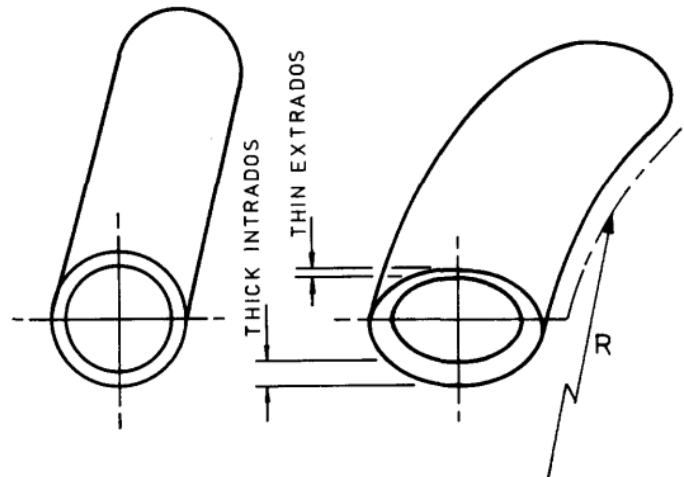
Figure 3-8 Ovalization of pipe after bending [12]

According to Haigh's assumption on the cross section of the pipe after bending, the mean radius can be described by the nominal radius plus a cosine term,

$$\frac{d'}{2} = \frac{d}{2} + X\,cos2\varphi \qquad\qquad (3-9)$$
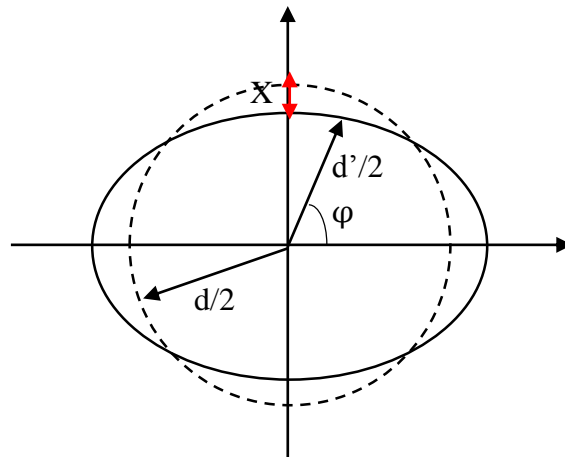
Figure 3-9 Assumption of Haigh's analysis

Substituting the Eq.(3-9) into equations from (3-1) to (3-4), F_v is found to be always larger than that under assumption of no ovalization.

$$F_v' \, ds = 2 \cdot \int_0^\pi p \frac{d}{2} \cdot (\mathrm{R} + \frac{d'}{2} cos\varphi) cos\psi \, d\psi \, d\varphi$$

$$= 2 \cdot \int_0^\pi p \frac{d}{2} \cdot [\mathrm{R} + (\frac{d}{2} + X \, cos2\varphi) cos\varphi] cos\psi \, d\psi \, d\varphi \qquad (3\text{-}10)$$

$$> F_v \, ds$$

On the other hand, the area of cross section decreases due to ovaliztion. This results in the decrease of the pressure force on the end-cap F_p'. In this case, the forces in Eq.(3-8) are no longer in balance, i.e.

$$F_v' \, ds + F_v' \, d\psi \; > \; 0 \qquad (3\text{-}11)$$

The resultant force acts as a moment to resist against the deflection of pipe, e.g. pipe bending, herein named Anti-deflection moment, M_p. It further increases the bending stiffness of the pipe. The equilibrium is illustrated in Figure 3-10.
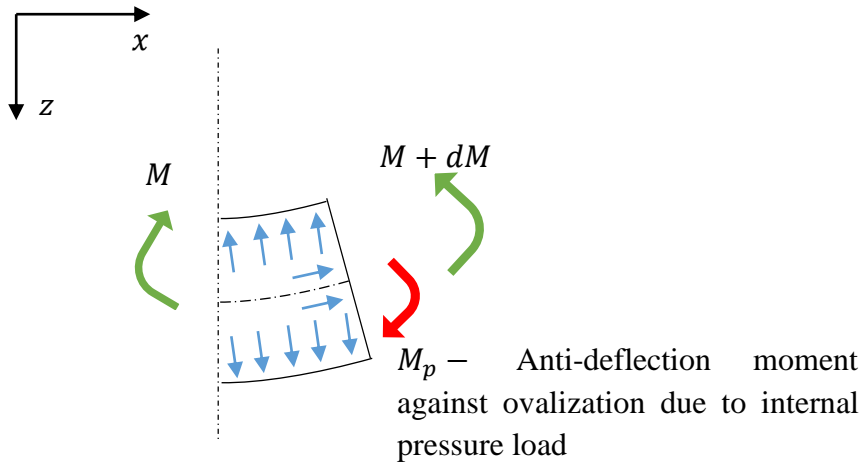
Figure 3-10 Anti-deflection moment, in case of pipe ovalization

In case of large internal pressure in high order of magnitude, the anti-deflection moment is significant, thus leading to the increase of the bending stiffness.

Nevertheless, the decrease of cross-section area can also result in the increase of

internal pressure, leading to larger bending stiffness. This is neglected in this thesis.

3.3.3 Stress behavior due to axisymmetric load

The response due to axisymmetric loads are primarily governed by the metallic layers which consist numbers of helices. By assuming that the wires rest stress free in the helix configuration, the initial torsion κ_1 and curvature components κ_2 and κ_3 along the helix can be expressed as

$$\kappa_1 = \frac{\sin\alpha\,\cos\alpha}{R} \tag{3-12}$$

$$\kappa_2 = \frac{\sin^2\alpha}{R} \tag{3-13}$$

$$\kappa_3 = 0 \tag{3-14}$$

Where σ is the lay angle of the helix, R is the helix radius.

Further, the long and thin wires can be described by the curved beam theory and the wire equilibrium equation can be expressed as [13]

$$-\kappa_2 Q_1 + \kappa_1 Q_2 + q_3 = 0 \tag{3-15}$$

$$-\kappa_2 M_1 + \kappa_1 M_2 + Q_3 = 0 \tag{3-16}$$

Where Q_i and M_i respectively represent the forces along and the moments about X^i axes, and q_3 is the contact line load in the radial direction. This is defined in the Figure 3-11.

((a)) Initial torsion and curvature quantities   ((b)) Wire stress resultants
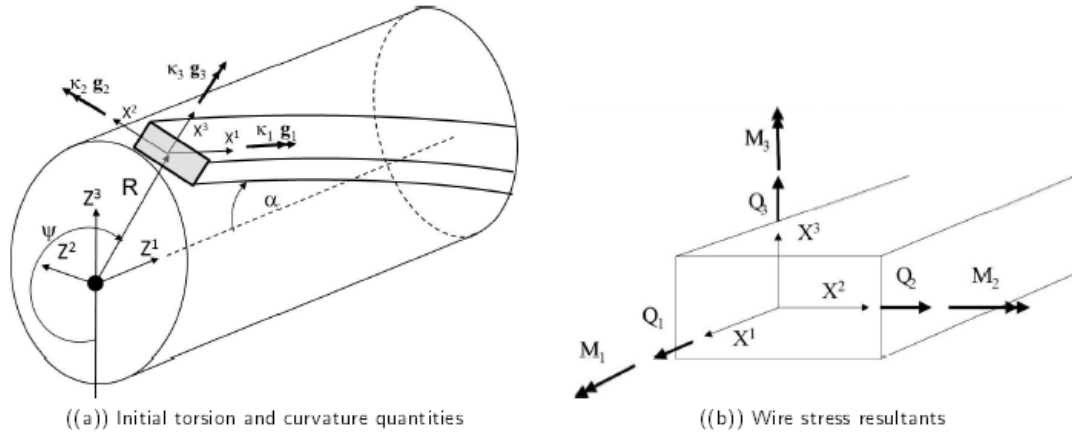
Figure 3-11 Definition of wire coordinate axes and the mechanical quantities

In most cases, the armour wire is slender and the contribution from M_i and Q_2 is small can be negligible. Therefore the contact pressure line load q_3 can be obtained as

$$q_3 = \kappa_2 Q_1 = \frac{\sin^2 \alpha}{R} Q_1 \qquad (3\text{-}17)$$

Basically by assuming that the steel layers are the main axial loads beading components, the pure axial equilibrium can be expressed as

$$\sum_{j=1}^{N\alpha} n_j \alpha_{11j} A_j \cos\alpha_j = T_\omega = T + \pi p_{int} R_{int}^2 - \pi p_{ext} R_{ext}^2 \qquad (3\text{-}18)$$

Where N_σ is the number of contributing layers, T_ω is true wall tension, n_j is the number of wires in layer j, α_{11j} is the axial stress in the layer. A_j is the cross-section area, T is the effective tension (the total cross-section resultant), p_{int} is the internal pressure, p_{ext} is the external pressure, R_{int} is the internal pipe radius where the internal pressure is acting (normally outside the carcass) and R_{ext} is the external pipe radius where the external pressure is acting.

From the equation above, it is seen that axial loading is mainly take by the tensile armour layer.

For a two layers of cross-wound structure where the lay angles are equal but opposite

in lay direction (torsion balanced), the following formulas can be used to estimate the stresses in the tensile armour.

$$\alpha_t = \frac{T_\omega}{nA_t \cos \alpha} = \frac{T_\omega}{2\pi R t_{tot} F_f \cos^2 \alpha} \qquad (3\text{-}19)$$

where n is the total number of tensile armour wires, At is the area of the wire, t_{tot} is the thickness including both layers and F_f is the fill factor.

The nominal external pressure from the tensile layers onto the pressure spiral wire armour can further be approximated by assuming same fill factor and number of tendons for two layer. It yields,

$$p_t = \frac{2q_3}{b} F_f = \frac{2(\alpha_t A_t \sin^2 \alpha)}{Rb} F_f = \frac{2(T_\omega)}{2n_j \cos\alpha} * \frac{\sin^2 \alpha}{Rb} * \frac{n_j b}{\cos\alpha 2\pi R} \qquad (3\text{-}20)$$

The primary effects due to axial loading are of concern in the later analysis. Further information on other effects can be referred to [1] [13] [10]

3.3.4 Stress behavior due to bending

3.3.4.1 Geodesic and Loxodromic assumptions

There are two main assumption towards along which path that each wire follows in the stressed state under bending.

1) **Loxodromic assumption**: represents the curve that would represent the initial path of each wire on the circular cylinder as if the path was fixed relative to the surface.

2) **Geodesic assumption**: represents the shortest distance between two points, respectively on the tensile and compressive sides of the pipe along the same helix.
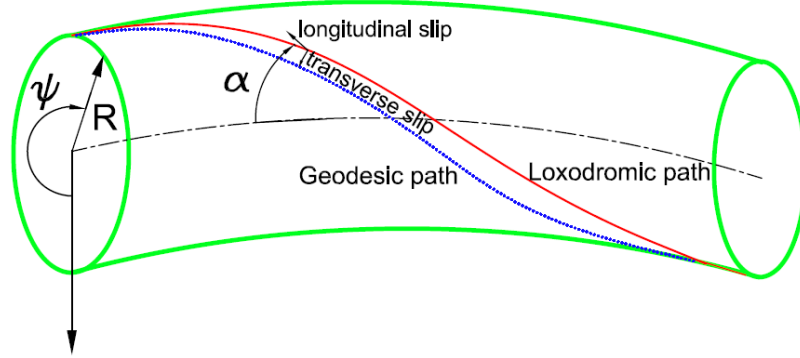
Figure 3-12 Definition of curve paths

However, the transverse wire displacements towards the Geodesic will be restrained by transverse friction forces. The dynamic bending torsion and curvature in each wire will be somewhere between the solutions based on the two limit assumptions. [14]

In case of no slip, the loxodromic curve applies and the torsion and the curvature can be determined with the reference to Figure 3-6(a).

$$\omega_{1p} = sin\alpha \; cos^3\alpha \; cos\psi\beta_2 \qquad\qquad (3\text{-}21)$$

$$\omega_{2p} = - \; cos^4\alpha \; cos\psi\beta_2 \qquad\qquad (3\text{-}22)$$

$$\omega_{3p} = (1 + sin^2\alpha) \; cos\alpha \; cos\psi\beta_2 \qquad\qquad (3\text{-}23)$$

Where β_2 is the global curvature at the cross-section center and ψ is the angular coordinate starting from the lower side of the pipe.

In case of longitudinal slip under Loxodromic assumption, if no axial friction is assumed, the longitudinal relative displacement can be expressed as

$$u_1 = \frac{R^2 \cos^2\alpha}{sin\alpha} \; sin\psi\beta_2 \qquad\qquad (3\text{-}24)$$

Hence the corresponding torsion and the weak axis curvature are changed into

$$\omega_{1p} = 2 sin\alpha \ cos^3\alpha \ cos\psi\beta_2 \qquad\qquad (3\text{-}25)$$

$$\omega_{2p} = - cos^2\alpha \ cos2\alpha \ cos\psi\beta_2 \qquad\qquad (3\text{-}26)$$

The transverse curvature ω_{3p} is not affected in this case.

In the later analysis, Loxodromic assumption is employed by restraining the transverse slip in the definition of the nodal boundary condition.

3.3.4.2 Moment-curvature behavior and associated friction stresses

The bending stiffness of the flexible pipes and umbilicals is the main focus in the analysis in the later chapters. It behaves differently in different kinds of structures and conditions.

The bending behavior of the non-flexible pipe is basic reference for the others. This is illustrated in the moment-curvature plot in the figure 3-13.
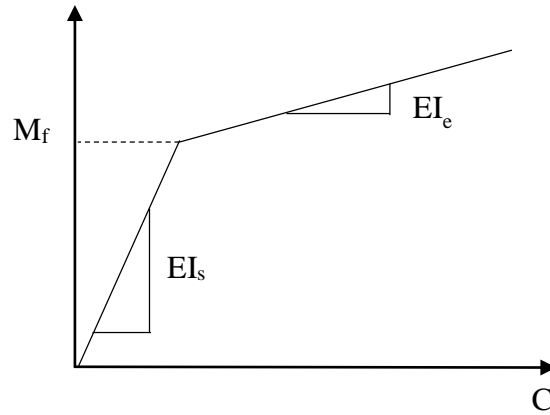
Figure 3-13 Typical moment curvature relation for non-bonded flexible pipe

This hysteresis behavior may be explained by the internal slip mechanism. Initially when the curvature is small, slip is prevented by the internal friction between layers, leading to a high initial bending stiffness. The moment needed to overcome the friction force, M_f, is named as the friction moment. M_f depends on the contact pressure between pipe layers, and consequently on the loads applied to the pipe.

As the friction moment is exceeded, the curvature increases linearly with the moment. In this case the bending stiffness EI_e is represented by the sum of contributions from elastic bending of the plastic layers and each individual wire.

With reference to Figure 3-6(a), considering plane deformation only, the axial force in the tendon can before slip can be expressed as:

$$Q_1 = -EA_t \cos^2 \alpha \ Rcos\psi\beta_2 \tag{3-27}$$

By differentiating the above equation with respect to the length coordinate X_1 and applying the relation $\psi = \frac{sin\alpha}{R}X^1$, the associated shear force q_1 per unit length along the wire is obtained,

$$q_1 = EA_t \cos^2 \alpha \ sin\alpha \ sin\psi\beta_2 \tag{3-28}$$

It is found that the maximum occurs at the neutral axis of bending as for the standard beam theory. The maximum possible shear stress q_{1c} is obtained:

$$q_{1c} = \mu(q_3^I + q_3^{I+1}) \tag{3-29}$$

Where μ is the coefficient of friction and the index I refer to the inner and outer surfaces of the tendons. By equation q_1 and q_{1c}, the critical curvature is further found as:

$$\beta_{2c} = \frac{\mu(q_3^I + q_3^{I+1})}{EA_t \cos^2 \alpha \ sin\alpha} \tag{3-30}$$

Based on the assumption of harmonic helix motion and no end effects, an arbitrary cross section can be divided into two zone, illustrated in the

Region I: stick domain

Region II: slip domain

ψ_0: transition angle
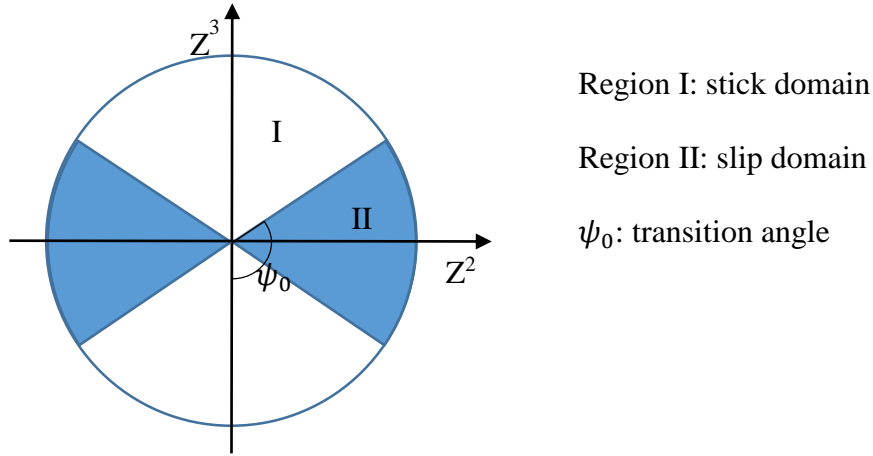
Figure 3-14 Cross-section stick and slip domain

Considering one quarter of the cross-section and at the tensile side, the transition between these two regions can be defined by the angle ψ_0:

$$\psi_0 = \cos^{-1}(\frac{\beta_{2c}}{\beta_2})$$

(3-31)

Where β_2 is the actual curvature of the cross-section at any stage beyond slip. At this stage, the stress distribution along Region II in this quarter can be expressed as:

$$\sigma_{11}(\psi) = \frac{\mu(q_3^I + q_3^{I+1})R}{sin\alpha A_t}\psi$$

(3-32)

And the stress distribution in Region I can be expressed as:

$$\sigma_{11}(\psi) = Ecos^2\alpha R\beta_2(sin\psi - sin\psi_0) + \frac{\mu(q_3^I + q_3^{I+1})R}{sin\alpha A_t}\psi_0$$

(3-33)

At the full slip, i.e. $\psi = \psi_0 = \frac{\pi}{2}$, the cross-section stress reaches its full value:

$$\sigma_{11} = \frac{\pi}{2} \frac{\mu(q_3^I + q_3^{I+1})R}{\sin\alpha A_t} \tag{3-34}$$

By integration, utilizing symmetry, the associated bending moment yields:

$$\text{M} = 4\text{F}_\text{f} \cos^2 \alpha \ R^3 t \left[\int_0^\psi \left(\frac{\mu(q_3^I + q_3^{I+1})R}{\sin\alpha A_t} \psi \right) + \right.$$
$$\left. \int_{\psi_0}^{\frac{\pi}{2}} E\cos^2\alpha R\beta_2(\sin\psi - \sin\psi_0) + \frac{\mu(q_3^I + q_3^{I+1})R}{\sin\alpha A_t} \psi_0 \sin\psi \right] d\psi \tag{3-35}$$

According to the bending moment equation above, the start slip and full slip bending moment can be determined to be:

$$M_c = \frac{R^2 \mu(q_3^I + q_3^{I+1})n}{2\tan\alpha} = \frac{F_f\left(\pi R^2 \cos^2 \alpha \mu(q_3^I + q_3^{I+1})\right)}{b\sin\alpha} \tag{3-36}$$

$$M_f = \frac{2R^2 \mu(q_3^I + q_3^{I+1})n}{\pi \tan\alpha} = \frac{F_f\left(4R^3 \cos^2 \alpha \mu(q_3^I + q_3^{I+1})\right)}{b\sin\alpha} \tag{3-37}$$

It is seen that the difference between start slip and full slip bending moment value is a factor of $\frac{\pi}{4}$, which agrees with the factor between the initial and full yield bending moment of a rigid pipe with a pure elastic-plastic material property.
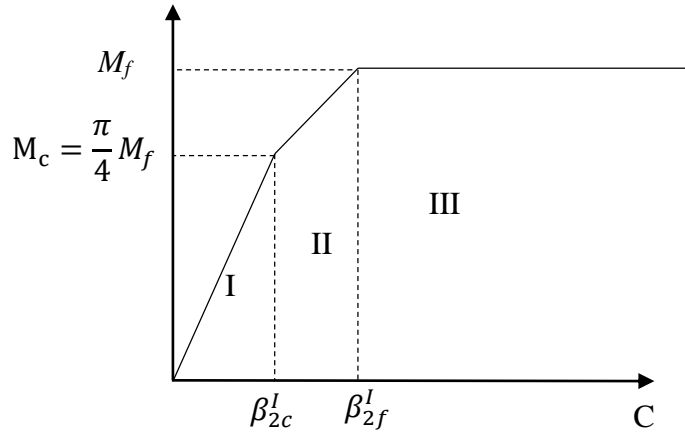
Figure 3-15 Moment curvature contribution from each layer

This diagram represents the friction contribution to the moment curvature relation from each tensile armour layer and can be represented as a three-linear function. The contact pressure will vary between layers and the total moment curvature diagram will therefore include a sum of three-linear relations, one for each layer.

Further assuming bi-linear relations instead in consideration of the small transition between start slip to full slip in each layer, the individual contribution from friction can be expressed as:

$$\beta_2 \leq \frac{4}{\pi} \beta_{2c} : EI_s = F_f \cos^4 \alpha \, \pi R^3 t$$

$$(3\text{-}38)$$

$$\beta_2 \geq \frac{4}{\pi} \beta_{2c} : EI_s = 0$$

The total bending stiffness can be found by summing contributions from all the layers:

$$EI = EI_e + \sum_{j=1}^{N_t} F_{fj} \cos^4 \alpha_j \, \pi R_j^3 t_j f(\beta_2, \beta_{2cj}) \qquad (3\text{-}39)$$

Where f is a situation factor that is 1 for $\beta_2 < \beta_{2cj}$ and is 0 for $\beta_2 > \beta_{2cj}$ for each layer.

EI_e represents the sum of elastic contributions from the plastic layers and local wire bending. If Loxodromic assumption applies, the estimate bending stiffness contribution can be expressed as:

$$EI_e = \sum_{j=1}^{N_{pi}} \frac{\pi}{4} E_j \left[\left(R_j^0\right)^4 - \left(R_j^i\right)^4 \right] + \frac{1}{2} \sum_{j=1}^{N_t} n_j \left[G_j I_1 4 \sin^2 \alpha_j \cos^5 \alpha_j + \right.$$

$$\left. E_j I_{2j} \cos^3 \alpha_j \cos^2 2\alpha_j + E_j I_{3j} \cos \alpha_j \left(1 + 2 \sin^2 \alpha_j + \sin^4 \alpha_j\right) \right] + \quad (3\text{-}40)$$

$$\sum_{j=1}^{N_t} F_{fj} \alpha_{11j} \pi R_j^3 t_j [3 \cos^4 \alpha_j \sin^2 \alpha + 4 \cos^2 \alpha_j + 6 \cos^4 \alpha_j + \frac{\cos^8 \alpha_j}{\sin^2 \alpha_j} + \frac{\cos^6_j \alpha_j}{\sin^2 \alpha_j} + 4$$

It is noted that the slip limit depends on the pressure and tension, several moment-curvature may have to be used.

For most cases, this model has proven to give good stress and fatigue for the tensile armour as compared to the test data. [13]

3.3.4.3 Influence of shear deformation in the plastic layers

As stated previously, the plastic layers influences the load distribution between all the layers. If the tensile layer is supported by thick plastic layers, shear deformations may occurs and the plane surfaces no longer remain plane before slip.
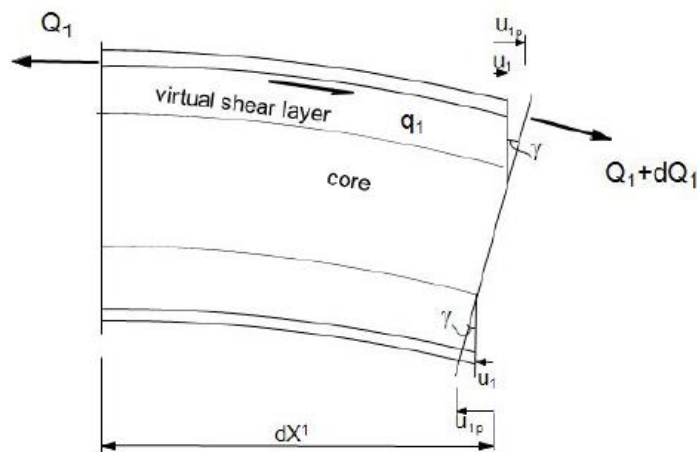
Figure 3-16 Shear deformation model [1]

Based on the equilibrium, the differential equation can be formulated along the tendon

as:

$$EAu_{1,11} - ku = -ku_{ip} \tag{3-41}$$

Where u_{ip} represents the relative displacement corresponding to plane surface remains plane condition. The shear stiffness parameter is defined by

$$\text{k} = \frac{\text{Gb}}{\text{t}} = \frac{E_p b}{2(1+v)+t} \tag{3-42}$$

Where E_p is the Young's modulus of the plastic layer. The slip curvature is obtained by only considering the particular solution:

$$\beta_{2c} = [1 + \frac{\sin^2 \alpha \ EA}{kR^2}](\frac{\mu(q_3^l + q_3^{l+1})}{EAcos^2\alpha \ sin\alpha}) \tag{3-43}$$

Therefore shear stiffness will result in the increase of the slip curvature, hence reducing the stress in the stick domain at the given curvature.

3.3 Non-linear FEM formulation

3.3.1 The Principle of Virtual Displacements

One of the most frequently used techniques in continuum mechanics is the *Principle of Virtual Displacement*, or the *Principle of Virtual Work*. Excluding volume forces, the principle of virtual work in an arbitrary equilibrium state of a body with deformed volume and surfaces V and S reads: [10]

$$\int_V (\rho\ddot{u} - f) \ \delta u \ dV + \int_V \sigma: \delta\epsilon \ dV - \int_S t \ \delta u \ dS = 0 \tag{3-44}$$

Where ρ is the material density, $\ddot{u}$ is the acceleration field, f is the volume force vector, σ is the Cauchy stress tensor, ϵ is the natural strain tensor, t is the surface

traction and u is the displacement vector. In this work most quantities are referred to the initial C_0 configuration where Green strain and 2nd Piola-Kirchohoff stress are energy conjugated quantities. It is noted that the strains are assumed small in this case. However, in the case of non-conservative loading, the resulting load will change as a function of the area change. This form refers to [15]

Two different formulations widely used. Total Lagrangian (TL) and the Updated Lagrangian (UL) formulations are used in the in finite element analysis of large deformation problems. The present work has been based on the Co-rotational formulation referring all quantities to the C_0 configuration. The equation of incremental stiffness is obtained by making use of Eq. (3-36) and study the virtual work in an infinitesimal increment Δ as follows only considering the static terms:

$$\int_V C : (\epsilon + \Delta E) : \delta(\epsilon + \Delta E) dV_0 - \int_S (t + \Delta t) \, \delta u \, dS_0 = 0 \qquad \text{(3-45)}$$

Where E is the Green strain tensor. This equation gives incremental equilibrium equation to be used as basis for the stiffness matrix. [10]

3.3.2 Non-linear effects

In the analysis of large displacement, three main non-linear effects should be taken into consideration. They are generally termed as Geometry Non-linearity, Material Non-linearity and Boundary Non-linearity.

1. Geometry Non-linearity

In the geometry non-linearity problems, the deflections of the structure are large compared with the original dimensions of the structure, so the stiffness and loads will change as the structure deforms.
The important step is to define time varying loads or restrains and boundary condition for the non-linear static loads, and then create the solution set and define the time increments for this solution.

2. Material non-linearity

Material behavior is based on the current deformation state or the past history deformation, and other constitutive variables, such as pre-stress and temperature, may

also have some influences. This property is mainly pronounced in the structures which undergo non-linear elasticity, plasticity, viscoelasticity, creep or inelastic rate effects, and is usually related to the Young's Modulus.

3. Boundary Non-linearity

The boundary condition may change in the contact area. These include force boundary condition and displacement boundary condition.

Those three nonlinearity sources are the most important. In addition, some other sources may be of concerns in some cases, e.g. non-linear pipe-soil interaction force, non-linear hydrodynamic loading, transient temperature

3.3.3 Finite element implementation

By application of Principle of virtual displacement using the interpolation function expressing the 3 dimensional displacement field of the element, the displacement interpolations for the moment based model and the sandwich beam model yield. The interpolation function is expressed as follows.

$$
\begin{bmatrix} E_{11} \\ E_{22} \\ E_{33} \\ 2E_{12} \\ 2E_{13} \end{bmatrix} = \frac{1}{C_\sigma} \begin{bmatrix} 1 & -v & -v & 0 & 0 \\ -v & 1 & -v & 0 & 0 \\ -v & 1 & -v & 0 & 0 \\ 0 & 0 & 0 & 2(1+v) & 0 \\ 0 & 0 & 0 & 0 & 2(1+v) \end{bmatrix} \begin{bmatrix} S^{11} \\ S^{22} \\ S^{33} \\ S^{12} \\ S^{13} \end{bmatrix} \qquad (3\text{-}46)
$$

Where C_σ is the Young's modulus and v is the Poisson's ratio and S^{ij} are the components of 2$^{\text{nd}}$ Piola-Kirchoff stress tensor. Then the displacement interpolation yields.

The FE assemble and solution procedure is based on solving the equilibrium in two steps. [16]

1. For each load step, the axisymmetric model is used to determine the inter-layer conditions from tension, torsion and pressure loads for each element along the flexible pipe. In addition to the appropriate boundary conditions in terms of contact pressure and friction stick–slip behaviour for the bending models, this also gives axial and torsion stiffness parameters that are applied to solve a reduced equation system when

applying bending loads.

2. In the reduced system, the radial DOFs are eliminated, hence only including the beam DOFs for the MM model and in addition the longitudinal tendon DOFs for the SBM model. The reduced equation system is applied to solve the bending problem where the MM and SBM models now respectively behave as ordinary non-linear beam and sandwich beam elements.

Detailed procedure refers to [15] [16] [1].

3.4 Bflex2010 program system

3.4.1 Introduction

Bflex2010 is a FEM based program system for non-linear static and dynamic analysis of flexible pipes. The program is based on the principle of virtual displacement. The Co-rotational Total Lagrangian formulation is applied to model the non-linear effects, while Newton-Raphson Iteration procedure is applied to carry out the non-linear FEA. Blex2010 takes the effect of multi-directional slip of the tensile armour into account, and the bending moment induced by each armour layer's response to the external curvature. [15] For more detail description, refer to Bflex theory manual and User manual. [10] [16]

In this thesis work, the modelling is mainly based on using the pipe elements and the helix contact elements, i.e. PIPE31 and HSHEAR363 for the core pipes, HSHEAR353 for the helix tendons, and HCONT453 or HCONT463 to simulate the contact between. Detailed modelling procedure is described in the following chapter, including specific structure data, material inputs, and control parameters.

3.4.2 Pipe element

3.4.2.1 Pipe element theory

The finite element model includes six beam dofs per node. The orientation and motion of the beam node is referred to a global coordinate system with base vectors I_i. The

element deformations are, measured relative to a local beam element system $\mathbf{i_i}$ that is attached to each beam element. The rigid deformations are neglected in the analysis. The motion of the beam model is illustrated in the figure below.
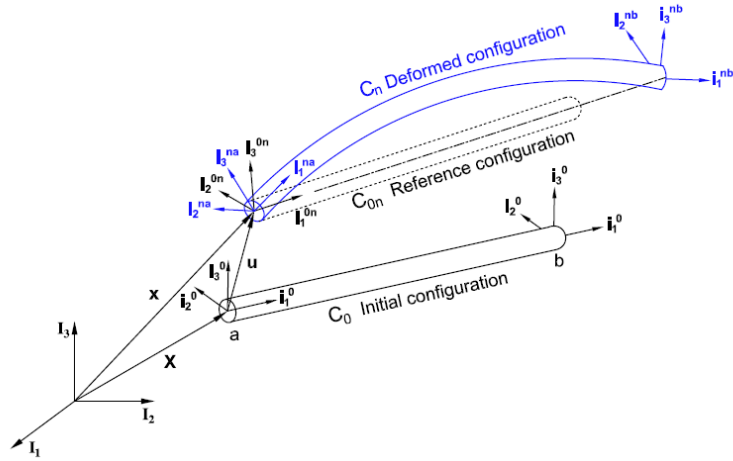

Figure 3-17 Motion of beam nodes [17]

The nodal $\mathbf{i_i}$ system and the elemental $\mathbf{j_i}$ system are in the initial state parallel to the global base vectors Ii and moves along with the node during deformation.

By assuming that the Bernoulli-Euler and Navier hypothesis apply, the beam contribution to the equilibrium equation is established. When formulating the incremental equilibrium equations, Green strain tensor is employed as strain measure. According to von Karman, the second order longitudinal strain term in the Green strain tensor is neglected. The same applies to the coupling terms between longitudinal strain and torsion. Shear deformations are also neglected. [10]

The displacement of an arbitrary point P in the local coordinate on the cross-section can be expressed as:

$$u_x(x, y, z) = u_{x0} - y u_{y0,x} - z u_{z0,x}$$

$$u_y(x, y, z) = u_{y0} - z\theta_x \tag{3-47}$$

$$u_z(x, y, z) = u_{z0} - y\theta_x$$

The longitudinal Green Strain is found to be:

$$E_{xx} = u_{x0,x} - y u_{y0,xx} + \frac{1}{2}(u_{y0,x}^2 + u_{z0,x}^2) \qquad (3\text{-}48)$$

3.4.2.2 PIPE31

The pipe31 element is 3D 2-noded beam element with thin walled tubular cross-section and constant radius and thickness along each element. It works in element level in order to consistently handle the pressure effect.

For pipe elements further simplification is introduced by utilizing the fact that the hoop stress is known using shell theory, which means that the hoop strain is known. Hence no degrees of freedom is related to the hoop effect.

In the thesis work, it is mainly used to simulate the core pipe, which is directly internal pressure bearing component. However, it is insufficient to pick up the radial expansion. This is shortcoming of the PIPE31 element.

3.4.2.3 HSHEAR353

HSHEAR353 is a 4-noded 26-dof curved beam element dedicated to the modelling of helices. It includes 12 beam dofs corresponding to those of pipe31 plus 6 helical DOFS at each end of the corresponding helix. In addition two internal dofs are used to allow accurate description of the longitudinal slip process.
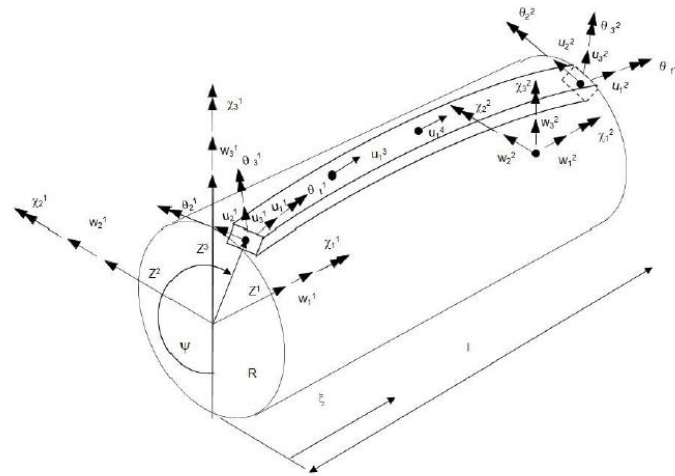
Figure 3-18 The dofs system of HSHEAR353 element

3.4.2.4 HSHEAR363

HSHEAR363 is a 4 noded 18 dof beam-shell element dedicated to the modelling of the pressure armour, the anti-buckling tape and the plastic layers. It includes 12 beam dofs corresponding to those of pipe31 plus 3 dofs associated to separate nodes having the same geometric location as the end beam nodes.
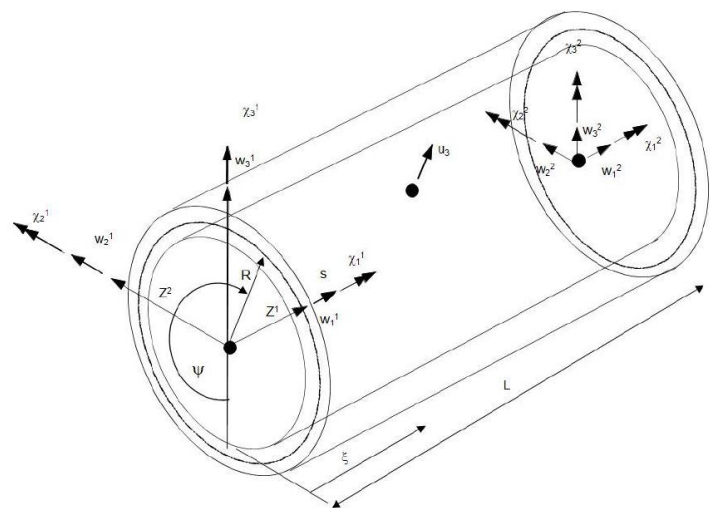

Figure 3-19 The Dofs system of HSHEAR363 element

For the HSHEAR363 element two additional nodes are introduced to allow the radial motion being described by local radial and ovalization motions in addition to the

standard beam quantities. It can be interpreted as a simplified shell element that allow the core (that may consist of the pressure armour, the thermoplastic layers and the anti-buckling tape layers) to be modelled in an approximate way. The redial displacement is assumed to be described as:

$$u_3 = (\gamma_1 + \gamma_2 cos2\psi + \gamma_3 sin2\psi) \tag{3-49}$$

Hence by application of HSHEAR363 element, the radial expansion due to internal pressure load can be picked up. The radial compression on the plastic layer is more correctly simulated.

3.4.3 Contact element

3.4.3.1 Contact kinematics

Contact elements are non-structural elements, instead they are virtual elements which contain the necessary material properties to simulate the connection and relative displacement between the structure layers.

Considering 2 bodies A and B each of which occupies a region. Here two situations are of concerns, i.e. gap opening and contact.

1. Gap opening

$$g = (\Delta \mathbf{u_B} \overset{.}{-} \Delta \mathbf{u_A}) \cdot \mathbf{n} + g_0 \geq 0 \tag{3-50}$$

2. Contact

$$g = (\Delta \mathbf{u_B} \overset{.}{-} \Delta \mathbf{u_A}) \cdot \mathbf{n} + g_0 < 0 \tag{3-51}$$

Where g_0 is the initial gap, g is the current gap at time $t + \Delta t$ in the direction of $\mathbf{n}$, n is the outward surface normal vector of body A.

Further, if contact has been established, relative slippage including friction work will occur when:

$$\gamma = (\Delta \mathbf{u_B} \overset{\cdot}{-} \Delta \mathbf{u_A}) \cdot \boldsymbol{t} + \gamma_0 \neq 0 \qquad (3\text{-}52)$$

Where t is the tangent vector pointing towards body B.

There are three commonly used principles when dealing with contact problems. Ther are Lagrange multiplier method(LM), Penalty method(PM) and Mixed Method(MM).

In LM, the constraint conditions for a contact problem are satisfied by introducing Lagrange parameters in the variation statement. In PM, the contact pressure is assumed proportional to the amount of penetration by introducing a pointwise penalty parameter, the final stiffness matrix does not contain additional terms. In MM, it is highly dependent on the selected order of the contact pressure. [18]

In the following section, two types of HCONT element are described. HCONT453 and HCONT463 are respectively 4 noded and 3 noded hybrid mixed contact elements used to connect the HSHEAR elements to the core and to describe contact between the HSHEAR elements.

3.4.3.2 HCONT453

The HCONT453 element is designed as a contact between two HSHEAR353 elements, which describes the interlayer contact forces and the friction with regard to the relative displacement. The element consists of 4 nodes, which are both the end nodes of the 2 HSHEAR353 helix element. Neglecting the torsion of both the helix elements, HCONT453 contains 20 DOFs, but totally 24 DOFs are set up in order to match the standard beam DOFs. The Dofs system is illustrated in the figure below.
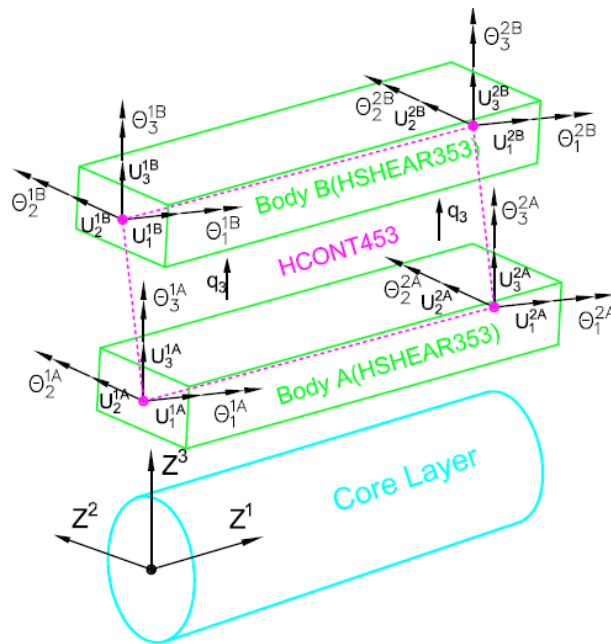
Figure 3-20 DOFs system of HCONT453 element

3.4.3.2 HCONT463

This contact element is to fit the quantities as defined for the HSHEAR353 and HSHEAR363 elements. As for the HSHEAR353, both the transverse and longitudinal directions are included at the end, whereas for the HSHEAR363 element, radial displacement is introduced only. To match the standard 6 DOFs in each node of the helix, the element is implemented with 15 DOFs, the DOFs system of HCONT463 element is shown in the figure below.
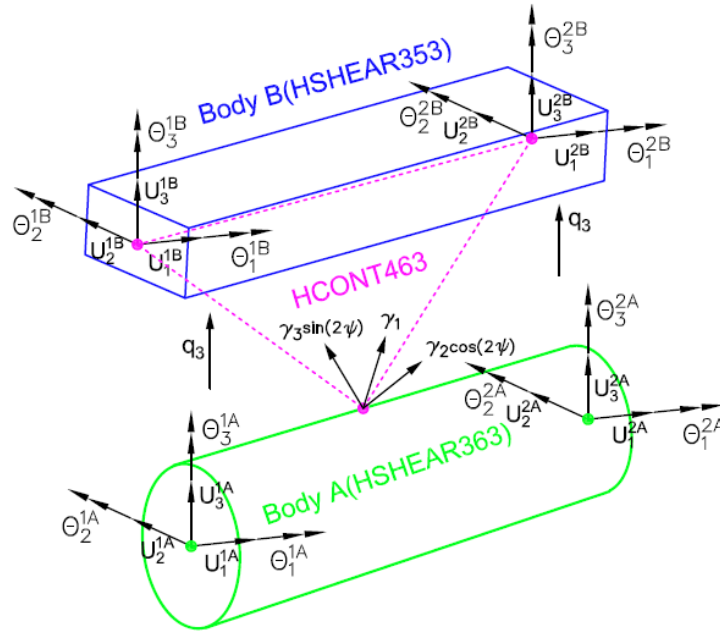
Figure 3-21 DOFs system of HCONT463 element, image

The radial displacement of the HSHEAR353 element is described by 4 DOFs, while in the HSHEAR363 element, 3 DOFs are included, so totally 7 DOFs in the radial direction.

3.4.4 Material properties

Various material types are available in Bflex2010 to describe different material properties of structural components. In this thesis work, the following types are employed.

3.4.4.1 LINEAR and ELASTIC

Both types are used to describe the linear elastic behavior of the core pipe. While ELASTIC is able to calculates the specific mechanical properties automatically e.g. bending stiffness about axes or torsion stiffness, LINEAR needs detailed specified mechanical properties which should be provided manually. Based on the elastic model and the application of plane stress assumption, the Hook's law applies.

3.4.4.2 CONTACT and ISOCONTACT

CONTACT is a user defined material surface property based on describing the material curve in the x and y and z- directions for the contact element types. As default, the force x and y components are multiplied with the z-force reaction and a friction coefficient.

By specifying USERDEFINED at the end of the contact card, the x- and y- curves are to be specified as displacement versus force curves. Then the curves will act independent of each other. Using this functionality together with hcont453, 463 the gap logic will further be turned off.

ISOCONTACT is the isotropic contact material. It can be applied to get isotropic friction behavior.

3.4.4.3 HYCURVE and EPCURVE

HYCURVE describes the hyper-elastic material behavior. The basic principle is that the resultant quantity is a one to one function of the associated deformation quantity without hysteresis (No history effect).
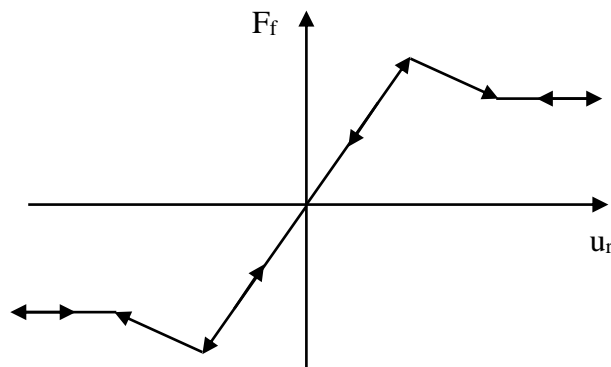

Figure 3-22 Sample curve defined by HYCURVE

Nevertheless, EPCURVE describes the elastoplastic material behavior with kinematic/isotropic hardening, i.e. Kinematic hardening and Isotropic hardening. This is illustrated in the Figure 3-18.
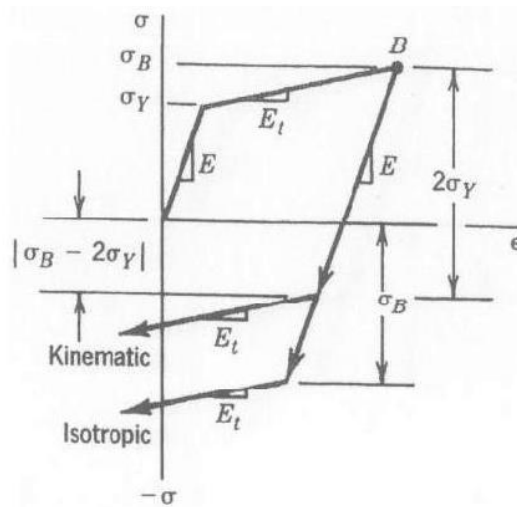
Figure 3-23 kinematic hardening and isotropic hardening

In the non-bonded model, EPCURVE is employed to define the Coulomb friction model.

As for the EPCURVE, the shear stiffness and the slip force limit are the important parameters that dominate the slip behavior.

The shear stiffness of the plastic layer and its effect have been discussed in section 3.3.5. Further problem and detailed discussion will be addressed in the modelling part in the later chapters.

Further information on the solution algorithms refers to the [10], including Newton-Raphson equilibrium iteration, the incremental time integration scheme and convergence criteria. The detail is not addressed here.

4. Non-bonded and boned pipe modelling and analysis

4.1 Introduction

Since a lot of works have been carried out on studies of non-bonded pipes, this chapter will start from the modelling of one non-bonded flexible pipe model. Then it will be modified according to the distinguishing differences to fit the bonded flexible model.

It should be noted that all the models are simplified models, but covering general characteristics of flexible pipes. The focus will be put on the bending stiffness of the flexible pipes, which shows the behavior of contact material dependent.

However, the problem comes when looking into the effects of internal pressure loads. The discussion will be based on the previous methodology chapter. Possible solution will be proposed in the end.

4.2 Non-bonded pipe modelling and analysis

First comes to the technical data of the flexible pipe. This is the basis for the modelling.

Detailed modelling procedure is addressed, with respect to the FE modelling, the material inputs, boundary conditions and constraint, following by the measurement method.

The analysis put the emphasis on the basic mechanical property, i.e. the bending behavior of the flexible pipe.

Finally the internal pressure effect is studied.

4.2.1 Modelling methods

4.2.1.1 Structure specification

The simplified non-bonded pipe model has the main typical components, including two layers of helical tendons and one core pipe.

Each tensile layers consists of numbers of helical tendons, which are the main components that bears the tensile loads and pressure load.

In reality, apart from the tensile layers, the non-bonded pipe also comprise other functional layers such as pressure armour, inner sheath and outer sheath and so on. Since we basically focus on the contact layers between the two tensile layers and the inner pipe, other component are not modelled in detail. Instead, they are integrated into one single core pipe layer, which reflects the main mechanical properties of all other layers.

The main structure components are illustrated in the Figure 4-1.
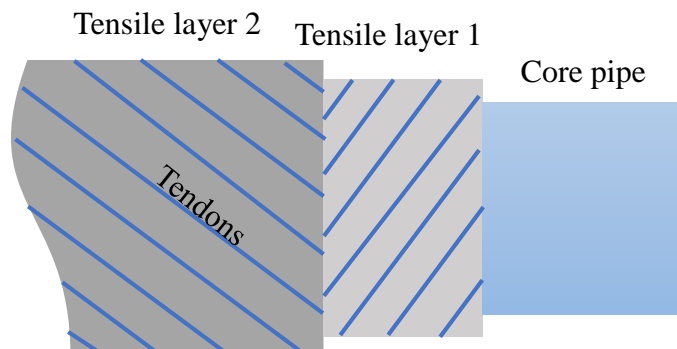
Figure 4-1 Illustration of the non-bonded flexible simplified model

The main structural data is tabulated in the table 4-1.

Table 4-1 Main technical data of non-bonded flexible pipe model

Non-bonded flexible pipe	
Length: 1196.00 mm Inner diameter: 112.80 mm Outer diameter: 162.00 mm	
Core pipe	Structural radius = 60.9 mm Axial stiffness EA = 4.58 MN Bending stiffness about y and z axis EI=8.78e3 MNm^2 Young's modulus E = 300MPa Shear modulus G =120 MPa
Tensile layer 1	Structural radius = 70.3 mm Tendon cross section geometry =5 * 2 mm^2, rectangular Tendon lay angle = -37.90º Tendon Young's modulus E = 2.1e5 MPa Tendon shear modulus G = 8.076e4 MPa Poisson ratio = 0.3 Fill ratio = 0.9 Number of tendons N = 61
Tensile layer 2	The same as tensile layer 1 but with: Structural radius = 74.3 mm Tendon layer angle = +37.90º

	Number of tendons N = 65

Apart from the main structural layers above, there are another two contact layers made of polymeric materials. The main contribution of the contact layers is to affect the load distribution by simulating the contact forces and relative displacement. The stick-slip behavior is directly affected by the contact layer material properties.

The description and the modelling of the contact layers are both addressed in section 4.2.1.3.

4.2.1.2 Finite element modelling

The main structural layers are modeled by application of the Bflex2010 PIPE and HSHEAR element types. In this case, the tendons layers are modeled by HSHEAR353 while PIPE31 is used to model the core pipe, in which all the other layers are integrated.

By application of Scale Factor, the number of tendons is scale down to speed up the calculation. This has been proved efficient and accurate enough. The tensile layer 1 has 61 helical tendons so that the scale factor is 3.85 when 16 tendons are simulated. As for the tensile layer 2, the scale factor is 4.06.

The model is divided into 80 segments so that there are 80 PIPE31 elements along the pipe length. Each tendon is also meshed into 80 elements.
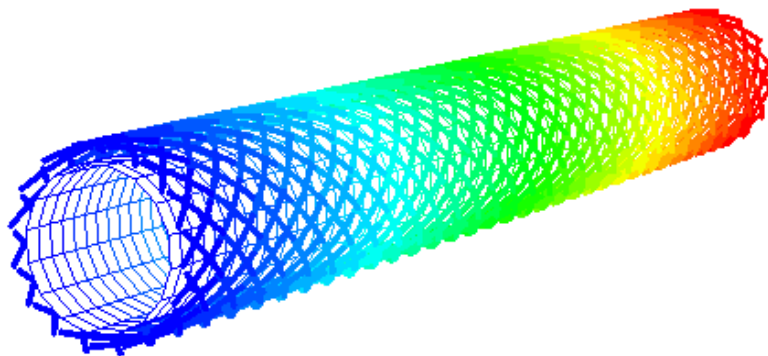
Figure 4-2 FE model of the non-bonded flexible pipe

4.2.1.3 Material properties

Structural layers

The main material data has been shown in the structural data table above. As for the tendons, they are modeled by material option ELASTIC, where the Young's modulus, shear modulus and Poisson's ratio are stored. The relevant information such as the bending stiffness and shear stiffness are automatically calculated by Bflex2010.

As for the core pipe, its material information is specified by option LINEAR, where the detailed information on all relevant mechanical properties is stored. The bending stiffness about y axis and z axis and torsion stiffness should be calculated manually and provided in advance.

Contact layers

The stick-slip behavior is directly dominated by the contact material and is the key difference between the non-bonded and the bonded flexible pipes. Since friction forces in x and y directions are dependent on the compression force in local z direction, they are separately specified under ISOCONTACT option of the contact material. Epcurve and Hycurve are used respectively for the material inputs in different directions.

In Bflex2010, the contact layer material properties is defined by using the Bflex2010 material type CONTACT or ISOCONTACT. They allow users to describe specific material behaviors in different directions, where material types EPCURVE and HYCURVE can be applied. Normally, EPCURVE is used to describe elastoplastic material behavior with kinematic or isotropic hardening, while HYCURVE is used to describe hyper-elastic material behavior.

As for the non-bonded pipe, the stick-slip behavior can be described by defining the stick limit and stiffness of the stick part by EPCURVE option in the directions where shear deformation occurs, i.e. x and y directions. This material curve is to be defined as a consecutive number of points defining displacement versus unit force per length. BFLEX2010 will scale the unit force value with μNL, where μ is the friction factor, N is the vertical reaction and L is the length of the pipe element in contact. Besides, the

contact layer also bears the radial contact pressure load in local z direction. This is described by HYCURVE.

The coefficient of friction is here set to be 0.2. It will be multiplied by the normal force and the corresponding factor to get the right friction. Besides, at the same normal force level, when the relative displacement exceeds the limit, the friction force will not increase anymore. This is the time when the slip behavior occurs.

4.2.1.4 Boundary condition and loads

The non-bonded pipe is clamped at the left end while the constraint is applied at the right end. It is demonstrated in the figure below.

Normally in the practical operations, the non-bonded flexible pipes are under high pressure inside the inner pipe. To keep the consistence both with the operations and tests, internal pressure is set to be 20 MPa in this case.

As we all know, generally high internal pressure makes pipes stiffer than the pipes at low internal pressure. This will be verified by the parametric study later.
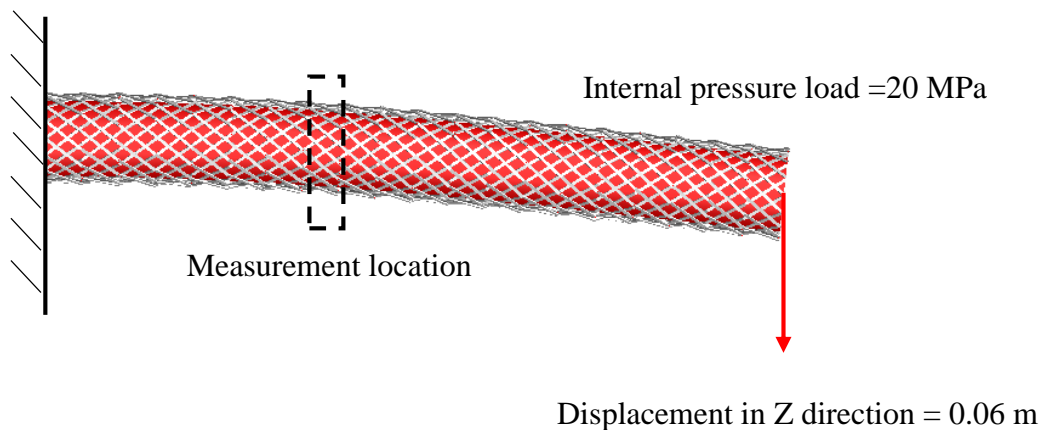
Figure 4-3 Boundary condition and the measurement location of the non-flexible pipe model

The internal pressure load is applied gradually previous to the loading of displacement constraint so as to avoid the coupling effect. The loading history is demonstrated in the

figure below.
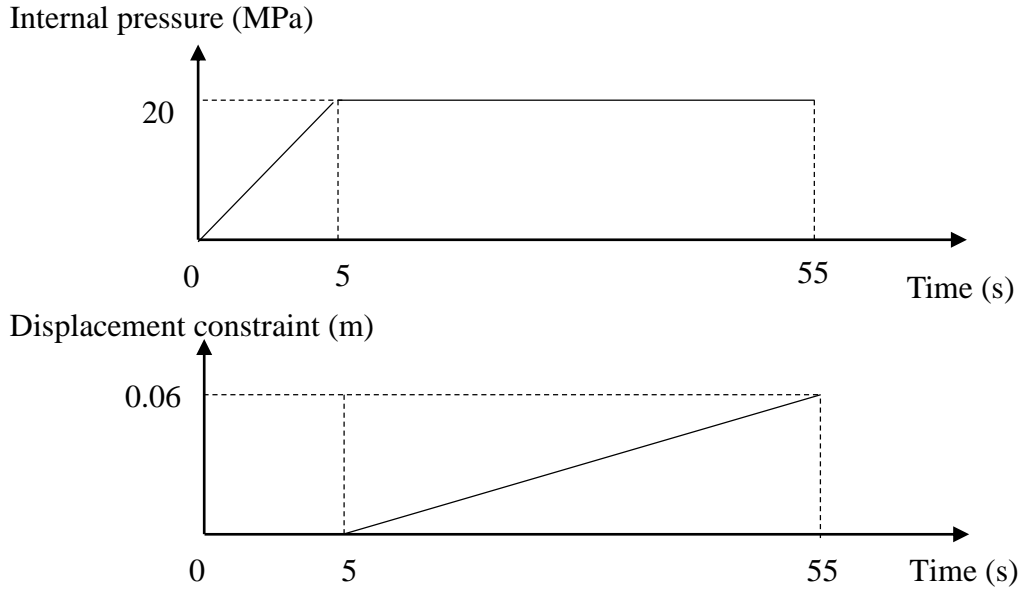
Figure 4-4 Loading history of the internal pressure and the displacement constraint

4.2.1.5 Measurement methods

The curvature and moment are needed at specific location to extract the bending stiffness, which can reflects the general mechanical property.

However, because of the rigid boundary condition at the left end, there is an obvious end effect in the global curvature plot shown in some figures. Practically the end effect should be avoided so as to measure the general bending stiffness. Hence in some tests the measure point is selected at a certain distance away from the pipe ends.

Therefore after the simulation is done, the necessary data is extracted at the measurement location, i.e. 0.48 m away to the left end. The measure location is illustrated in the figure 4-3.

4.2.2 Results analysis

4.2.2.1 Bending stiffness of the non-bonded pipe

The bending stiffness is the focus of the analysis. And the bending stiffness of the non-bonded pipe will be compared with that of bonded pipe in the later section.

In figure 4-5, the first curve shows the continuous increase of curvature at the measure point. Small change occurs when the displacement is about 0.2m that the increase speed slows down a little bit. The corresponding change is obvious in the moment history plot. The increase of moment slows down at the same time as the curvature curve.
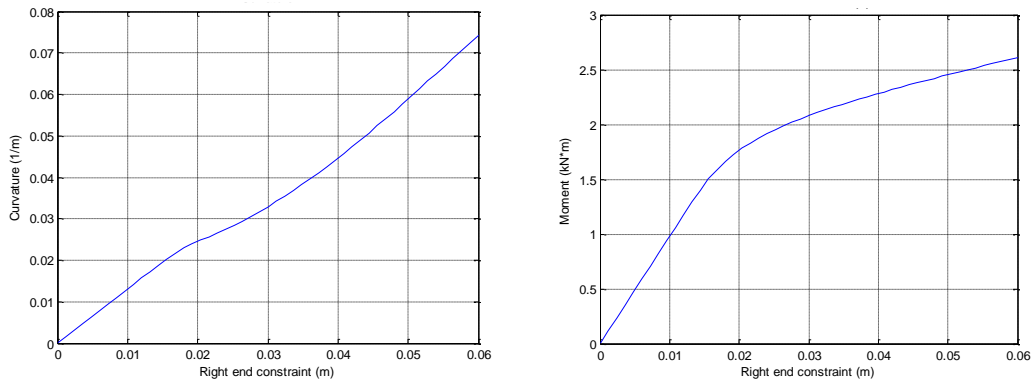
Figure 4-5 Curvature and moment history of the non-bonded flexible pipe

The curvature and moment is together plotted by setting the curvature as the x coordinate and moment as y coordinate, which is shown in the figure 4-6.
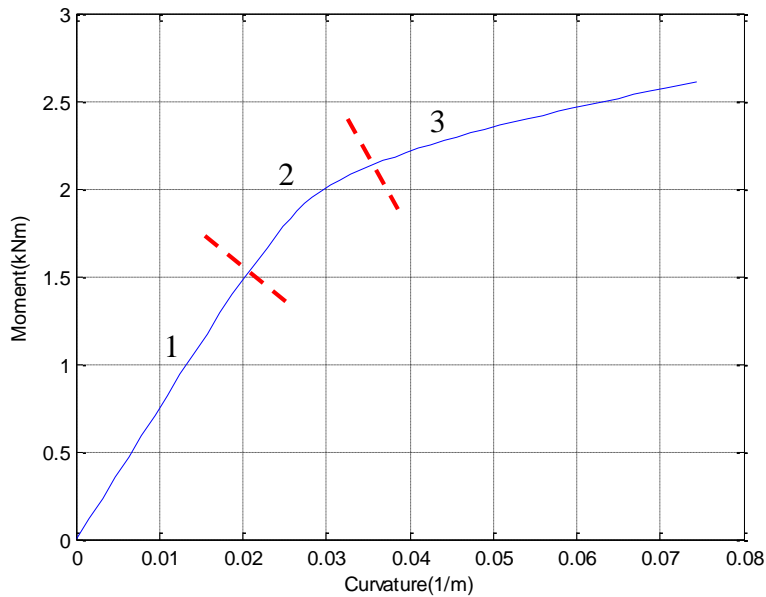
Figure 4-6 Moment-curvature of non-bonded flexible pipe

The curvature vs. moment curve can be also divided into 3 main phases, respectively corresponding to the three main stages described in previous methodology chapter, i.e. full stick, transition, and full slip.

During phase 1, it has a large initial bending stiffness and keeps constant from beginning till curvature of 0.024 m^{-1}. This initial bending stiffness $EI_1 = 75$ kNm^2. Similar as the umbilical pipe we have analyzed, this initial bending stiffness is related to the stiffness of the stick part defined in the material input.

Phase 2 is the transition between the full-stick and full-slip behavior of the contact layers. The bending stiffness smoothly changes to small value.

In phase 3, the moment increases slowly with the increase of curvature while the tangential bending stiffness keeps constant about 12.0 kNm^2. In this case the contribution of the bending stiffness mainly comes from the core pipe, partly from the increasing longitudinal stress on the tendons due to change of pipe geometry.

By looking at the individual contact element, we can find the detailed behavior related to the contact material. The following figure indicates the contact force on the typical contact element. It show that when the displacement reach certain value, the friction force does not increase as sharply as previous. Instead, it stays at certain value with

little fluctuation.
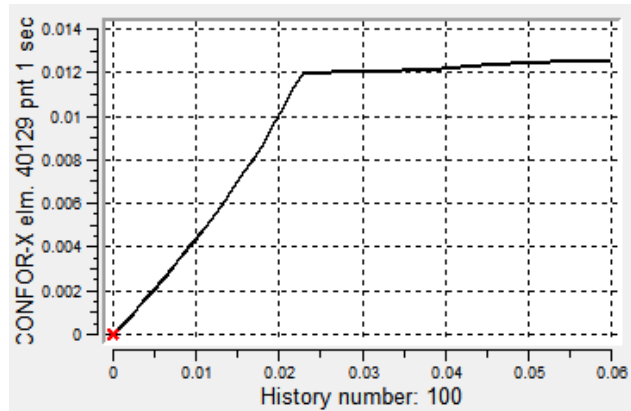
Figure 4-7 Longitudinal contact force on a typical contact element

As a whole, it is the all contact element that make up the contact layer and affect the stick-slip behavior. That is why the moment-curvature curve has a great initial bending stiffness but turn small afterwards.

4.2.2.2 Global deformation

Seen from the global displacement plot and the global curvature plot below, the main bending occurs close to left end, where the pipe is clamped. At the right part close to the free end, the deformation is small and the pipe is almost straight.

Apparently there is an end effect near the left end. The curvature reaches it maximum of 0.25 m^{-1} at this part and decreases swiftly at the location of 0.1m to the left end. There is a sagging part at the region where stress concentration locates. This is discovered in the stress analysis. However, this end effect should be avoided in the measurement.
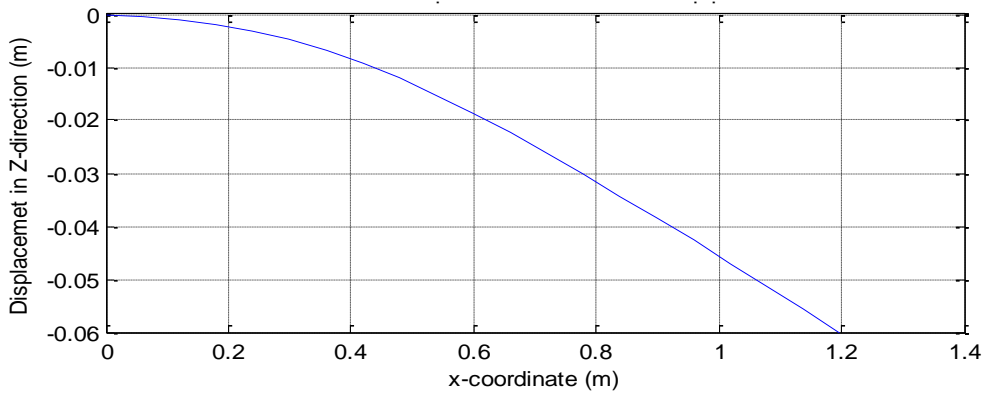
Figure 4-8 Global displacement of the non-bonded pipe
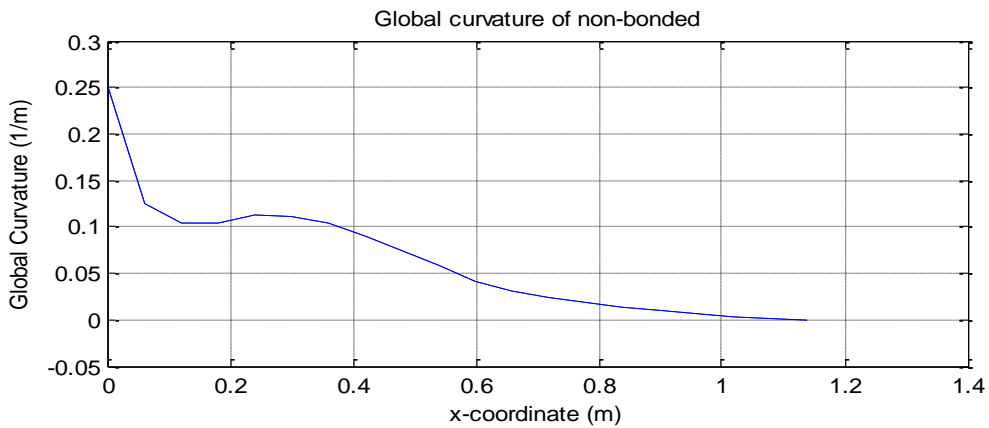
Figure 4-9 Global displacement of the non-bonded pipe

4.2.2.3 Cyclic loading

Seen from the following figure 4-10, when the load reverses its direction, the curve at the same time turns its direction and flows down. The tangential bending stiffness keeps consistent with the initial bending stiffness and again turns its direction at the second phase 2. This resembles the kinematic hardening.
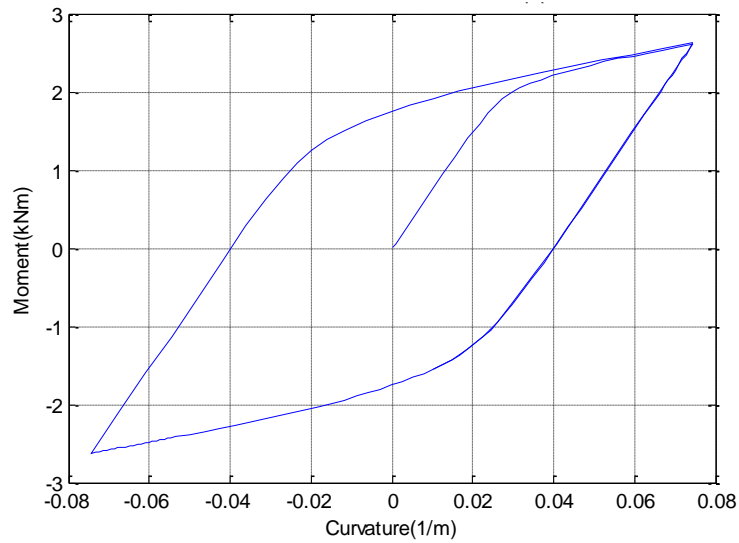
Figure 4-10 Moment-curvature of non-bonded pipe at cyclic loading

4.3   Bonded pipe experimental test review

4.3.1 General

SINTEF used to carry out one experimental test on the stiffness properties and damping behavior of flexible pipes. One Pag-o-flex pipe sample was tested to comply with the dynamic riser application and design pressure of 200 bar. [19]
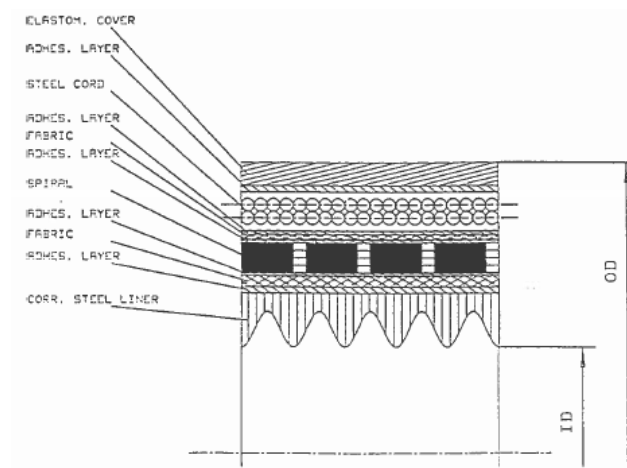
Figure 4-11 Detail section of the Pag-o-flex sample pipe [19]

The cross section of the pipe is illustrated in the figure 4-11. The detailed structural data is attached in the Appendix. In the modelling of bonded flexible pipe, the model will be a simplified to resemble the Pag-o-flex sample pipe, but integrating all the other layers into one inner core pipe and let the helix tendons be the separate tensile layers.

4.3.2 Test set-up

To avoid the end effect, on one hand it used lightly clamped boundary condition at the left end, and the sample pipe is long enough, i.e. 6 m, longer than the test length. On the other hand, the measure point was selected at a distance away to the left end to avoid the end effect. This measurement method is used in the thesis.
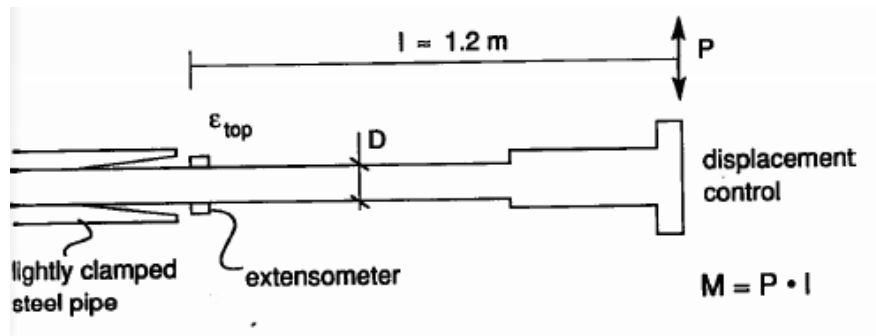
Figure 4-12 Test set-up of the sample bonded flexible pipe

4.3.3 Bending stiffness property

The following figure 4-13 shows the curvature vs. moment plot. The moment increases linearly from the origin, indicating a constant bending stiffness the load is being applied. The pipe is regarded as bonded pipe cause there is no slip behavior.

The hysteresis is about 2% and is small enough that can be ignored. The elastic to plastic behavior of the contact layer material may account for this hysteresis but the detailed reason is not discussed in the thesis.
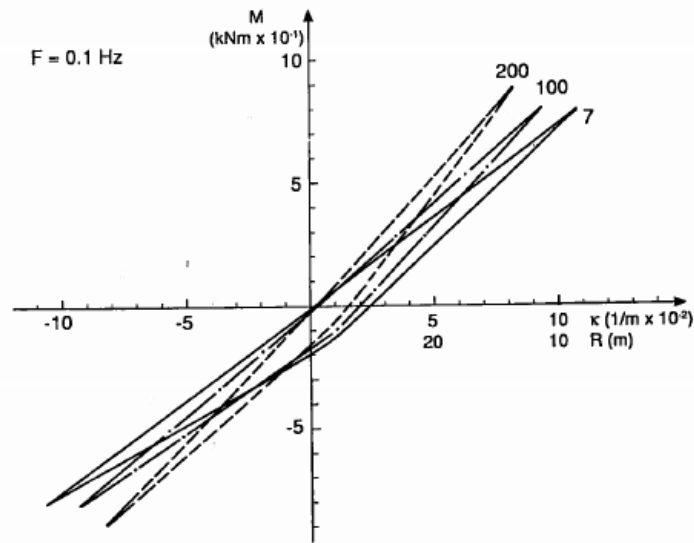
Figure 4-13 Moment-curvature curves at different internal pressure levels of Pag-o-flex sample pipe [19]

4.3.4 Effect of internal pressure load

The results also show the significant increase in bending stiffness for increasing internal pressure. The bending stiffness under different internal pressure level is tabulated in the table.

Internal pressure (bar)	Max curvature (m^{-1})	Max moment (kNm)	Bending stiffness (kNm^2)
200	0.082	0.89	10.85
100	0.093	0.80	8.60
7	0.16	0.79	4.94

We mainly account for the phenomenon by the rising resistance between the layers and the anti-deflection moment due to high internal pressure.

4.4 Alternative methods in modelling and analysis of the bonded pipe

4.4.1 Introduction

Generally the main structural data of the bonded model remains the same as the non-bonded. The main change is to modify the material to resemble the bonded pipe without slip behavior. Friction is inactivated by attaching the USERDEFINED option under the definition of the contact material so as to make the shear force in x and y direction independent of the force in z direction.

The key problem is how to properly model the core pipe to simulate the effect on the internal pressure load which has been approved one significant factor to the bending stiffness. Herein, PIPE31 has been employed, but the results show it insufficient to pick up the radial expansion. Hence the HSHEAR363 is used as the core pipe which could properly pick up the radial expansion.

4.4.2 Modelling Methods

4.4.2.1 Structure modification based on non-bonded flexible pipe model

The main structure and components are kept the same as the non-bonded pipe, including the length, inner diameter and outer diameter, structural layers etc. Those can be referred to the table of the structural data in previous section. The only changes are the geometry of the helical tendon and its lay angle.

Firstly, to keep consistent with the Pag-o-flex test sample pipe, the geometry of the helix tendon is changed from rectangular to current circular cross section. In the meanwhile, the cross sectional area is set to be equal to the rectangular tendon, in consideration of keeping axial stiffness consistent.

Table 4-2 Geometry and mechanical properties of the helical tendons

Geometry	Young's modulus(MPa)	Axial stiffness EA(MN)	Bending stiffness about y axis EIy (MNm^2)	Bending stiffness about z axis EIz(MNm^2)
Circular, D=3.75 mm	2.10E+05	2.10	1.67E-06	1.67E-06
Rectangular, 5*2 mm^2	2.10E+05		7.00E-07	4.38E-06

Secondly, the lay angle is changed to be 55.0°, in consideration of the typical bonded flexible loading hose with no restrict requirement on the tensile strength.

Last, surely the contact layer of the non-bonded pipe is replaced by rubber. This is specified in the following section regarding material inputs.

4.4.2.2 Alternative FE models using PIPE31 or HSHEAR363

Previously in the non-bonded case, PIPE31 element is employed to model the core pipe. As shown in the theory chapter, PIPE31 element is 3D beam with consistent axial strain and torsion. Nevertheless, PIPE31 has been proved insufficient to pick up the radial force in the non-bonded case, although the radial compression due to internal pressure load is properly picked up. Herein it is necessary to have a more accurate model to pick up the radial expansion together with the radial compression. Here comes HSHEAR363.

HSHEAR363 is a 4 noded 18 DOF beam-shell element which can be used to model the flexible pipe layers such as pressure armour, outer sheath and anti-buckling tape. It includes 12 beam degrees of freedom corresponding to those of PIPE31 plus 3 dofs associated to separate nodes having the same geometric location as the end beam nodes. Those additional dofs make it capable of picking up the radial expansion.

Besides, the main differences also lie in the types of contact layers, the node system and material type of core pipe. HCONT463 is needed to connect the HSHEAR363 core pipe and the first HSHEAR353 tensile layer, while HCONT353 is employed to connect two HSHEAR353 tensile layers. However, to model the contact between PIPE31 and HSHEAR353, one additional set of node system is established as a supporting layer in order to use the HCONT453 as the contact layer element.

4.4.2.3 Material Properties

Core pipe

Those two types of core pipe use alternative option to describe their own material properties.

LINEAR type is the only available material option to describe PIPE31 core pipe. But the mechanical properties such as bending stiffness about y axis and torsion stiffness should be calculated manually. ELASTIC is another option to describe HSHEAR363 core pipe, and the Young's modulus, Poisson's ratio and other basic material information are the only needed inputs.

No matter which option is used, it is important to keep the core pipe's bending stiffness consistent so that this change has no influence on the whole structure.

Contact Layer

Pure linear property assumption

The contact layer is the most significant difference between non-bonded and bonded flexible pipes.

The stick-slip behavior of non-bonded pipe is directly dominated by the properties of the contact layers. The most important characteristic is that the friction is dependent of the radial compression and does not increase significantly after the slip behavior occurs.

Unlike the non-bonded pipe, it is assumed that the boned pipe has a linear stress-strain property, meaning that no matter how large the relative displacement it has, the contact force will increase linearly to the relative displacement. This linear characteristic applies to all the direction and is described by HYCURVE respectively. This is illustrated by the figures below.
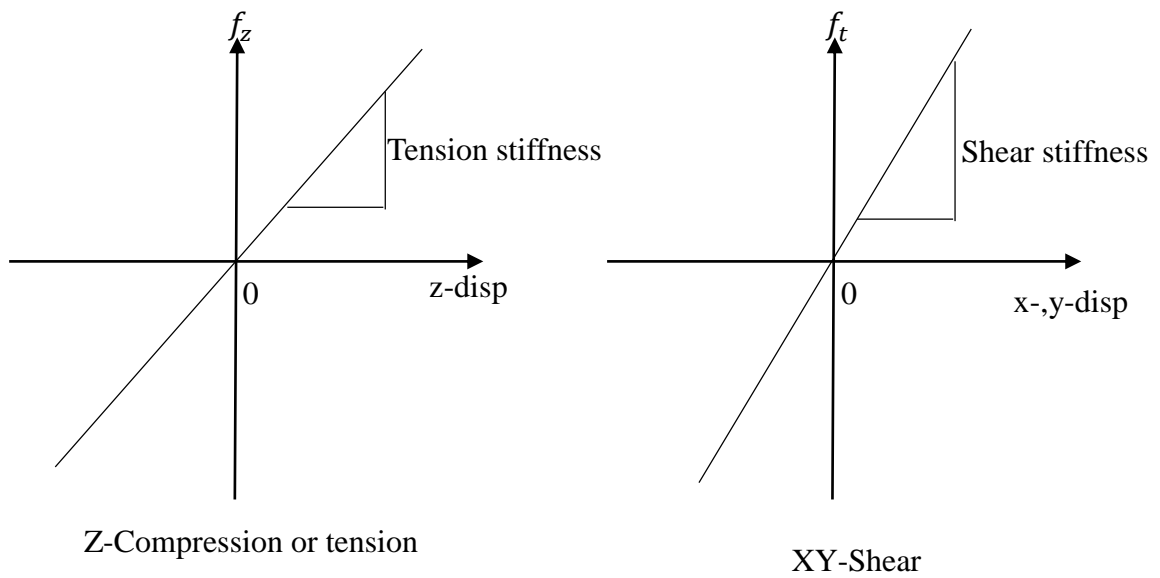
Figure 4-14 Illustration of tension stiffness and shear stiffness

However, the assumption is to some extend somewhat rough that may not cover several points as follow.

1. The relative displacement limit will not exceed the thickness of the contact layer. Hence the contact force would increase sharply asymptotic to infinite in this case. Generally the force vs. relative displacement plot is supposed to be like the figure below.
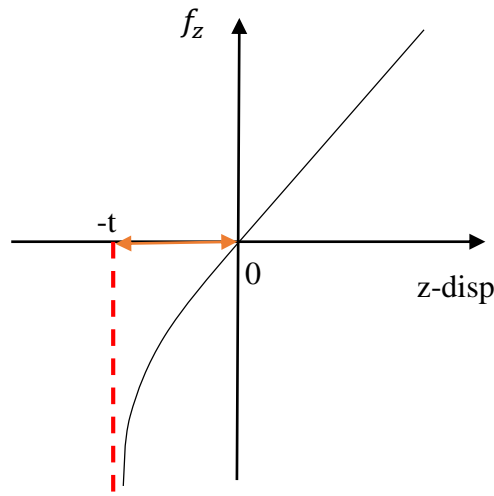
Z-Compression /tension

Figure 4-15 Illustration of tension stiffness considering the relative displacement limit

2. It seems that the coupling effect is not caught, i.e. no direct correlation between the radial compression and the shear force, since each of them takes their own role independently from the other. This will be verified by the results in the case studies later.

Considering the force behavior at large deformation, it seems this pure linear property is not very accurate. Nevertheless, in this thesis it is basically assumed that the relative displacement is small and the pure liner property still applies with sufficient accuracy.

Calculation of material inputs

The compound rubber is set to have typical material properties, as shown in the following table.

Table 4-3 Basic material data of the compound rubber

Elastic modulus (MPa)	Shear modulus (MPa)	Poisson's ratio
26.0	10.0	0.30

The contact layer material properties is defined by Bflex2010 material option CONTACT. This allows users to describe specific material behaviors in different directions, where material types EPCURVE and HYCURVE can be applied. Normally, EPCURVE is used to describe elastoplastic material behavior with kinematic/isotropic hardening, while HYCURVE is used to describe hyper elastic material behavior.

As for the bonded pipe and umbilical, HYCURVE is employed in all directions. Together with the USERDEFINED option, the CONTACT can ensure the shear and compression deformation independent of each other.

Under the assumption of pure linear force-displacement property, the unit force per length is defined by a linear function of the corresponding relative displacement. In the tangent direction where shear deformation occurs, this unit force per length function is,

$$f_t = \tau * b = (G * \frac{b}{t}) * u \qquad (4\text{-}1)$$

While in z direction of the helix tendon, the radial compression force per length is

$$f_z = \sigma * b = (E * \frac{b}{t}) * u \qquad (4\text{-}2)$$

Where τ is the shear strain, b is the contact interface width, G is the shear modulus and E is the elastic modulus of contact layer, u is the relative displacement of the layers in contact, t is the thickness of the contact layer.

Herein the tension stiffness and shear stiffness in the hyper-elastic curve can be defined according the equations above, respectively the value in the brackets, i.e.

Contact element shear stiffness = $(G * \frac{b}{t})$

Contact element tension stiffness = $(E * \frac{b}{t})$

In the later section, the parametric studies will be carried out regarding those stiffness

values.

Looking back at the f_t and f_z equations, the contact interface width b needs to be specified.
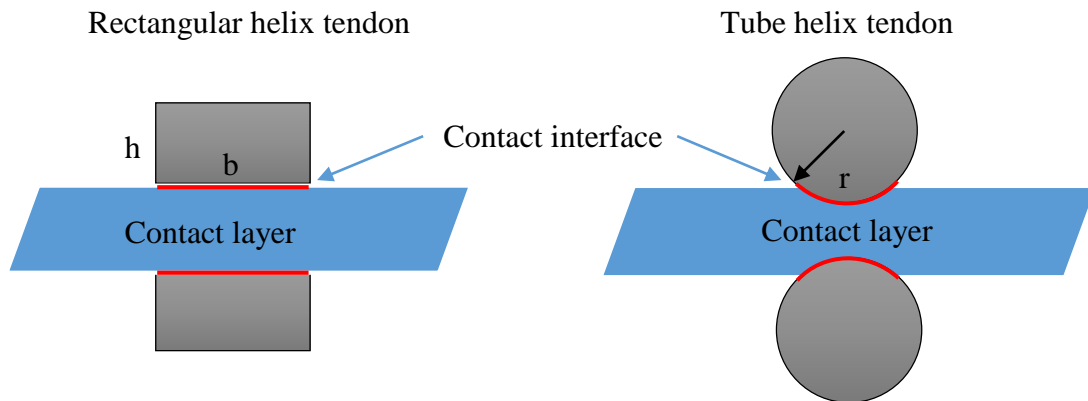
Figure 4-16 Illustration of the contact interface width

As for the rectangular helix tendon, the contact interface width b equals the width of the shear helix tendon. However, there is still no clear definition for the tube shape helix tendon on the width b. In the thesis it is assumed that b equals the radius r of the tendon in case that the tendon is not wrapped by the contact layer material. However, this is a rough estimate, but the uncertainty can be compensated by the parametric study on the contact material to see how much influence it has.
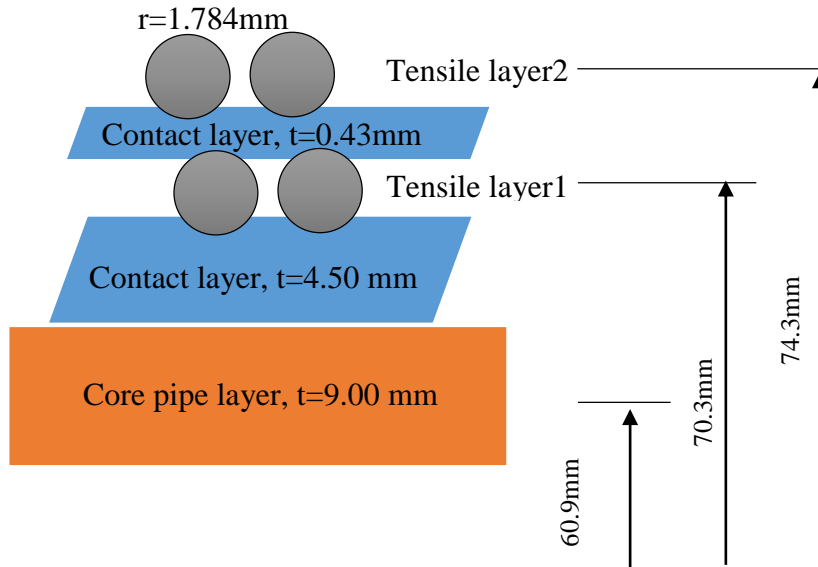
Figure 4-17 Cross section of the bonded flexible pipe model

Based on the assumptions and structure, both stiffness values can be obtained. Detail inputs data could be found in appendix.

4.4.2.4 Simulation set-up

The same structural boundary condition is applied, which could be referred to the non-bonded case. Besides, as for each node of the tensile layer, Loxodromic assumption applies. The loxodromic curve represents the curve that would represent the initial path of each wire on the circular cylinder as if the path was fixed relative to the surface. The transverse relative displacement is restrained, only relative displacement along the longitudinal direction is considered.

The constraint, internal pressure load are the same as the non-bonded case as described previously.

The measurement point still locates at 0.48m to the left end to avoid the possible end effect.

As for the Bflex2010 time control parameters, ALL iteration norms are used, including force, displacement and energy. In addition, the convergence radius is set to be 1E-5. Detailed control parameters could be referred to the appendix.

4.4.3 Analysis of PIPE31 bonded pipe model

The results of PIPE31 model are simply presented, due to its inaccuracy of the core pipe compared with the HSHEAR363 model. More detailed discussion and analysis will be addressed in the second case of the HSHEAR363 model.

The parameter study's description and the effect of internal pressure load are the main issue in this case.

4.4.3.1 Bending stiffness EI

As a whole, the PIPE31 bonded pipe model is directly modified from the non-bonded pipe. The only key change is the material of the contact layers which has no slip behavior. As we can see, concerning the linear moment-curvature property, the bonded pipe resembles the steel pipe to some extent. The curvature vs. moment curve is plotted in the following figure. Other plots, such as curvature history plot, moment history plot, all have linear property. They are not displayed here.

As shown in the figure 4-18, the moment at the measure point increases linearly with the curvature. The lines keeps straight from the origin to the maximum point where the curvature reaches 0.059m^{-1} and moment reaches 0.62 kNm^2.
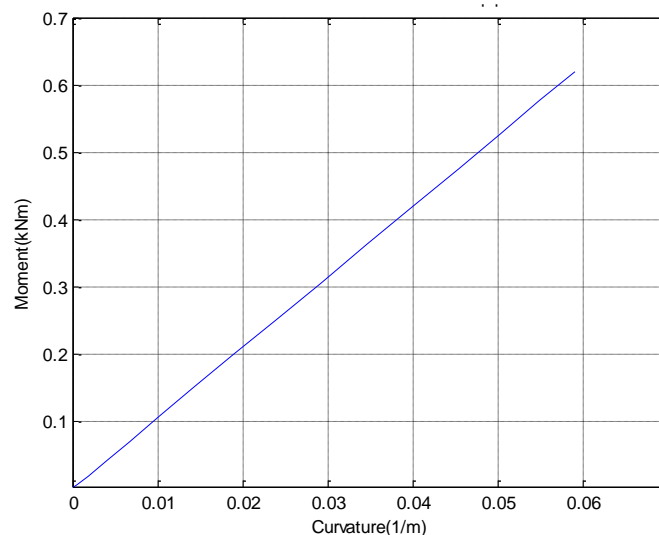
Figure 4-18 Moment-curvature of the PIPE31 bonded flexible pipe model

Since the relationship keeps linear, the bending stiffness can be directly extracted from the slope of straight line. In this case, the bending stiffness EI = 10.56 kNm^2.

Here we can compare the bending stiffness with the results from Pag-o-flex test. They are plotted together in the figure4-19.
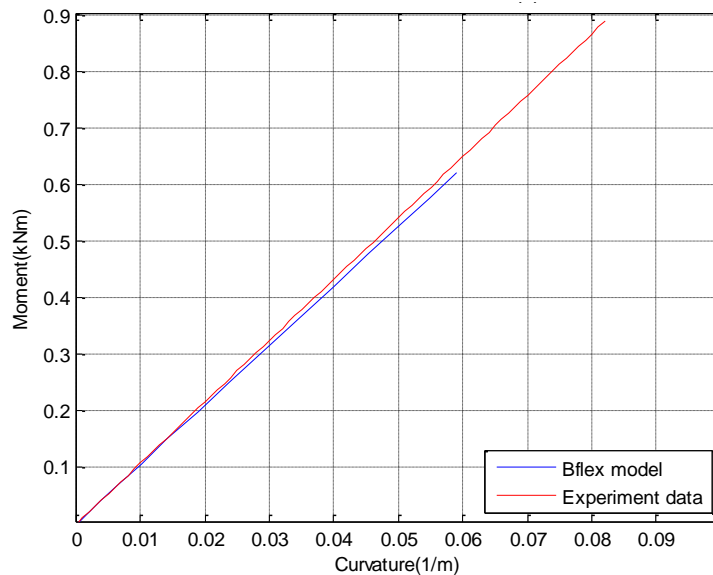
Figure 4-19 Moment-curvature plots of the PIPE31 model and Pag-o-flex sample pipe

The bending stiffness of the Pag-o-flex sample pipe EI =10.85 kNm^2. We can find the small difference between this model and the test sample, but it should be noted that this small difference has no significant meaning and does not indicate that the simplified model fully resembles the test sample pipe.

4.4.3.2 Global deformation

The figures below show similar global deformation of the bonded pipe as the non-bonded pipe.
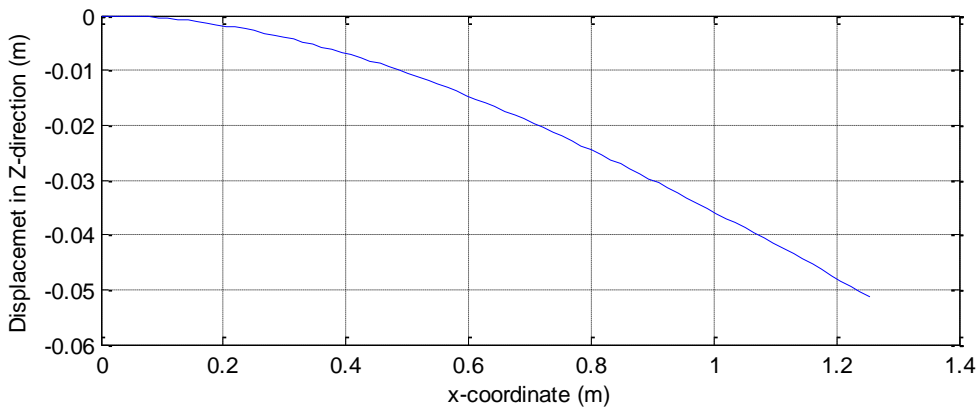
Figure 4-20 Global deflection of the PIPE31 bonded flexible pipe model

But as illustrated by the second figure of the global curvature, the model has a relative smooth transition at the left end, i.e. relative small end effect. Considering the sectional moment decreases linearly from the maximum at the left end to zero at the right end, this curve of global curvature indicates a consistent bending stiffness along the pipe length.
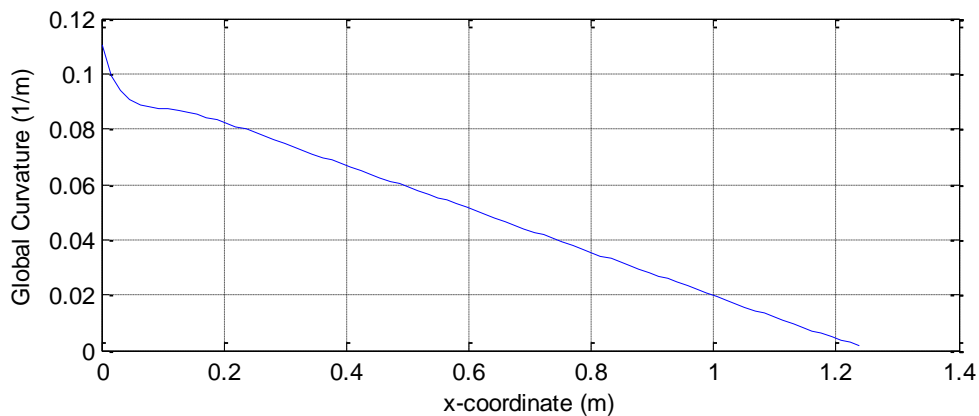
Figure 4-21 Global curvature of the PIPE31 bonded flexible pipe model

This will be compared with the HSHEAR363 model later.

4.4.3.3 Parameter study on the material inputs

Previously we have defined the so called contact element shear stiffness and tension stiffness, which are the slope of the corresponding hyper-elastic curve. This set of stiffness play a significant role in the shear deformation and compression.

Three main cases of parameter study have been implemented:

Case 1:

Multiply both values of stiffness by a factor β. This is based on the assumption of isotropic material property.

$$\text{Contact element shear stiffness} = \beta * (G * \frac{b}{t})$$

$$\text{Contact element tension stiffness} = \beta * (E * \frac{b}{t})$$

Case 2:

Multiply the contact element shear stiffness by a factor β_x but keep the corresponding tension stiffness constant. This is to see how the shear stiffness influences the shear deformation independently, as a reference to the first type.

$$\text{Contact element shear stiffness} = \beta_x * (G * \frac{b}{t})$$

$$\text{Contact element tension stiffness} = (E * \frac{b}{t})$$

Case 3:

Multiply the contact element tension stiffness by a factor β_z but keep the corresponding shear stiffness constant.

$$\text{Contact element shear stiffness} = (G * \frac{b}{t})$$

$$\text{Contact element tension stiffness} = \beta_z * (E * \frac{b}{t})$$

The latter two types of parameter study are not only the references to the first one, but also the basic investigation of the non-linearity of the material.

The typical β, β_x and β_z are tabulated in the following table together with corresponding bending stiffness in different cases.

Table 4-4 Bending stiffness in the parameter study, PIPE31 model, unit: kNm^2

Case no. Factor	case1- β	case 2- β_x	case 3- β_z
0.01	8.57	8.45	9.87
0.1	8.92	8.94	10.01
1	10.56	10.56	10.56
10	18.83	11.61	12.19
100	57.41	11.59	-

Case 1

The results of the first case parameter study is plotted in the figure below. It is seen the bending stiffness EI increases sharply after the factor β exceeds 1. On the opposite side, the bending stiffness decreases asymptotic to 8.5 kNm^2 which means that the only source of bending stiffness comes from the core pipe with no contribution from the tensile layers. This is also can be regarded a loss of contact between the core pipe and the tensile layers.
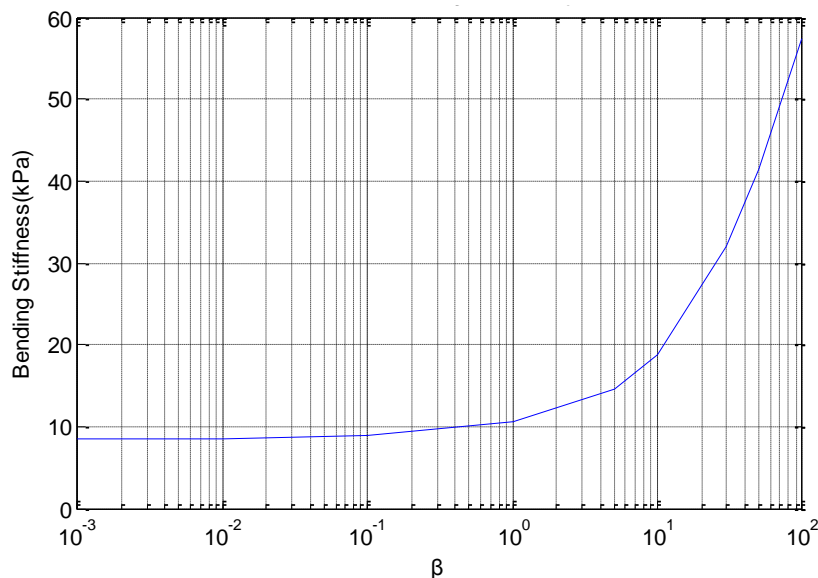
Figure 4-22 Parameter study result of case 1

However it is interesting to see the other two cases. By separately multiplying the stiffness with the corresponding factor β_x and β_z, the bending stiffness in both cases does not increase significantly. This is illustrated in the figure 4-23.

Case 2&3
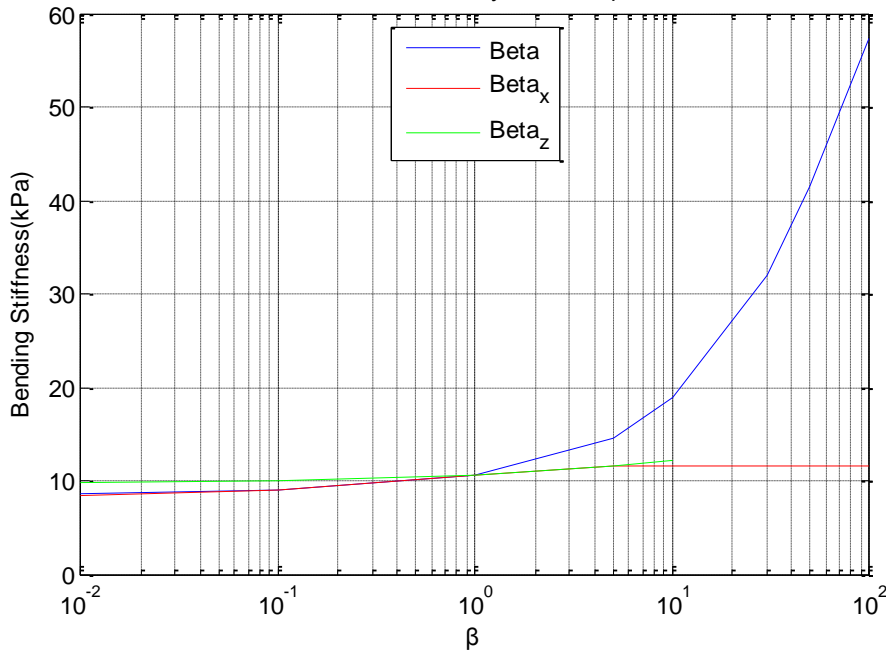
Figure 4-23 Parameter study results of case 1, 2, 3

The red curve indicates the change of bending stiffness when the element shear stiffness is multiplied by factor β_x. It increases along the same path as the type 1 (blue line) when the factor is smaller than 1. Afterwards, it increase a little bit but not significant. The green one corresponds to β_z. The bending stiffness also has a negligible rise.

But β_x and β_z, at least one of them, are supposed to have similar influence on the bending stiffness as case 1. This is compared with the HSHEAR363 model later.

4.4.3.4 Effect of internal pressure load

Have been proved by Pag-o-flex test, the bending stiffness EI increases significantly from 4.94 KNm^2 at 7 bar up to 10.85 KNm^2 at 200 bar.

Contrary to the test results, this bonded pipe model using PIPE31 element as core pipe behaves totally different. The bending stiffness does not increase but decreases a little bit instead. The results are plotted together with the test results below.
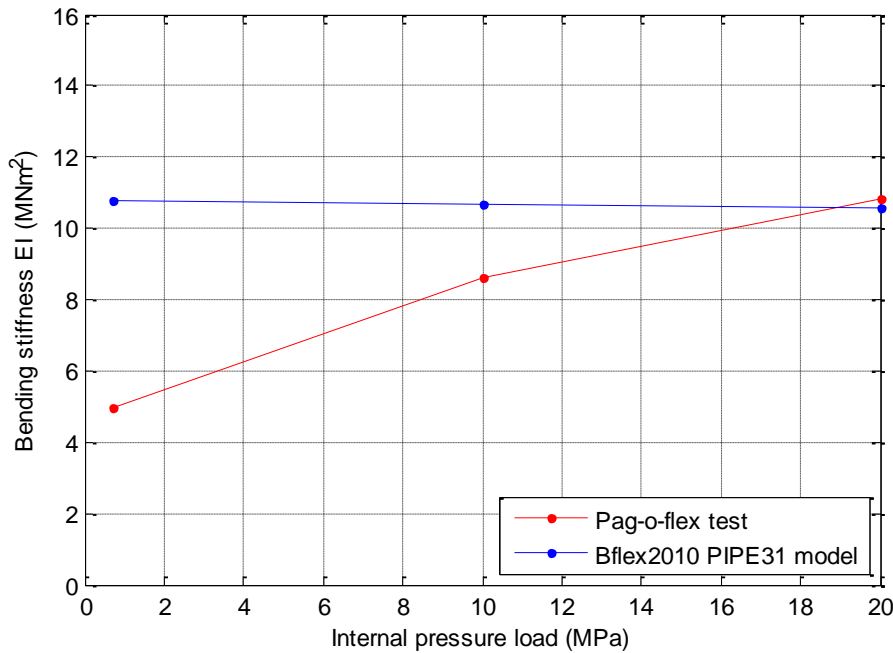
Figure 4-24 Effect of internal pressure on EI, in PIPE31 model

The inappropriate core pipe element may account for this phenomenon, since PIPIE31 is a 3D beam element with consistent axial strain and torsion. Additionally, proved by non-bonded model, PIPE31 element is not able to pick up the radial expansion correctly.

As discussed in previous section, generally for a flexible there are two main reason to ensure large bending stiffness at high internal pressure level. But it seems neither of them work in this model.

Hence, more accurate model using different core pipe element is needed. This is the main work of next analysis, with a new pipe model using HSHEAR363 element to replace the PIPE31.

4.4.4 Analysis of HSHEAR363 bonded pipe model

4.4.4.1 Bending stiffness EI

Same as PIPE31 pipe model, the curvature vs. moment shows pure linearity by a straight line from the origin to its maximum point.
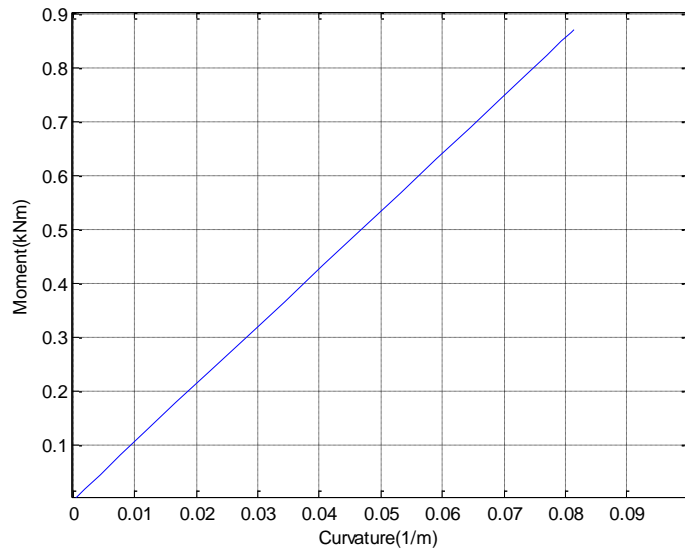
Figure 4-25 Moment-curvature of the HSHEAR363 model

In this case, the bending stiffness is directly extracted from its slope, i.e. 10.72 KNm^2. As discussed already, the bonded components with no slip is the main reason to account for this linearity. The linearity also exists in other plot, such as the moment, curvature and displacement history plots. Those can be referred to the appendix.

4.4.4.2 Global deformation

The global displacement remains similar as the previous model.
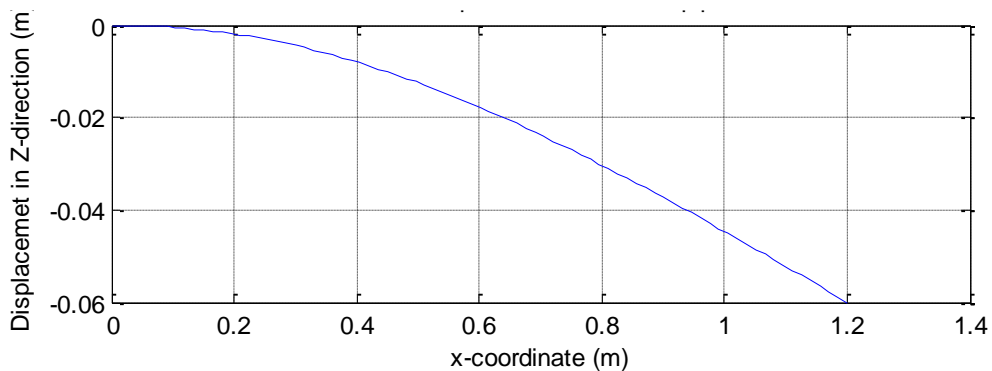
The displacement constraint is applied at the right end, making the sectional moment increases linearly to its maximum at the clamped left end. If assuming consistent bending stiffness along the pipe length, the curvature would also show the same trend like the sectional moment.

However, the end effect is more significant than the previous PIPE31 model. The curvature at the clamped left end is very large but jumps and then recovers sharply between 0 and 0.2 m.

Global curvature of bonded pipe
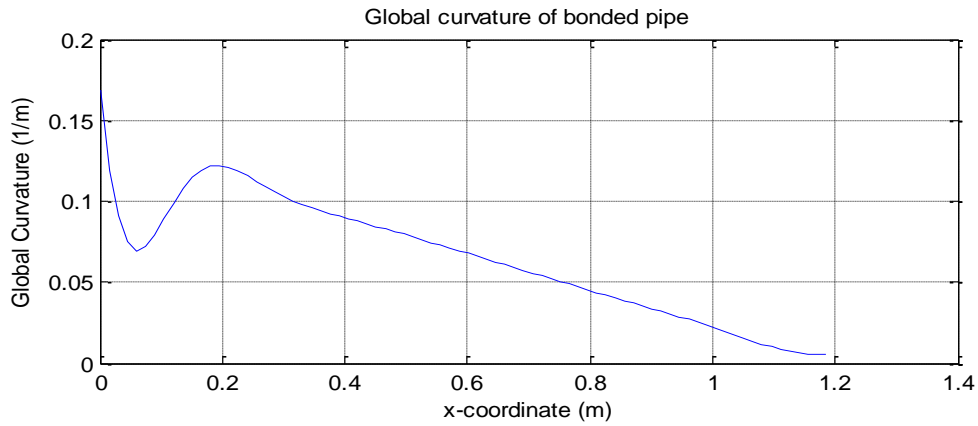
Despite of the significant end effect, the measure point successfully avoids this uncertainty. The curvature decreases smoothly to zero between the 0.4 m to 1.2 m.

4.4.4.3 Parameter study on the material inputs

Same as before, case 1 is to multiply both shear stiffness and tension stiffness of the HYCURE by factor β, while case 2 and 3 are to multiply the shear stiffness by β_x and to multiply the tension stiffness by β_z.

Some typical values of the factors and the corresponding bending stiffness are tabulated in the table as follows.

Table 4-5 Bending stiffness in the parameter study, HSHEAR363 model, unit: kNm^2

Case no. Factor	case1-β	case 2- β_x	case 3- β_z
0.01	6.07	6.10	10.70
0.1	6.65	6.68	10.70
1	10.72	10.72	10.72
10	38.92	38.24	10.89
100	92.07	88.86	10.95

Case 1

In case 1 where homogenous material property is assumed, similar increase occurs when β rises from 1 to 100. The maximum value reach 92.7 KNm^2 at β = 100 level.
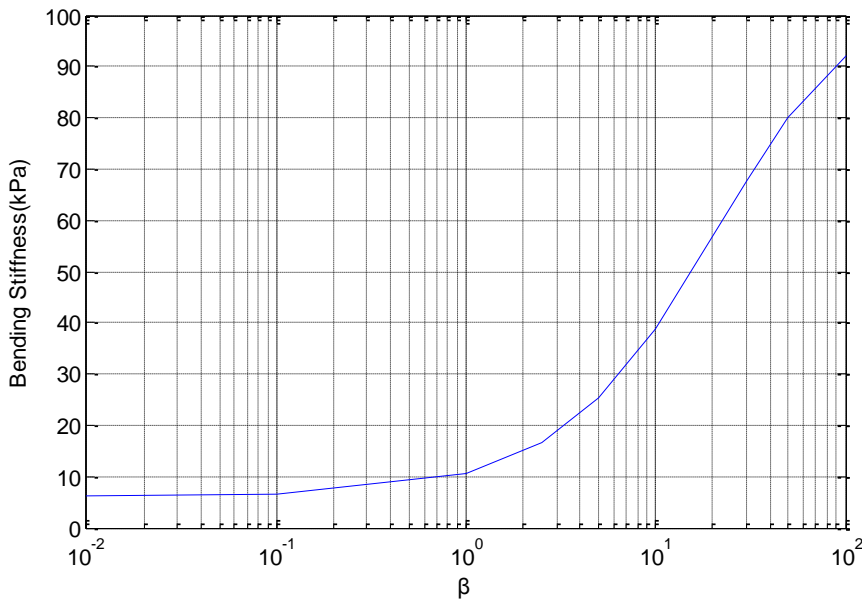
Figure 4-26 Parameter study result of case 1

Problem raises when looking at the opposite side where β is smaller than 1. The bending stiffness EI decreases continuously asymptotic to the value even below the inherent bending stiffness of the core pipe. On the contrary, in the first model, the core pipe bending stiffness is 8.78 kNm^2, and the integrated EI stays around 8.7 kNm^2 when the factor β is very small.

Herein some techniques during the modelling should be mentioned. During the transition from LINEAR in previous model to current ELASTIC option , it is of importance to keep the mechanical properties, e.g. the bending stiffness of the core pipe, consistent between those two models. However, the result turns out that the integrated bending stiffness of the bonded pipe specified by ELASTIC is smaller than the first model of PIPE31. To make the integrated bending stiffness consistent, the elastic modulus is tuned by a factor to make it stiffer. That is why the values of the bending stiffness shown by the curvature-moment plot are similar, both about 10.5 KNm^2.

Comparison between the two models on case 1
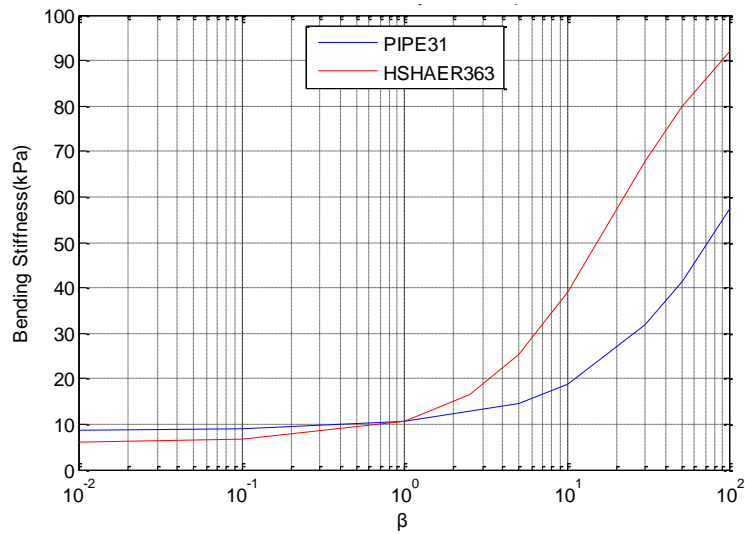
Figure 4-27 Comparison on the results of case 1 in two models

The difference is directly illustrated by the figure 4-27 above. It is seen the HSHEAR363 model has comparative larger bending stiffness than that of PIPE31 pipe model. The difference is insignificant when factor β is lower than 1.

Case 2&3

The results in all the three cases in HSHEAR363 model are plotted together in figure
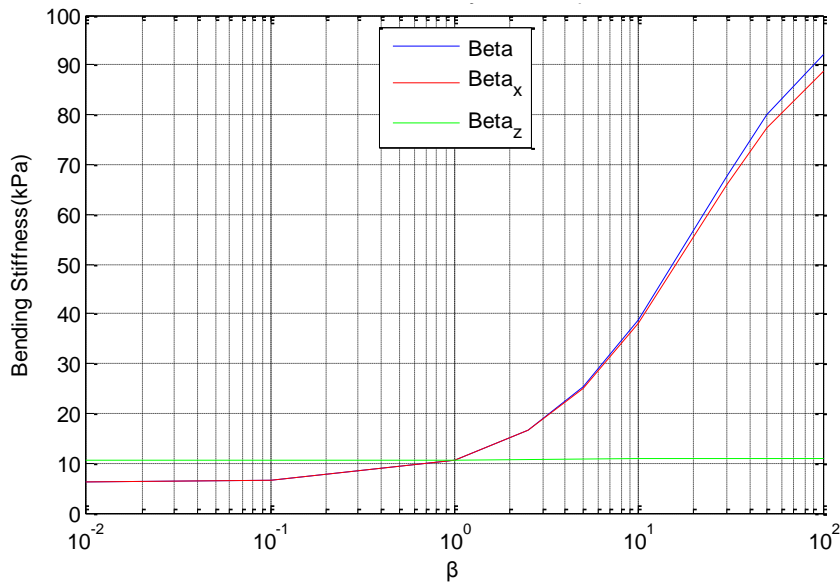
Figure 4-28 Parameter study results of case 1, 2, 3

This is much more meaningful than that of first model, for the separated characteristic influence from different element stiffness, i.e. shear stiffness and compression stiffness.

1. As seen, the bending stiffness of case 2 increases synchronously with case 1, which means the shear stiffness is the dominating factor to affect the bending stiffness, rather than the compression stiffness.

2. The factor β_z has no obvious influence on the bending stiffness, with almost constant EI shown by the green curve.

Therefore it comes to this conclusion that, as for the effect form the contact material, the bending stiffness is dominated by the shear stiffness, with no influence from the radial compression force.

Further on, there is no correlation between the effects from different directions.

4.4.4.4 Effect of internal pressure load

Although new core pipe using HSHEAR363 element is established to pick up the radial expansion, there is no significant change.
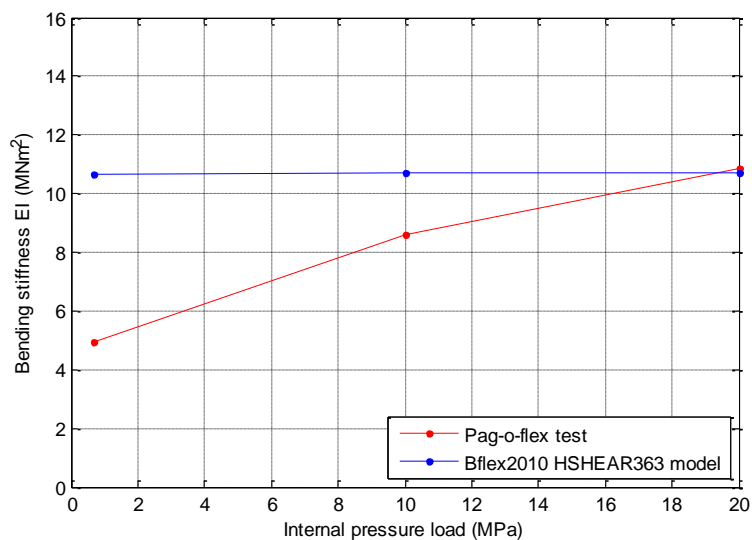
Figure 4-29 Effect of internal pressure on EI, in HSHEAR363 model

When compared with the first model, small difference occurs and the bending stiffness increases a little bit. However, this is still too unobvious.
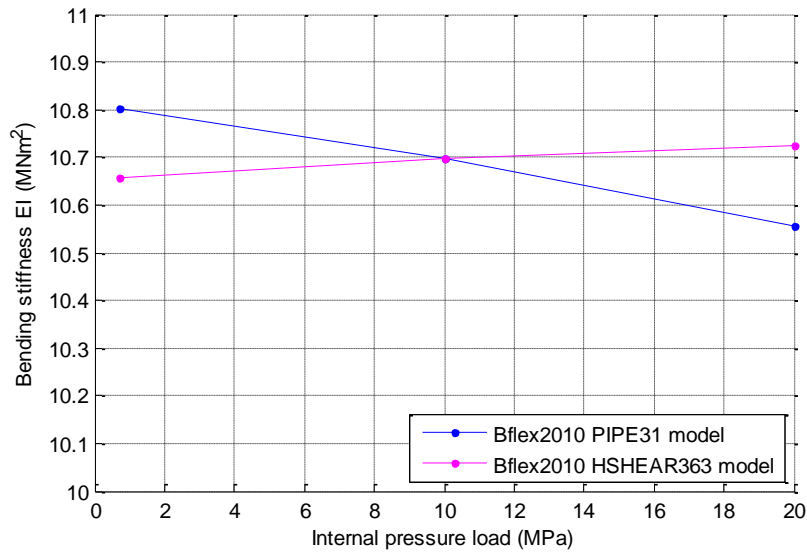
Figure 4-30 Comparison of the effects of internal pressure on EI from two models

But we have now found out the reason from the parameter study on the stiffness factor. Because there is no correlation between the radial compression force and shear force, thus the internal pressure load has no direct effect on the shear stiffness. Finally, the bending stiffness is independent of the internal pressure in the model.

4.5 Possible solutions to simulate the internal pressure load effects

According to the possible reasons described in Section 3.3.2 to account for the increase of bending stiffness, possible solutions are proposed to simulate the effect of the internal pressure load.

1) Set a pressure-dependent shear stiffness

In case of the rise of the internal pressure load, the shear stiffness of contact material can be tuned to some extent to fit proper increase of the elasticity. Therefore a large amount of parameter studies should be carried out to have an insight of material property's effect.

2) Add the curvature-dependent anti-deflection moment M_p into equilibrium iteration

Discussed in section 3.3.2, the anti-deflection moment M_p resists against the ovalization of the pipe cross section during bending. This curvature-dependent moment results in the increase of the bending stiffness.

If the deformation of the core pipe is simulated properly, the resultant force due to internal pressure can be calculated, and then M_p. Since this procedure is time dependent, this procedure should be taken into account in the equilibrium iteration.

5. Umbilical modelling and analysis

5.1   Introduction

This chapter firstly describes the modelling methods of one umbilical, comprising of the simplification methods used, the description of the pipe components, the boundary condition and measurement methods etc.

The results analysis starts from global deformation, with respect to the global deflection, moment and curvature. By simply assuming constant bending stiffness along the pipe, one estimated global curvature is calculated by dividing the moment by this estimated bending stiffness. This is compared with the numerical results.

Later on, the middle section is looked into in detail. The main mechanical property, EI, is illustrated by the curvature-moment curve.

To have an insight of the contact material behavior, the contact element force history and displacement history are plotted. This is studied together with the stick limit and stick stiffness defined by the material inputs.

Since the inputs information on the stick limit and stick stiffness are still uncertain, parametric studies are carried out in the end so as to see the effect of those parameters.

5.2   Modelling methods

5.2.1 Structure specification

The umbilical pipe model has a length of 6.026 m, with inner radius of 81.7 mm and outer radius of 96.7 mm. It has three main layers, i.e. inner tube, tensile armour layer and outer sheath. Then inner layer and outer sheath protect the umbilical from corrosion and make sure of the integrity. The tensile tendon layer consists of 140 tendons, designed with a small layer angle of 12°, making it sufficient to bear large axil load. The fill factor is 0.95.
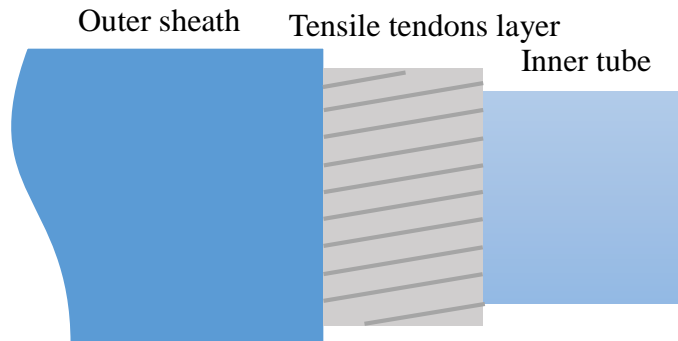
Figure 5-1 Main structural components of umbilical model

To carry out the experimental test, both ends of this umbilical pipe specimen are connected to termination structures. They are made of high strength steel and can be regarded as rigid during the test process. Tension load and constraint are applied on those structures.

The test umbilical model is illustrated in the following figure.
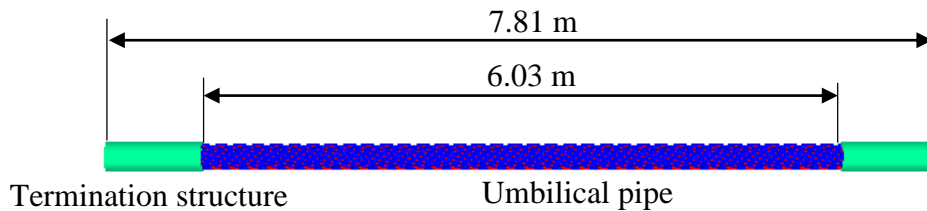
Figure 5-2 Configuration of the umbilical model

5.2.2 Finite element modelling

The main umbilical pipe layers are modelled by application of Bflex2010 shear element, respectively HSHEAR353 for tensile tendons layer, and HSHEAR363 for the inner tube and outer sheath. The finite element model has a quite small mesh size in the longitudinal direction, dividing the umbilical pipe into 154 segments.

Figure 5-3 FE model of the umbilical pipe

Since it is quite time-consuming and complicated to simulate all the 140 tendons, Bflex2010 uses a simplified method to simulate part of them with a scaling factor to estimate the total effect. In this finite element model, 16 tendons are created with a scaling factor 8.75. It should be bear in mind that the scaling factor and mesh size should be always not too large.

The finite element model is illustrated in the figure below, including inner tube and tensile tendon layer. The outer sheath is not shown in the figure.
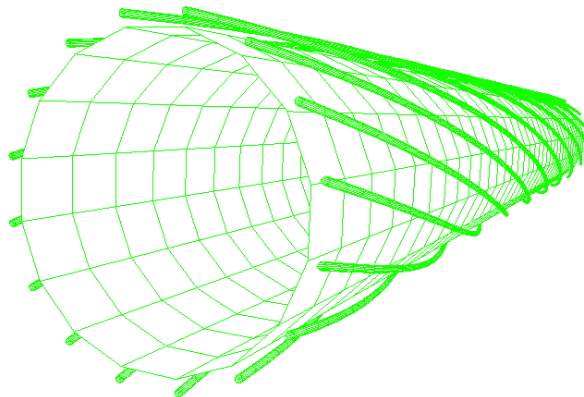
Figure 5-4 FE model of the inner tube and helical tendons of umbilical

5.2.3 Material properties

5.2.3.1 Inner tube and outer sheath

Anti-corrosion material is used for manufacture of inner tube and outer sheath. It demonstrates elastic material behavior, hence ELASTIC material option of Bflex2010 is employed in the FE model, giving a Young's modulus of $8.33E+8$ Nm^{-2} and a Poisson ratio of 0.45.

5.2.3.2 Helix tendon

The helical tendon has a circular cross section, and is simulated by LINEAR material option of Bflex2010, in which all the mechanical material properties are stored, such as axial stiffness, bending stiffness and torsion stiffness, etc. Different from the inner tube and outer sheath, it has a Poisson's ratio of 0.3 and a Young's modulus of 2.07E+11 Nm$^{-2.}$

5.2.3.3 Contact layer

Different from the bonded pipe that uses vulcanized rubber as contact layer, normally the umbilical pipe uses bitumen as the filling material.

As described in Chapter 2 on the material of contact layer, when the solid elements are soaked in a viscoelastic material, such as for steel wires corrosion protected by bitumen, the stress distribution may be governed by shear forces, not friction. Therefore the slip threshold model of the contact layer can be estimated by a shear deformation before slip, and a constant contact force afterwards.

This stick-slip behavior occurs in the x direction, and is independent of the radial compression force on the contact layer, while for the non-bonded pipe, the stick-slip behavior in x direction is dependent of the compression force. Hence in the case of umbilical with bitumen as contact material, USERDEFINED option is employed so as to describe independent behaviors in different directions.

To define the stick-slip behavior, a sloped straight line from the origin describes the linearly increasing shear force in the contact element. Later on, after the force exceed the certain value, i.e. stick limit, the contact force in the x direction does not increase anymore and keeps constant all along. This procedure is demonstrated in the following figure.
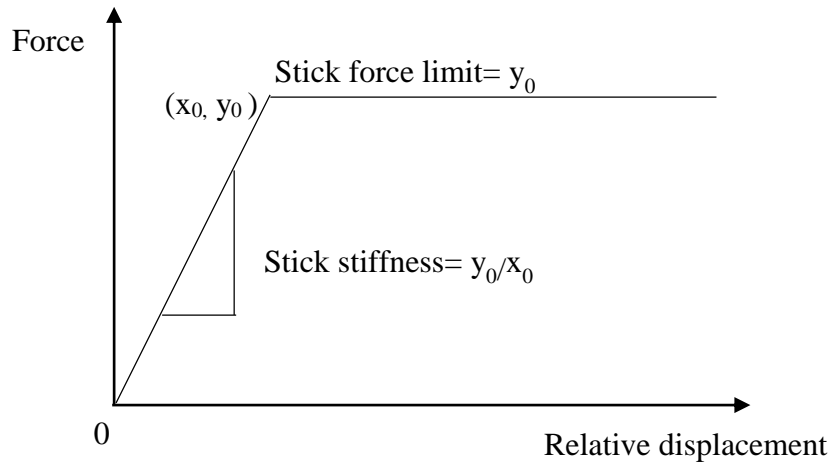
Figure 5-5 Stick-slip model of the bitumen contact material

5.2.4 Boundary condition

The umbilical is simply supported at the steel termination structures at both ends. The left end is constrained in the all direction but is rotational about y axis. The right end is only rotational about y axis and is movable along the x axis.

The relative displacement of tensile layer should also be restricted. It is assumed that the left end section and right end section follow the deformation of the end points, under the assumption of plane surface remaining plane. Loxodromic assumption also applied to the tensile tendons to restrict the relative displacement in local y axis.

5.2.5 Constraint and loads

To study the bending stiffness of the umbilical pipe middle point, both ends are under 45° introverted angle constraint. This is gradually applied from 0° to 45° after the tension load is applied. This angle constraint makes the umbilical turn its direction to 90°.

It is assumed the umbilical is under tension load of 20.0 kN in normal operation. The tension load is applied previously to the angle constraint.
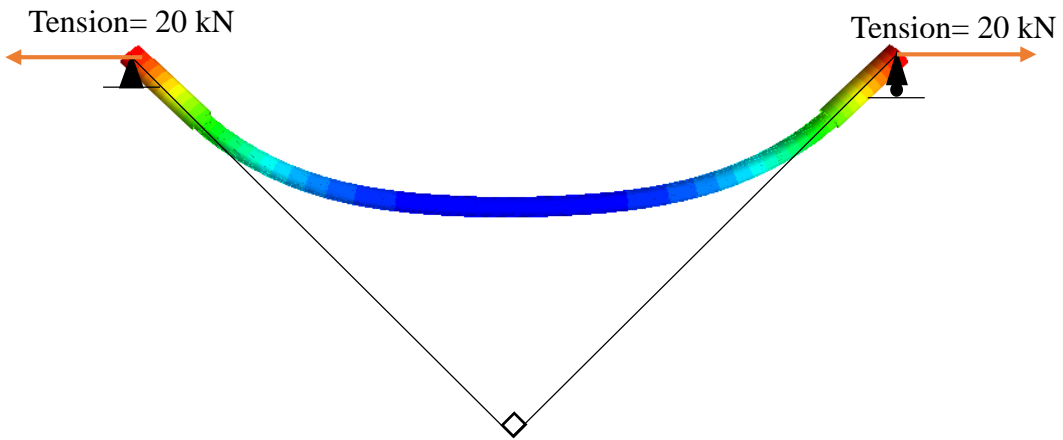
Figure 5-6 Boundary condition and angle constraint of the umbilical

To ensure a fluent transition during the loading history, Bflex2010 provides a RAMPCOS option under THIST_R to describe the load history as a cosine function. The loading history is demonstrated below.
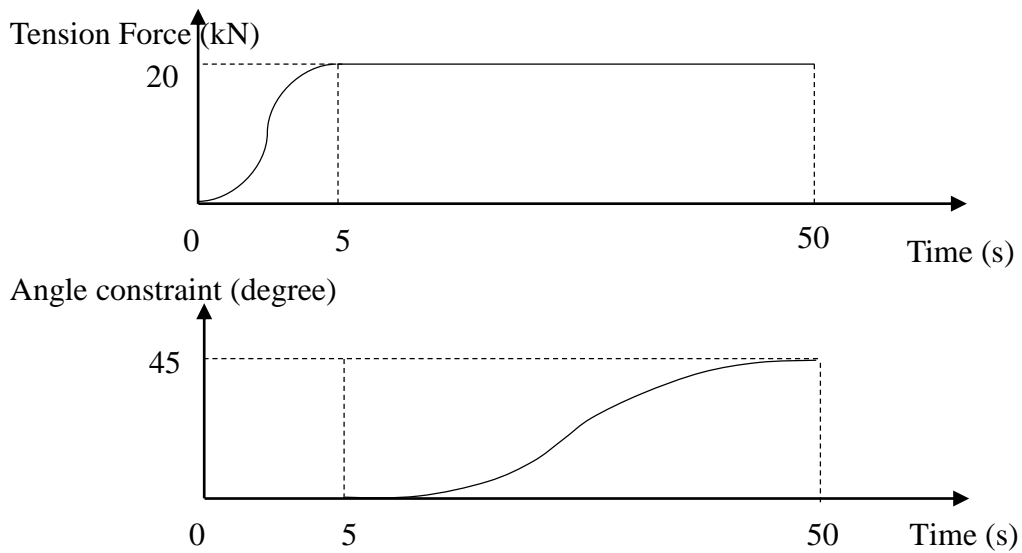
Figure 5-7 Load history of the simulation of umbilical

5.2.6 Measurement method

The relation between the curvature and moment at the middle point is the focus. The

curvature of mid-point could be extracted directly by Bflex2010 using element plot method ELPLOT at the middle element.

According to the small displacement theory, the initial moment are expected to be constant along the pipe length because of the symmetry. But since the pipe has a large deflection under 90 degree angle transition, the secondary moment effect duo to tensile load should be taken into account. The equilibrium is illustrated in the following figure.
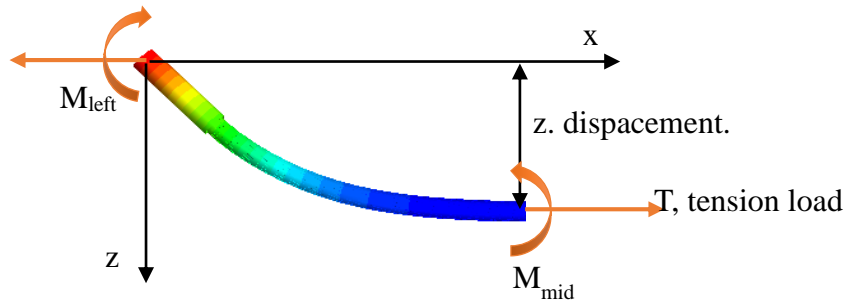
Figure 5-8 Equilibrium of the umbilical at the measurement location

From the equilibrium shown above, the mending moment of the umbilical middle point can be expressed as;

$$M_{mid} = M_{left} - z\,T \qquad (5\text{-}1)$$

Where M_{mid} is the moment at the middle section, M_{left} is moment at the left end, z is the displacement in z direction, T is the tension load at the ends.

The displacement and the moment of left end can be extracted by NOPLOT and NRPLOT respectively in Bflex2010.

5.3   Results analysis

5.3.1 Bending stiffness of umbilical middle section

The bending stiffness of the umbilical pipe is the focus of the analysis and is the priority ahead of others. In current stage, end effect is not considered. In addition it is assumed that the umbilical pipe's length is long enough that the middle part can properly

represent the general mechanical property of the umbilical of this kind.

The following figures respectively present the curvature, displacement and moment of the umbilical middle section while angle constraint gradually increases from 0 to 45 degree.

5.3.1.1 Curvature of middle section

As a whole the curvature increases linearly from the origin till 0.1 m^{-1}. But looking at the start region, it is seen that the umbilical pipe has a relative larger increase speed from 0 to 2.5 degree.
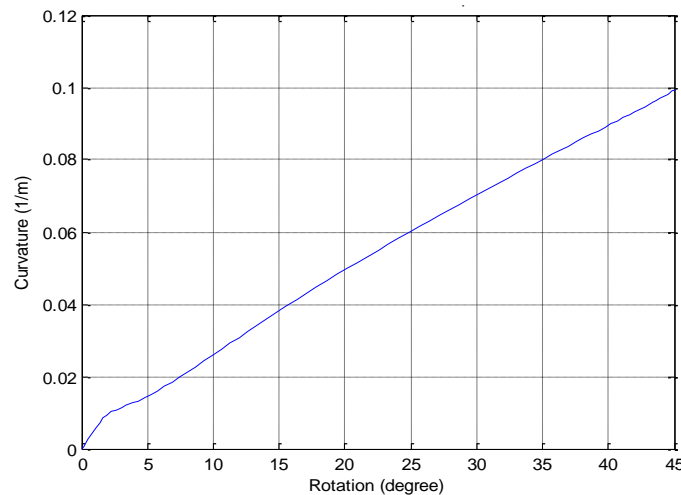
Figure 5-9 Curvature of the umbilical middle section

5.3.1.2 Moment of middle section

Due to the tension load, the umbilical pipe has a secondary moment to counteract the end moment. Section 5.2.6 has proposed the measurement methods and has given the equilibrium equation.

In the following figure 5-10, the moment of middle section is plotted together with the left end moment.
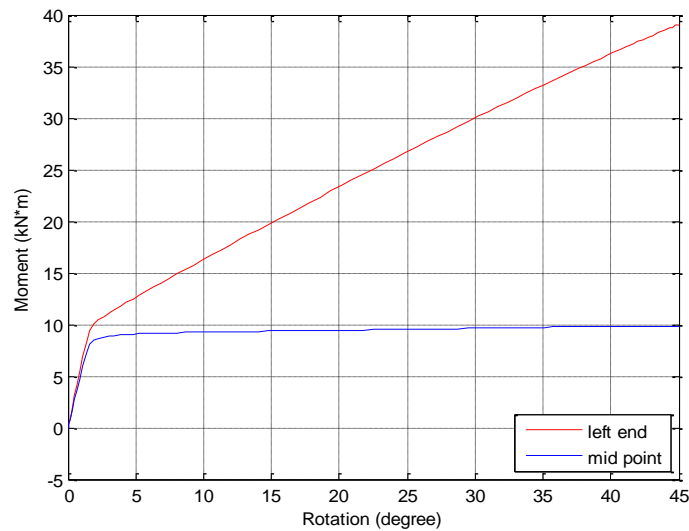
Figure 5-10 Moment history at the let end and middle section of umbilical

It is seen that both moments at the two locations increase sharply in the beginning of the angle constraint from 0 to around 2 s, but have significant changes afterwards. While the end moment increase gradually from 10.0 kNm to 39.4 kNm, the moment of the middle section almost keeps constant. This constant moment of middle section may be related to the constant contact force after slip occurs.

5.3.1.3 Curvature vs. moment of middle section

The curvature and moment of middle section are together plotted by setting the curvature as the x coordinate and moment of middle section as y coordinate, shown in figure 5-11.
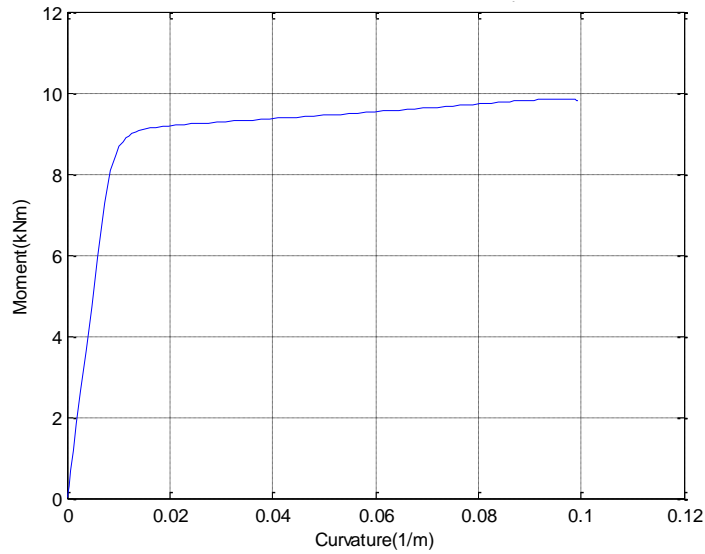
Figure 5-11 Moment-curvature of umbilical middle section

Viewing from the moment-curvature plot, the initial bending stiffness is extremely large and experiences a significant drop when the curvature exceeds 0.06m^{-1}. It decreases to small and nearly constant value after the transition.

The secant stiffness is calculated at the end of loading. By dividing the moment with the curvature, the secant bending stiffness at the final stage is 98.2 kNm^2.

Figure 5-12 shows the tangential bending stiffness at the middle section.
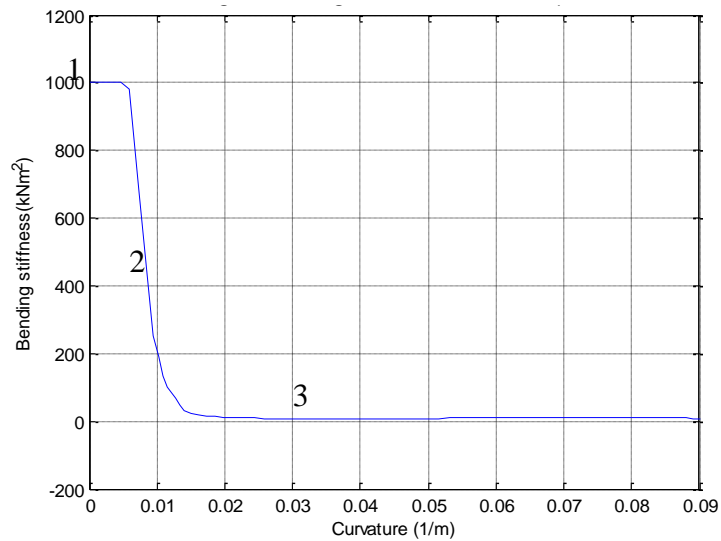
Figure 5-12 Tangential bending stiffness history, divided into three phases

The history of the tangential bending stiffness can be divided into three parts according to the main characteristics. The detailed data of the bending stiffness by time step is tabulated in the appendix. The following table 5-1 contains the main data, categorized into three main phases.

Table 5-1 Data of the bending stiffness at umbilical middle section

Phase	Curvature (m^{-1})	Bending Stiffness(kNm^2)	Average(kNm^2)
1	1.18E-03	1000.75	1000.78
	…	…	
	4.71E-03	1000.81	
2	5.96E-03	980.43	191.8
	7.31E-03	675.9	
	…	…	
	1.86E-02	12.89	
	1.99E-02	10.96	
3	2.13E-02	9.99	9.02
	2.28E-02	9.54	
	2.43E-02	8.8	
	8.71E-02	9.09	
	8.81E-02	8.84	
	8.90E-02	8.59	
	...	…	

During phase 1, the tangential bending stiffness keeps constant about 1000.0 kNm^2 at curvature from 0 m^{-1} to 0.0055 m^{-1}. In phase 2, it jumps sharply from 1000 kNm^2 to small order of magnitude. In phase 3, the bending stiffness keeps almost constant about 9.02 kNm^2

The sharp decrease of the umbilical bending stiffness is accounted for by the stick-slip behavior of the contact layer. The maximum stress point around the middle section is found to be at the contact element no.71217. By using Xpost, the contact force history and displacement history can be extracted at this location. It is seen that at 13 s, the contact force reaches the stick force limit, while the relative displacement continually increases after exceeding the stick displacement limit, i.e. 0.0001 m.
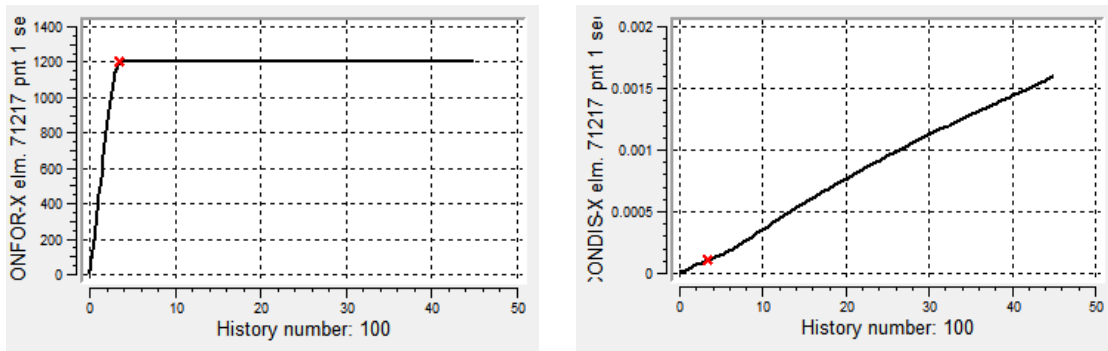
| (a) Contact force -x | (b) Relative displacement -x |

Figure 5-13 Contact force and relative displacement in local x direction

5.3.2 Global analysis

The Global analysis main focuses on the global deformation of the umbilical, including the deflection, moment and curvature.

5.3.2.1 Global deflection

Under symmetric angle constraint at both ends, the umbilical pipe deflects mainly in the z direction. The displacement in z direction is illustrated .in Figure 5-14.
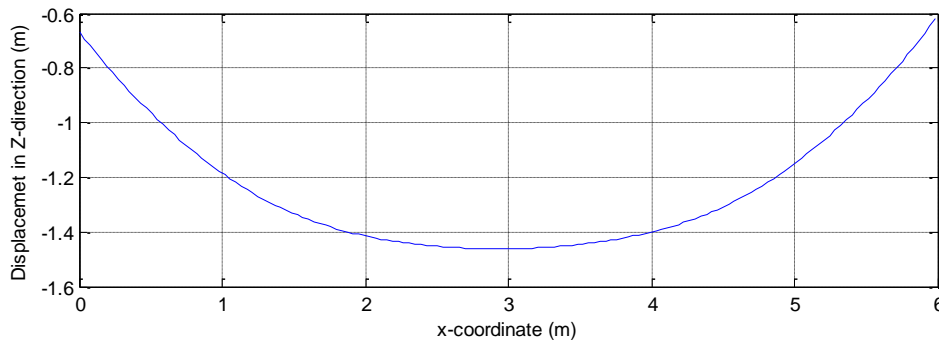
Figure 5-14 Global displacement in z-direction

The global displacement along the x direction is not covered in this thesis.

5.3.2.2 Global moment

Like the calculation of the moment of middle section, it is the same method to get each sectional moment by subtracting the sectional secondary moment from the end moment. Therefore the result has the same shape like global displacement in z direction. It is illustrated in the figure 5-15.
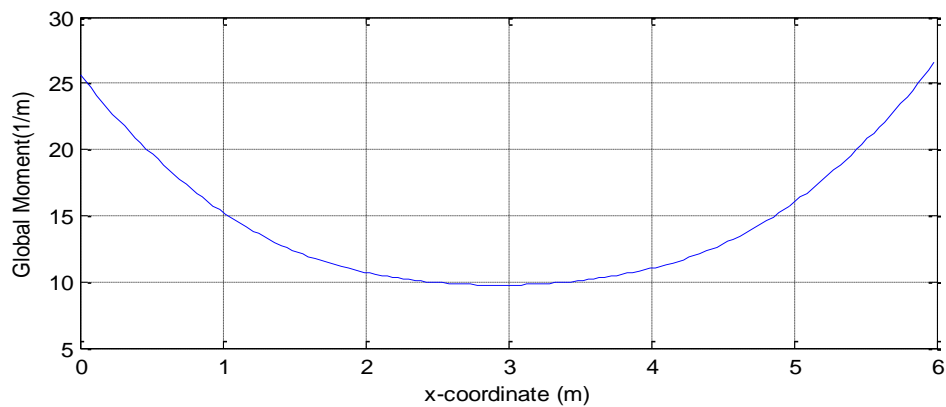
Figure 5-15 Global moment of umbilical

5.3.2.3 Global curvature

The global curvature is directly extracted at pipe element by ELPLOT option.

In practical operations, the umbilical pipes have nearly consistent global curvature under bending condition. But this is only in the case pipes are long enough so that the end effects nearby the termination structures can be ignored.

In this case, the umbilical has a length of 6 m. The curvature has a fluent transition along the umbilical pipe but the end effect is significant which is nearly 6 times of the curvature at the middle section.
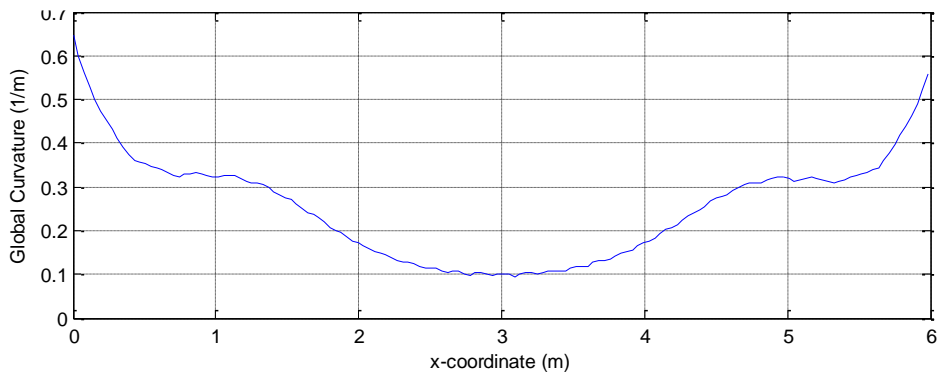
Figure 5-16 Global curvature from numerical result

By roughly assuming consistent bending stiffness along the pipe length, we can have an estimated global curvature. This EI_s is simply the secant bending stiffness extracted from Figure 5-11 at the final loading. Herein the estimated consistent bending stiffness is set to be $EI_{estimate}$ =100 kNm^2. The estimated bending stiffness is plotted together with the numerical result.
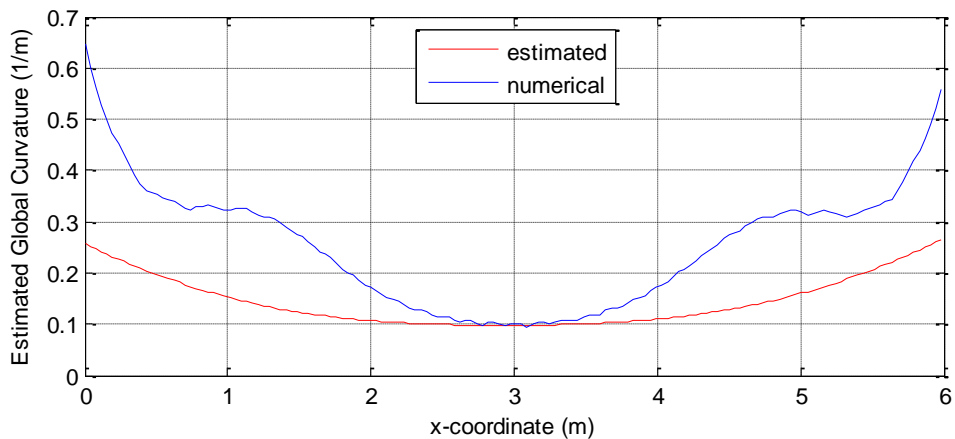
Figure 5-17 Global curvature from numerical result and estimation

It is seen the curvature around the end region increase sharply than the estimated results. Contrary to the assumption of consistent bending stiffness, it means that the bending stiffness decreases at the umbilical ends.

History plot of global curvature around the EI transition region

It is of interest to see how the global curvature changes during the loading, especially at the transition region where bending stiffness decreases significantly. Herein three history points are selected separately within the three main phases.
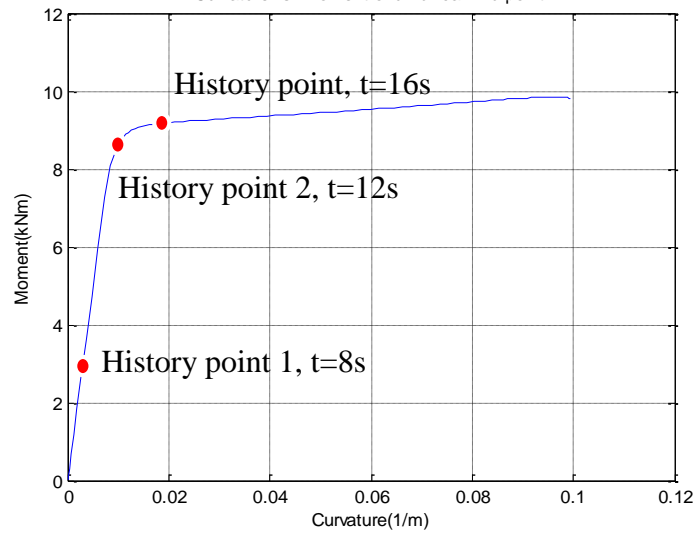
Figure 5-18 Selection of history points on the moment-curvature curve
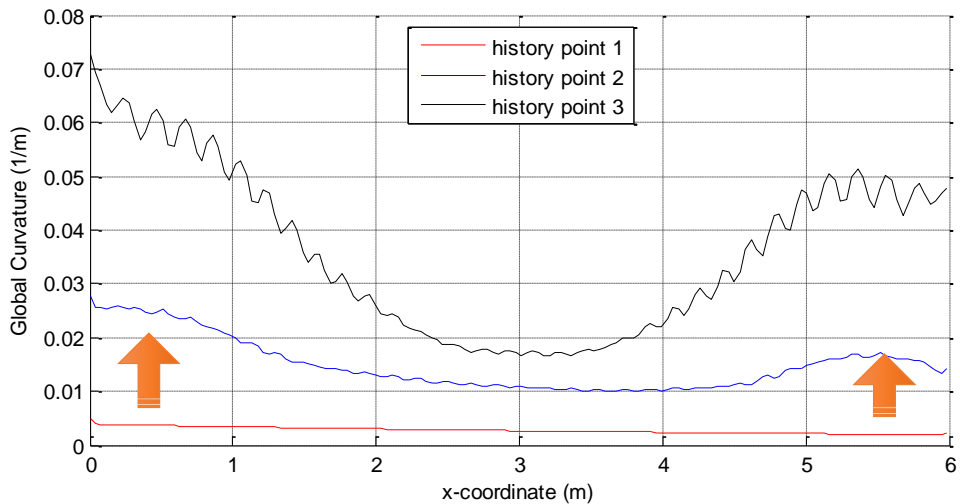
Figure 5-19 History plot of the global curvature

At history point 1, the global curvature keeps almost consistent along the umbilical pipe. In this stage, it is proved that the contact force of the contact layer is well below the stick-slip threshold.

Obviously seen from the above, the bending stiffness rises significantly at the both end regions from history point 1 to 2, exceeding the value at the middle section of the umbilical pipe. Later on the bending stiffness of the whole pipe increases linearly to history 3.

5.3.3 Stress Analysis

In this section, focus is the stresses of the middle section. End region is also studied where extreme stresses locate. Besides, stresses are separately analyzed in the different components of umbilical pipe.

End region   Middle Section
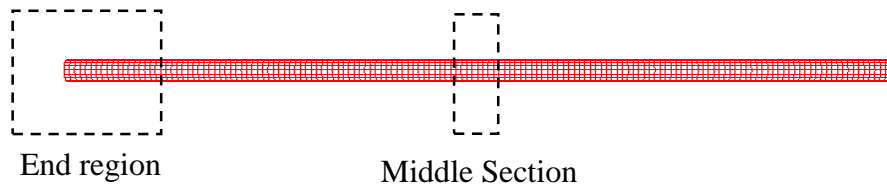
Figure 5-20 The illustration of the end region and middle section

5.3.3.1 Inner tube and outer sheath

The stress distribution of the inner pipe and outer sheath is directly affected by the radial compressive forces from the tensile layer and the influence of the termination structures. The overall distribution of the longitudinal stress σ_{xx} is illustrated in the figure below.
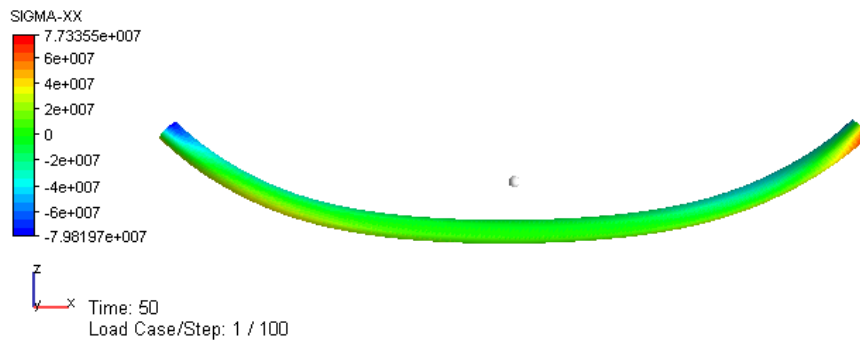
Figure 5-21 Global distribution of the longitudinal stress σ_{xx}

The maximum longitudinal stress locates at the both ends of the inner tube and outer sheath. The result from Xpost shows the maximum is 77.34 MPa
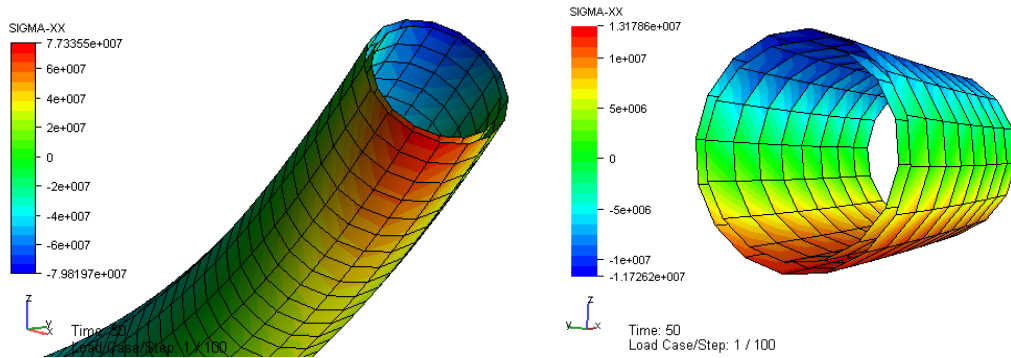
Figure 5-22 Longitudinal stress σ_{xx} at the end region and middle section, inner tube and outer sheath

The middle section has a relatively small longitudinal stress, with maximum about 13.18 MPa at the lower part. The stress distribution is smooth along the length.

5.3.3.2 Tensile layer

The tensile layer has the similar stress distribution but with one bigger order of magnitude.
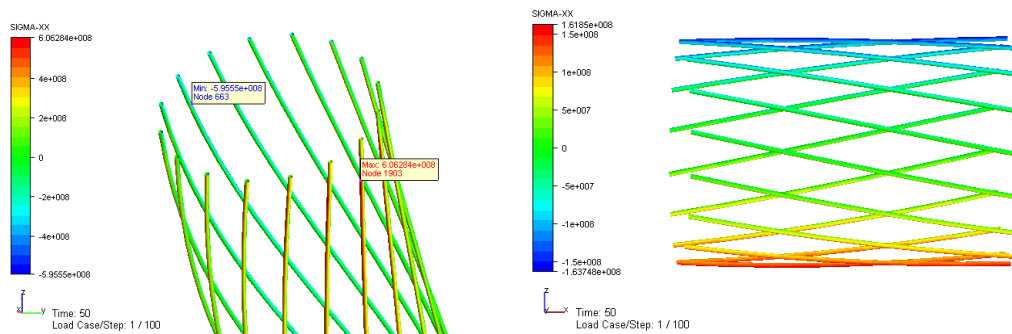
Figure 5-23 Longitudinal stress σ_{xx} at the end region and middle section, tensile layer

The maximum longitudinal stress σ_{xx} at the middle section is 161.85 MPa when it is at the curvature of about 0.01 m^{-1}.

This longitudinal stress σ_{xx} is the total resultant of the several different kinds of stresses, including the axial stress, longitudinal stress due to bending about axis. The next figures show the distributions of stresses of different kinds.

Seen from the plot of the axial stress, the tendons at the bottom of the umbilical pipe has the positive maximum stress while at the opposite side the stress is at the negative

maximum.
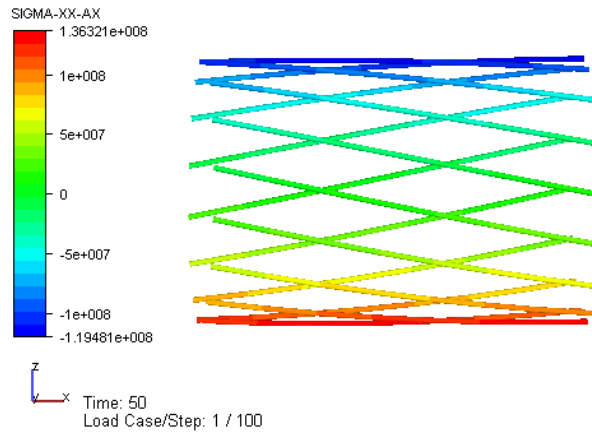
Figure 5-24 Axial stress on the tendons at the middle section

The longitudinal stresses due to bending about local y axis and local z axis have different stress distributions. They are illustrated in the figure 5-25.
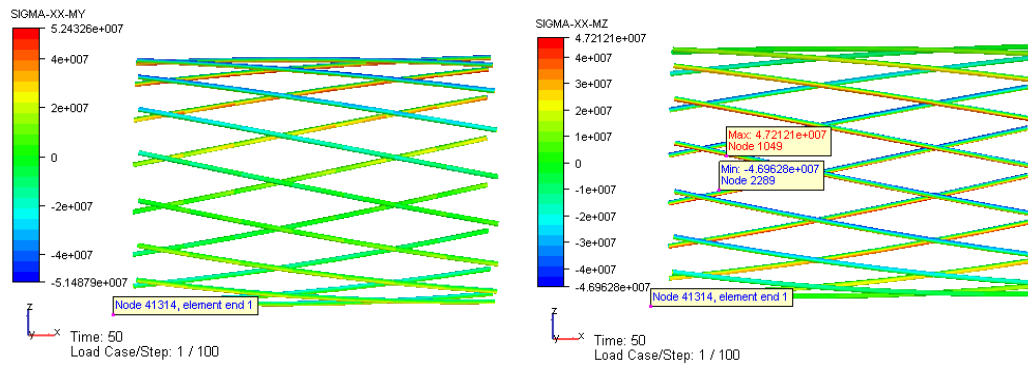
Figure 5-25 Distribution of longitudinal stresses due to bending, middle section

5.3.3.3 Contact layer

When the umbilical pipe deforms, there is tendency that the tendons slides between the inner tube and outer sheath. The contact material prevents the tendons from sliding by providing opposite shear force in opposite direction. But due to the existence of stick limit, when the contact force reaches the limit, the resistance force does not grow and the tendons will slip between the structures in contact.
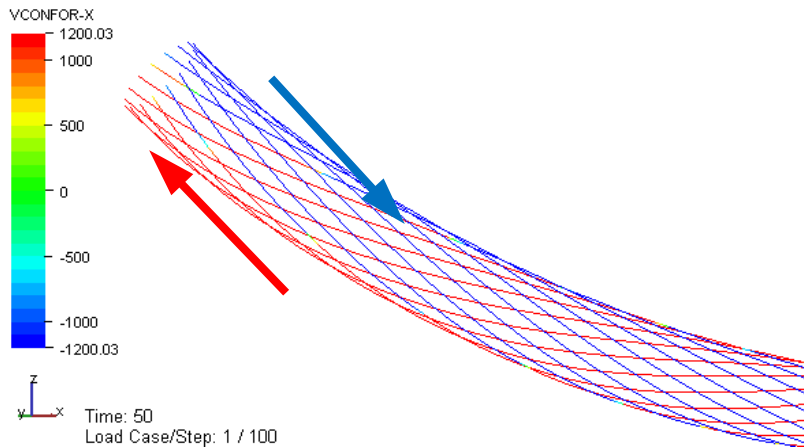
Figure 5-26 Distribution of the contact force in local x direction

After reaching the limit, the force does not grow but the relative displacement continuously increases. From the result, the displacement even reaches about 0.02 m around the end region. The middle section has a moderate smaller relative displacement compared with that at the end region.
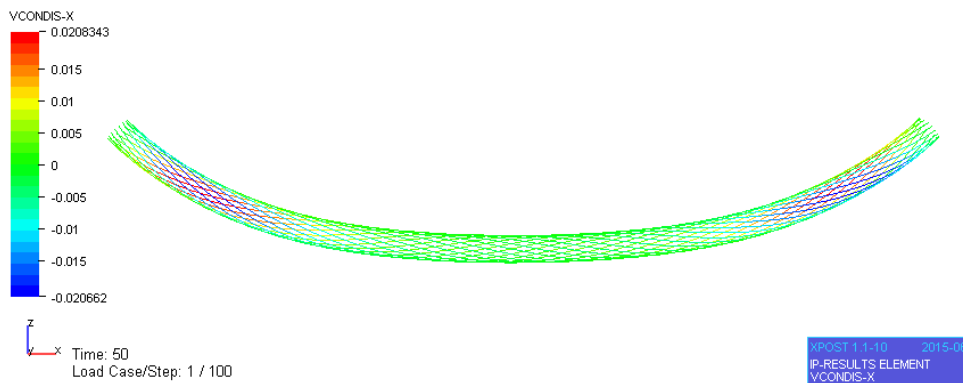
Figure 5-27 Distribution of the relative displacement in local x direction

History data of contact force and relative displacement at left end and middle section

The contact force and relative displacement at different locations are extracted from the numerical results at the representative history points around the transition region.

Table 5-2 History data of contact force and relative displacement on the contact layer

	End region		Middle section	
Time (s)	max contact force(Nm^{-1})	max relative displacement (e-5 m)	max contact force(Nm^{-1})	max relative displacement (e-5 m)
8.0	478.81	3.99	434.88	3.62
9.5	1072.45	8.94	973.94	8.11
10.0	1200	11.99	1193.58	9.95
12.0	1200	68.34	1200	19.86
16.0	1200	237.22	1200	43.11
50.0	1200	2066.20	1200	353.34

It shows that the contact force and the end region reaches the stick limit earlier than the middle section. After slip behavior occurs, the relative displacement at the end region increases much faster than that at the middle section. Finally the relative displacement reaches 3.35 mm, while it reaches about 20.66 mm at the part close to the ends.

5.3.4 Parameter study

The stick limit and the stiffness of the stick part have been defined in the previous section by setting the turning point (x_0, y_0). Stick force is directly y_0, meaning that after reaching this force limit, the contact force would not increase, while the relative displacement goes on growing. The shear stiffness is defined by y_0/x_0.

5.3.4.1 Parameter study on the shear stiffness

In this parametric study on the shear stiffness of the stick part, the stiffness is changed by defining stepped x_0, while the stick limit is kept constant equal to 1200 Nm^{-1}. This is demonstrated by the figure below.
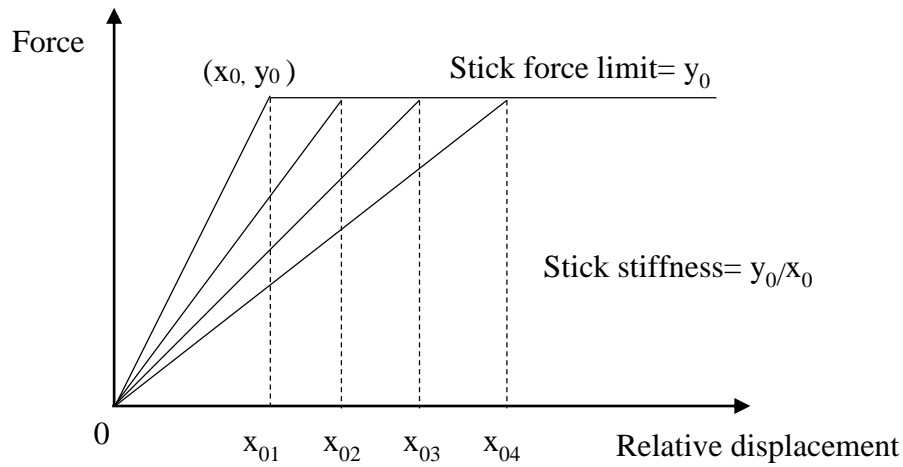
Figure 5-28 Threshold model of shear stiffness in the parameter study

7 pairs of (x_0, y_0) are defined, keeping the stick limit constant at 1.20E3 but giving series of stick stiffness values ranging from 4.00E+05 Nm^{-2} to 2.40E+07 Nm^{-2}. The detailed parametric study material inputs are tabulated in the table below.

Table 5-3 Parameter study on the shear stiffness, keeping stress slip limit constant

Case no.	$x_0(m)$	$y_0(Nm^{-1})$	Shear stiffness(Nm^{-2})
1	5.00E-05		2.40E+07
2	1.00E-04		1.20E+07
3	2.00E-04		6.00E+06
4	5.00E-04	1.20E+03	2.40E+06
5	1.00E-03		1.20E+06
6	2.00E-03		6.00E+05
7	3.00E-03		4.00E+05

The result of the parameter study is shown in figure

Phase 1 corresponds to the full stick behavior of the umbilical. With the increase of the shear stiffness, the initial bending stiffness rises significantly. In the meanwhile, the duration of phase 1 decreases sharply.

Phase 2 is the transition between full stick region and full slip region. When the stiffness of stick part decreases, the change ratio slows down and the transition duration becomes

long. This is demonstrated by the tangential bending stiffness plot.

However, after the stick limit is reached and the contact becomes full slip, the tangential bending stiffness becomes consistent in all the cases, average about 10 kNm^2. Since the contact forces are same during phase 3 in all the cases, the only source of the tangential bending stiffness comes from the inner tube, outer sheath and geometry deformation of the tensile layer.
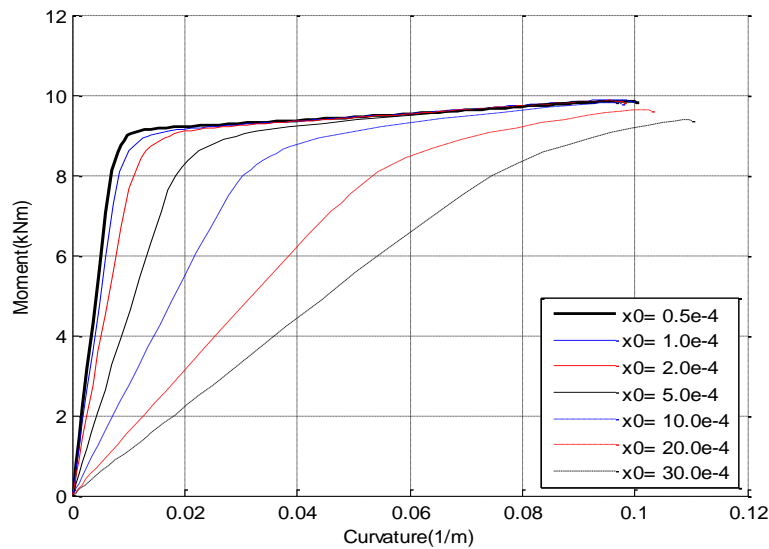
Figure 5-29 Moment-curvature result in parameter study on the shear stiffness
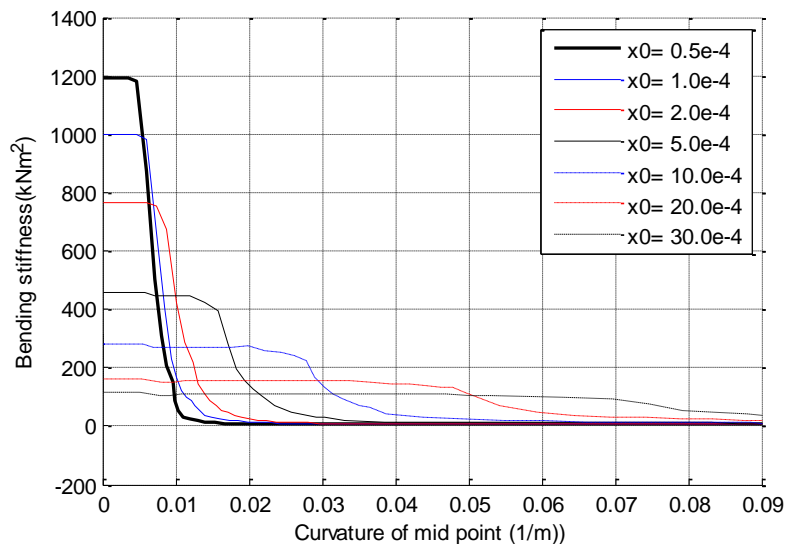
Figure 5-30 Tangential EI in parameter study on the shear stiffness

The values of initial bending stiffness are extracted with respect to shear stiffness. This

is shown in figure 5-31.
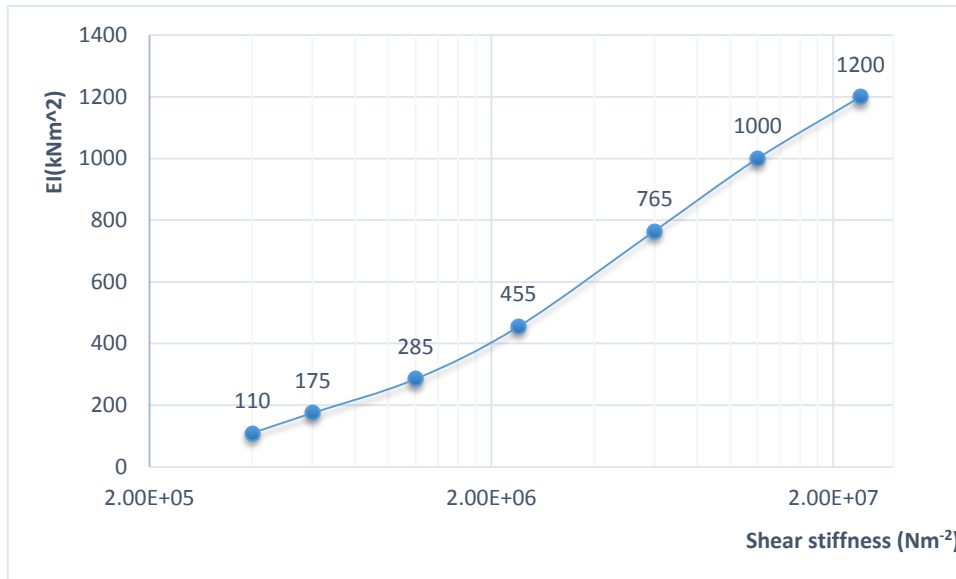
Figure 5-31 Initial EI in parameter study on the shear stiffness

As shown in figure 5-31, the initial bending stiffness increases sharply when the shear stiffness is small. It is because the force distribution is transferred to all the layers.

The increase speed slows down when the shear stiffness is extremely large. In this case, the relative displacement between the layers becomes difficult.

5.3.4.2 Parameter study on the stick stress limit

In this parametric study on the stick force limit, the stick limit is changed by defining stepped points (x_0, y_0) along the same sloped line, i.e. keeping the stiffness consistent in all cases.
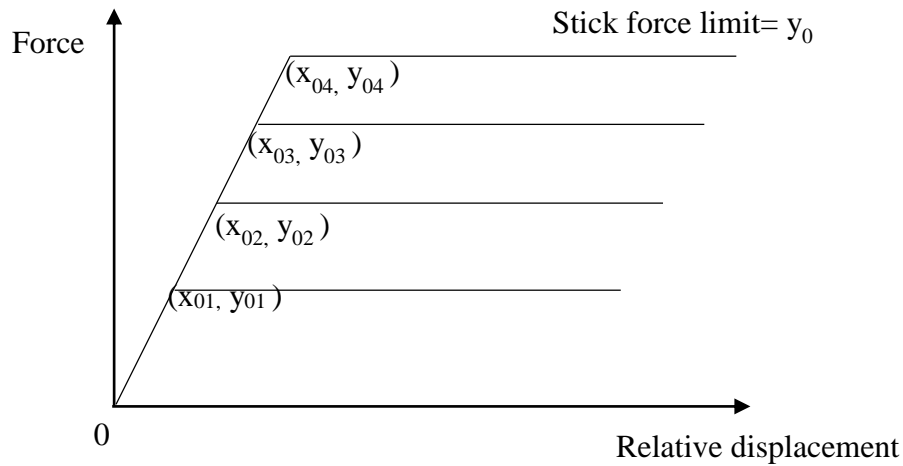
Figure 5-32 Threshold model of stick limit in the parameter study

6 pairs of (x_0, y_0) are defined, keeping the stick stiffness consistent at 1.20E7 Nm^{-2} but giving series of stick limit values ranging from 5.00E+02 Nm^{-1} to 5.00E+03 Nm-1. The detailed material inputs are tabulated in the table below.

Table 5-4 Parameter study on the stick limit, keeping shear stiffness constant

Case no.	x_0(m)	y_0(Nm^{-1})	Shear stiffness(Nm^{-2})
1	4.167E-05	5.00E+02	
2	8.333E-05	1.00E+03	
3	1.667E-04	2.00E+03	1.20E+07
4	2.500E-04	3.00E+03	
5	3.333E-04	4.00E+03	
6	4.167E-04	5.00E+03	

Seen from the following figures, with the increase of stick limit, the duration of phase 1 increases. The initial bending stiffness keeps consistent in all cases. The transition duration from full-stick to full-slip becomes long and smooth.

Same as the first parametric study on the stick stiffness, the final tangential stiffness in phase 3 approaches to be consistent about 10 kNm^2 in all cases at different limit levels.
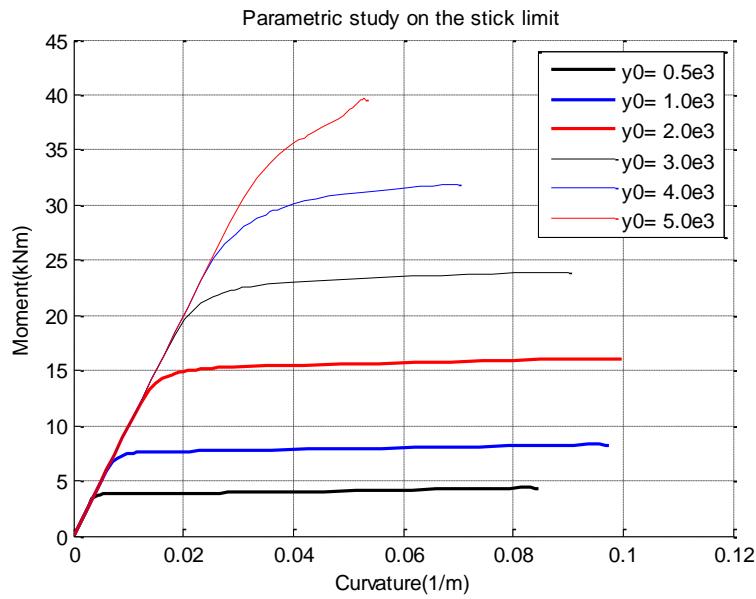
Figure 5-33 Moment-curvature result in parameter study on the stick limit
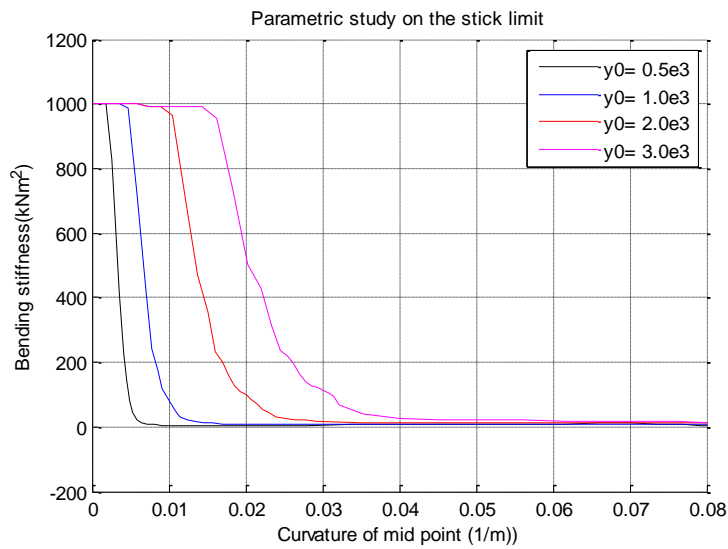
Figure 5-34   Tangential EI in parameter study on the stick limit

Nevertheless, the most obvious difference is the change of moment at the middle section. It shows that when the stick limit increases, the umbilical pipe bears larger moment. This is because of larger contact force resulted by the increased stick force limit.

5.4   Discussion on modelling errors

It should be bear in mind what kind of errors the simulation model may have, and the effects of the errors from the simulation.

5.4.1 Scale factor of the helix tendons number

The first simulation error I have come across is the simplification method on the number of tendons. In the beginning 4 helix tendons is modelled along the umbilical pipe. However, in reality the number of helix tendons is 140, leading to a large scaling factor of 35.

The result shows that the global curvature fluctuates a lot. But in reality, since the 140 helix tendons surround tightly between the inner tube and outer sheath, the global curvature is supposed to be smooth without much fluctuation.

This is due to the large scale number of 35 that only 4 helix tendons are modelled. In addition, because of the small lay angle of 12 degree, the spacing between the four tendons is relatively large. That is why the tendons behave separately in different location, leading to large difference and thus the fluctuation.
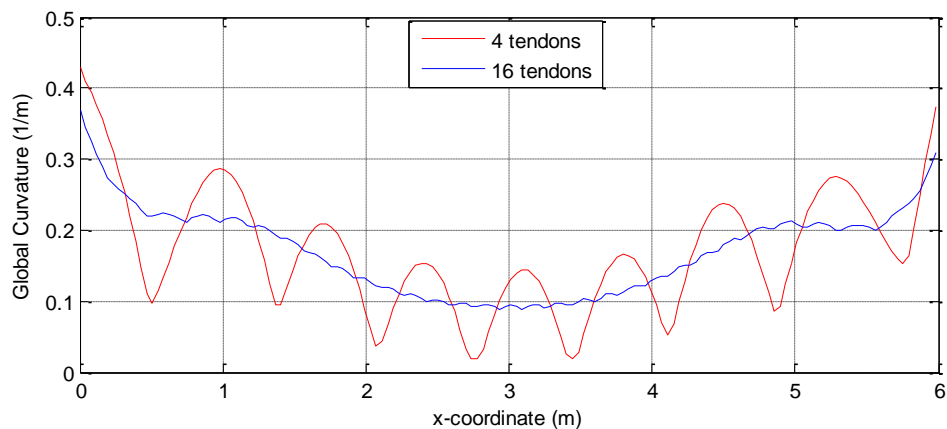
Figure 5-35 Effect of small scale factor to simulate tendons

Hence 16 helix tendons with a relatively small scale factor of 8 have been modelled. The results improve significantly and fluctuation decreases a lot, making the results reliable enough.

As we can expect, the fluctuation would vanish if even smaller scale factor is used.
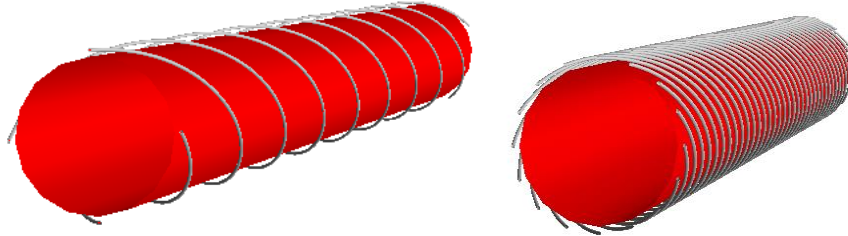
Figure 5-36 Helical tendons model based on different scale factors

5.4.2 Material input

Besides, as for the stick limit and stick stiffness, the input data is based on previous experience, with no clear calculation methods or assumption regarding the stick stiffness. Therefore the material input is not directly linked to the material properties of the bitumen contact layer. This issue should be studied further to have a good analytical input apart from data only based on experience.

5.4.3 Mesh sensitivity

Similar as the effect of scale effect, by using fine mesh and make the model as detailed as possible, the simulation would approach the reality.

In this thesis, it is assumed that 154 sections along the pipe length of 6 m is accurate enough and has been proved sufficient.

5.4.4 Simulation control data

The result is significantly affected by the iteration criterion, the convergence radius, and the step length.

In this simulation, convergence radius is set to be 1.0E-5. As for the iteration criterion, option ALL is activated to cover all the incremental norms, including incremental displacement norm, incremental energy norm and incremental force norm.

However, there is still one uncertainty shown in the curvature vs. moment plot. At the end of the loading, the bending stiffness decreases a little bit from stable value. This phenomenon is not obvious and has a short duration.
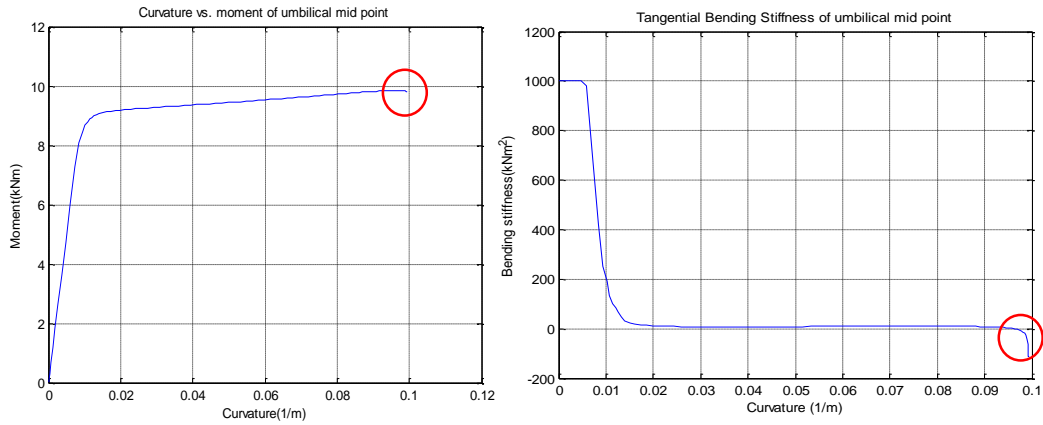
Figure 5-37 End effect error caused by numerical simulation

This is an unclear point of this thesis. Even though it does not affect the main analysis of the results, it should be reviewed again to get rid of the error.

6. Conclusions

This thesis work basically focuses on the general mechanical properties of the bonded flexible and umbilical, and the corresponding stress behavior affected by the structural components and materials.

Bonded flexible pipe model

1) Because of the elasticity of rubber compound material used as the contact layer, the bending stiffness is not affect by slip behavior. The curvature vs. moment shows a pure linear relationship.

2) In the parameter study on the shear stiffness and compression stiffness, it shows the effect of contact layer's deformation is limited. But when assuming the contact layer is extremely stiff, i.e. great value of factor β, the contact layer becomes the dominating factor on the bending stiffness EI. On the contrary, if assuming the contact layer is extremely soft, the bending stiffness will only depend on the inherent EI of the core pipe, with no contribution from the tensile layers.

3) When implementing the parameter study on the independent influence from the shear stiffness and the compression stiffness, the results indicate that there is no correlation between the shear force and radial compression. This may account for the effect of internal pressure load.

4) When looking into the effect of internal pressure load, the results conflict with the results from the Pag-o-flex test results. With the increase of internal pressure load, the bending stiffness does not increase significantly as the test.

Umbilical model

1) Different from non-bonded flexible pipe, the stick-slip behavior is dominated by the viscoelastic properties of bitumen, instead of friction. The slip threshold model of the contact layer can be estimated by a shear deformation before slip, and a constant contact force afterwards.

2) When the umbilical is under bending, the initial bending stiffness is extremely large to hundreds. This corresponds to the full-stick behavior. It experiences a sharp decrease during the transition and stays nearly constant about $10 \ \mathrm{kNm}^2$ during the full-slip phase.

3) The parameter study shows that the shear stiffness influences the tangential

bending stiffness, while the stick limit only affects the durations of stick or stick-slip transition, with no significant influence on the bending stiffness values at stable stages.

7.Further work

Due to the time limit, there are still some unsolved issues left. The main problems lie in the uncertainty on the detailed insight of the theory, the simplification of modelling, and the analysis methods.

Some further works are proposed briefly on these main issues as follow.

1) Analytical result

This is one of the most important result and is regarded as an evaluation of the numerical solution. However, since large amount of time has been spent on the modelling part to simulate the results to compare with the test, the analytical results are not provided in this thesis work.

Nevertheless, roughly seen the numerical results comply with the normal range of the mechanical properties, and the behaviors of the different type of flexible models are sufficiently pronounced, the results are reliable to much extend.

The analytical methods should basically focus on the initial bending stiffness of the bonded flexible pipe model and the umbilical model.

2) Effect of internal pressure load

This is the key problem that is not correctly pronounced by the numerical solution. In Chapter 2, possible reasons for the nature increase of the bending stiffness under large internal pressure load have been proposed, with respect to the contact stiffness and the anti-deflection moment.

As for the contact stiffness of the material, it needs more researches on the insight into the compressibility of material, and the detailed description on the embedding behavior of the steel into the rubber.

Secondly, the concept of Anti-deflection moment against ovalization should be reviewed and verified. This is regarded as the main contribution to the bending stiffness. However, to take this effect into numerical solution, it needs the ovalization behavior should be accurately simulated. More importantly, the force change on the end-cap should be caught. Since it is the decrease of the end-cap force that acts as the governing

factor that results in the anti-deflection moment.

If possible, the increase of internal pressure should be added to increase the accuracy.

3) Modelling in detail

All the models in this thesis work are simplified. Only the key components are modelled such as the tensile layers and the core pipes. However, some important numerical options are not activated, such as FLEXCROSS, ITCODE, etc.

Hence, the detailed modelling with necessary numerical algorithm shall be carried out, and this may play as a significant role in the analysis of specific behavior and influence.

Besides, mesh size of the FE model, and the time increment in the iteration, may also increase the accuracy and make the result reliable.

References

[1] MARINTEK, NTNU, 4Subsea , Handbook on design and operation of flexible pipes, 2014.

[2] American Petroleum Institute, API RECOMMENDED PRACTICE 17B, 2014.

[3] S. Sevik, On stresses and fatigue in flexible pipes, NTH, Trondheim, Norway., 1992.

[4] Nexans Norway AS, Submarine Cables, Umbilicals and Services, Subsea Technology, 2008.

[5] Z. Y. Qingzhen Lu, Design of Cross-Sectional Layout of Steel Tube Umbilical, 2014.

[6] S. K. K. A. H.-Z. Elise Olsen, "VISCOELASTIC BEHAVIOUR OF BITUMEN IN DYNAMIC CONTROL UMBILICALS," in *OMAE2014*, 2014.

[7] H. &. S. K. H. Sjur Kristion Lund, "UMBILICAL FILLING". United States,Patent Application Publication 2006.

[8] V. M. Custodio AB, "A nonlinear formulation for the axisymmetric response of umbilical cables and flexible pipes," *Appl Ocean Res 2002;24: 21–9.,* 2002.

[9] S. Sævik, "Theoretical and experimental studies of the axisymmetric behaviour of complex umbilical cross-sections".*Applied Ocean Research.*

[10] S. Sævik, "Bflex2010- Theory Manual," 2013.

[11] C. G. Andrea Catinaccio, "PIPES UNDER INTERNAL PRESSURE AND BENDING," 2009.

[12] J. H. S. A. AUSTIN, "STRESSES IN A PIPE BEND OF OVAL CROSS-SECTION AND VARYING WALL THICKNESS LOADED BY INTERNAL PRESSURE".

[13] S. Sevik, "Theoretical and experimental studies of stresses in flexible pipes. Computers and Structures," 2011.

[14] S. Sevik, "A finite element model for predicting stresses and slip in flexible pipe armouring tendons at bending gradients," *Computers and Structures, 46(2).,* 1993.

[15] O. D. Ø. G. S. B. a. J. K. G. Svein Sævik, BFLEX 2010 Version 3.1.0 - Beta User Manual, 2015.

[16] S. Sævik, Theoretical and experimental studies of stresses in flexible pipes, Institute of Marine Technology, Norwegian University of Science and Technology, 2011.

[17] K. M. Mathisen, "Large Displacement Analysis of Flexible and Rigid Systems Consdiering Displacement-Dependent Loads and Non-Linear Constraints," *PhD thesis,* 1990.

[18] S. Sævik a. J. K. Ø. Gjøsteen, "Strength analysis modelling of flexible umbilical members for marine structures," *Journal of AppliedMathematics,* 2012.

[19] S. Sævik e. B. Skallerud, "Stiffness properties and damping behavior of flexible pipes," *Flexible pipe technology ,* 1992.

Appendix

Appendix A. Bflex2010 input files

A.1 Bonded flexible pipe model with PIPE31 core pipe

```
#--------------------------------------------------------------------------
# Control data
#            Maxit   Ndim   Isolvr Npoint Iprint   Conr    Gac        Istres
CONTROL      500     3      2       16     01       1.e-9   0.0        stressfree
#        Matat   Alpha1   Alpha2   Alpha
DYNCONT   1       0.0      0.09    -0.05
#            T      Dt    Dtvi  Dt0    Type     StepType Iterco  Itcrit  Maxit  Maxdiv    Conr
TIMECO     25.0    1.0   1.0   10.0   STATIC   auto      NONE    all     100    5         1e-5
#--------------------------------------------------------------------------
## Nocoor input#
#
#The core layer
#       Type           Node      Xcor    Ycor   Zcor
Nocoor Coordinates   1        0         0       0
                     81       1196.0e-3  0       0
#
#Supporting first layer
#       Type    x0    y0    z0    Beta1    Beta2    Beta3    R        Node    Xcor       Theta
Nocoor Polar   0.0   0.0   0.0   0.0      0.0      0.0      70.3e-3   30001   0.00        0
                                                                     30081   1196e-3     -26.197
#       N       Nodeinc   Xinc      Thetainc
Repeat 16       81        0.0       0.392
#
# Tensile layer 1
#       Type    X0    Y0    Z0    Beta1    Beta2    Beta3    R        Node    Xcor       Theta
Nocoor Polar   0.0   0.0   0.0   0.0      0.0      0.0      70.3e-3   10001   0.0        0
                                                                     10081   1196.0e-3  -26.197
#       N       Nodeinc   Xinc      Thetainc
Repeat 16       81        0.0       0.392
#
# Tensile layer 2
#       Type    X0    Y0    Z0    Beta1    Beta2    Beta3    R        Node    Xcor       Theta
Nocoor Polar   0.0   0.0   0.0   0.0      0.0      0.0      74.3e-3   20001   0.0        0
                                                                     20081   1196.0e-3  24.7871
#       N       Nodeinc   Xinc      Thetainc
Repeat 16       81        0.0       0.392
```

```
#       Mode            Factor      Result
Visres Integration   1              Sigma-xx-ax Sigma-xx Vconfor-z      VCONDIS-z
#---------------------------------------------------------------------
### The core layer
#       Elgroup       Elty          Matname Elid Node1 Node2 Node3 Node4
Elcon   core          pipe31        CoreMat   1    1      2
#       N     Nelinc    Nodinc
Repeat  80    1          1
#
## Tensile Layers
#
# Tensile Layer 1
#       Elgroup       Elty          Flexcrossname    Elid Node1 Node2 Node3 Node4
Elcon   tenslayer1 hshear353       tendon            10001   1     2    10001  10002
                                                     10016   1     2    11216  11217
#       N     Nelinc    Nodinc
Repeat  80    16          1
#
# Tensile Layer 2
#       Elgroup       Elty          Flexcrossname    Elid   Node1 Node2 Node3   Node4
Elcon   tenslayer2 hshear353       tendon            20001    1     2    20001  20002
                                                     20016    1     2    21216  21217
#       N     Nelinc    Nodinc
Repeat  80    16          1
#
### Contact Layers
#
# Contact Layer1-between core and tensile layer 1
#       Elgroup       Elty          Flexcrossname    Elid    Node1 Node2 Node3 Node4
Elcon   contlayer1 hcont453    contmat               40001   30001 30002 10001   10002
                                                     40016   31216 31217 11216   11217
#       N     Nelinc    Nodinc
repeat 80     16          1
#
# Contact Layer 2-between tensile layer 1 and tensile layer 2
#       Elgroup       Elty          Flexcrossname    Elid    Node1 Node2 Node3 Node4
Elcon   contlayer2 hcont453    contmat1_1             50001   10001   10002   20001 20002
                                                      50016   11216   11217   21216 21217
#       N     Nelinc    Nodinc
repeat 80     16          1
#---------------------------------------------------------------------
```

```
# Orient input
#
# The core layer
#          Type              Elid      X    Y        Z
Elorient Coordinates       1        0   1e3      0
                           80       0   1e3      0
#
# Tensile Layer 1
#          Type              Elid      X    Y        Z
Elorient Coordinates     10001      0   1e3      0
                         10016      0   1e3      0
#          N    Inc Xinc Yinc Zinc
repeat 80 16    0      0      0
#
# Tensile Layer 2
#          Type              Elid      X    Y        Z
Elorient Coordinates     20001      0   1e3      0
                         20016      0   1e3      0
#          N    Inc Xinc Yinc Zinc
repeat 80 16    0      0      0
#
# Contact Layer1
#          Type              Elid      X    Y    Z
Elorient Eulerangle      40001      0    0    0
                         41280      0    0    0
#
# Contact Layer2
#          Type              Elid      X    Y    Z
Elorient Eulerangle      50001      0    0    0
                         51280      0    0    0
#
##Contact interfaces
#          GroupName       MasterName     SlaveNamei    IS1     ISn     IStx       ISty       IStz     MaxIT
IGap
#                          1 means that friction is independent (tape between layers) else (isotropic model)
CONTINT contlayer1     core           tenslayer1    1       3       0          0          0        60     1
CONTINT contlayer2     tenslayer1     tenslayer2    1       3       0          0          0        60     1
#
#----------------------------------------------------------------
#
# Element property input
```

```
#
#         EleGroupName    EleType       Rad       Th              RCd    TCd    RMAdd   TMAdd   MD
MS     ODP    ODW    RKS
ELPROP core     pipe                 6.09e-2   0.0001e-3    1.0    0.1    2.0     0.2     100e-6   0.00
138.6e-3 138.6e-3 0.5
#         EleGroupName    EleType       GeoType    Width   Th          DryMass   SubmergedMass
ScaleFact  PHistory GHist    AxiSym    AxiSym=1 turn off axisymmetric shear inetraction
#
=2 turn off bending shear interaction
#
=3 turn off both
ELPROP  tenslayer1        shearhelix  tube       1.784e-3   0.001e-3    0.0785e-6       0.0          3.81
300        400        10 d d d d
ELPROP  tenslayer2        shearhelix  tube       1.784e-3   0.001e-3    0.0785e-6       0.0          4.06
300        400        10 d d d d
#       EleGroupName    EleType       Gap0   TuneTime   AUTOMNPC    AutoSearch
ELPROP contlayer1       layercontact  D      D            D           0
ELPROP contlayer2       layercontact  D      D            D           1
#-------------------------------------------------------------------
# Boundary condition data
#       Type    NodId   DOF
BONCON GLOBAL 1         1
BONCON GLOBAL 1         2
BONCON GLOBAL 1         3
BONCON GLOBAL 1         4
BONCON GLOBAL 1         5
BONCON GLOBAL 1         6
BONCON GLOBAL 81        2
#
BONCON GLOBAL 10001       1
repeat          16      81
BONCON GLOBAL 10081       1
repeat          16      81
BONCON GLOBAL 20001      1
repeat          16      81
BONCON GLOBAL 20081      1
repeat          16      81


BONCON GLOBAL 10001       2
repeat          1296     1
```

```
BONCON GLOBAL 20001     2
repeat          1296    1


BONCON GLOBAL 30001     1
repeat          1296    1
BONCON GLOBAL 30001     2
repeat          1296    1
BONCON GLOBAL 30001     3
repeat          1296    1
BONCON GLOBAL 30001     4
repeat          1296    1
BONCON GLOBAL 30001     5
repeat          1296    1
BONCON GLOBAL 30001     6
repeat          1296    1


BONCON GLOBAL   10001    4
repeat          1296    1
BONCON GLOBAL 20001     4
repeat          1296    1
BONCON GLOBAL   10001    5
repeat          1296    1
BONCON GLOBAL 20001     5
repeat          1296    1



#---------------------------------------------
#
# Constraint input R=1m, theta=1m/R/2, theta=k*L/2, L=0.5m,   0.5*0.1/2=0.025
#       Ctype Pdtype   NodId DOF Dispval HistNo
CONSTR PDISP GLOBAL   81     3    1     100
#---------------------------------------------
#
#Load input data
#       Hist   Dir   NODE Load      no2 r2          n m
#CLOAD   200    1    21   1.056e6
#       Hist    Elnr1 T1    Elnr2 T2
#TLOAD   200    1       23.0 10    23.0
#       Preshist Gravhist
PELOAD 300          400
```

```
#          Hist Elnr1 P1   Elnr2   P2
PILOAD   200  1      20  80       20
#-----------------------------------------------------------
# History data
#      pdisp
#      NO      T1      FAC1
THIST_R 100    0.0       5.0      rampcos 0.0
               5.0      25.0    rampcos 60.0e-3


#
#      internal pressure
#      NO      T1      FAC1
THIST_R 200    0       5 rampcos 1.0
               5      400 rampcos 1.0


THIST 300      0       0.0
               400     0.0
THIST 400      0       0.0
               400     0.0


#-----------------------------------------------------------------------------
#   Material data
#            Matname        Mtype        Poiss   Density   Talfa  Tecond  Heatc   EM       GM
Etrans
#MATERIAL tendon          elastic    0.3      7850e-6       11.7e-6 50       800    2.1e5    8.076e4
2.1e5
MATERIAL tendon        linear      0.3      11.7e-6    50       800     0      2.1     1.67e-6    1.67e-6
1.28E-06    2.1e5    8.076e4   7850e-6      2.1e5


#            Matname    Mtype      Poiss   Talfa    Tecond   Heatc   Beta EA      EIY      EIZ
GIT       EM       GM        Density   Etrans
MATERIAL CoreMat      linear      0.0      11.7e-6    50       800     0      4.58    8.78e-3    8.78e-3
6.27e-3    300    120    1000e-6      300
#   Contact :
#        Mname      Type        MuX    MuY    XName    XName   ZName
#        Mname      Type        MuX    MuY    XName    XName   ZName
MATERIAL contmat     contact     0.2    0.2    ax      ax      az    userdefined
MATERIAL contmat1_1 contact     0.2    0.2    bx      bx      bz    userdefined


MATERIAL ax        hycurve        -1000    -2.0e3*2
                                 1000     2.0e3*2
```

MATERIAL az	hycurve	-1000	-5.15e3*2
		1000	5.15e3*2
MATERIAL bx	hycurve	-1000	-41.3e3
		1000	41.3e3
MATERIAL bz	hycurve	-1000	-107.4e3
		1000	107.4e3

A.2 Bonded flexible pipe model with HSHEAR363 core pipe

```
#-------------------------------------------------------------------------
# Control data
#          Maxit   Ndim   Isolvr Npoint Iprint   Conr    Gac      Istres
CONTROL    500     3      2       16     01       1.e-9  0.0       stressfree
#          Matat   Alpha1  Alpha2  Alpha
DYNCONT    1       0.0     0.09    -0.05
#          T       Dt     Dtvi  Dt0    Type      StepType Iterco  Itcrit  Maxit  Maxdiv   Conr
TIMECO     25.0    1.0    1.0   10.0   STATIC    auto     NONE     all    150    5        1e-5
#-------------------------------------------------------------------------
## Nocoor input#
#
#The core layer
#       Type           Node     Xcor   Ycor   Zcor
Nocoor Coordinates    1        0        0        0
                      81       1196.0e-3  0      0
Nocoor Coordinates   101       0        0        0
                     180       1196.0e-3  0       0


#
# Tensile layer 1
#       Type    X0     Y0     Z0     Beta1   Beta2   Beta3   R       Node  Xcor     Theta
Nocoor Polar   0.0    0.0    0.0    0.0     0.0     0.0     70.3e-3 1001  0.0       0
                                                                   1081  1196.0e-3 -26.197
#       N       Nodeinc   Xinc    Thetainc
Repeat 16       81        0.0     0.392
#
# Tensile layer 2
#       Type    X0     Y0     Z0     Beta1   Beta2   Beta3   R       Node  Xcor     Theta
Nocoor Polar   0.0    0.0    0.0    0.0     0.0     0.0     74.3e-3 20001 0.0       0
                                                                   20081 1196.0e-3 24.7871
#       N       Nodeinc   Xinc    Thetainc
Repeat 16       81        0.0     0.392
#       Mode            Factor    Result
Visres Integration    1           Sigma-xx-ax Sigma-xx Vconfor-z      VCONDIS-z
#
#----------------------------------------------------------------------
### The core layer
#       Elgroup         Elty          Matname Elid Node1 Node2 Node3 Node4
```

```
Elcon   core           hshear363      CoreMat   1   1     2    101
#       N     Nelinc    Nodinc
Repeat  80    1         1
#
## Tensile Layers
#
# Tensile Layer 1
#       Elgroup    Elty          Flexcrossname   Elid Node1 Node2 Node3 Node4
Elcon   tenslayer1 hshear353     tendon          1001   1     2    1001  1002
                                                 1016   1     2    2216  2217
#       N     Nelinc    Nodinc
Repeat  80    16        1
#
# Tensile Layer 2
#       Elgroup    Elty          Flexcrossname   Elid   Node1 Node2 Node3  Node4
Elcon   tenslayer2 hshear353     tendon          20001   1     2   20001  20002
                                                 20016   1     2   21216  21217
#       N     Nelinc    Nodinc
Repeat  80    16        1
#
### Contact Layers
#
# Contact Layer1-between core and tensile layer 1
#       Elgroup    Elty          Flexcrossname   Elid     Node1 Node2 Node3 Node4
Elcon   contlayer1 hcont463      contmat         40001   101 1001   1002
                                                 40016   101 2216   2217
#       N     Nelinc    Nodinc
repeat 80     16        1
#
# Contact Layer 2-between tensile layer 1 and tensile layer 2
#       Elgroup    Elty      Flexcrossname   Elid    Node1 Node2 Node3 Node4
Elcon   contlayer2 hcont453  contmat1_1      50001   1001   1002  20001 20002
                                             50016   2216   2217  21216 21217
#       N     Nelinc    Nodinc
repeat 80     16        1
#------------------------------------------------------------------------
# Orient input
#
# The core layer
#       Type           Elid    X   Y      Z
Elorient Coordinates   1       0   1e3    0
```

```
                              80      0   1e3     0
#
# Tensile Layer 1
#          Type           Elid     X   Y      Z
Elorient Coordinates     1001     0   1e3      0
                         1016     0   1e3      0
#          N    Inc Xinc Yinc Zinc
repeat 80 16   0      0      0
#
# Tensile Layer 2
#          Type           Elid     X   Y      Z
Elorient Coordinates     20001    0   1e3      0
                         20016    0   1e3      0
#          N    Inc Xinc Yinc Zinc
repeat 80 16   0      0      0
#
# Contact Layer1
#          Type           Elid     X   Y   Z
Elorient Eulerangle     40001    0   0   0
                        41280    0   0   0
#
# Contact Layer2
#          Type           Elid     X   Y   Z
Elorient Eulerangle     50001    0   0   0
                        51280    0   0   0
#
##Contact interfaces
#          GroupName      MasterName    SlaveNamei    IS1    ISn    IStx      ISty      IStz   MaxIT
IGap
#                      1 means that friction is independent (tape between layers) else (isotropic model)
CONTINT contlayer1     core          tenslayer1    1      3      0         0         0      60     1
CONTINT contlayer2     tenslayer1    tenslayer2    1      3      0         0         0      60     1
#
#----------------------------------------------------------------
#
# Element property input
#
#          EleGroupName   EleType      Rad    Th              RCd    TCd    RMAdd    TMAdd    MD
MS    ODP    ODW     RKS
#ELPROP core      pipe                 7.09e-2   0.001e-3    1.0    0.1    2.0      0.2      100e-6      0.00
138.6e-3 138.6e-3 0.5
```

```
ELPROP core        shearhelix    tube      60.9e-3  9.0e-3   2.0    0.2    1.0    300    400    10
#          EleGroupName  EleType       GeoType      Width   Th       DryMass    SubmergedMass
ScaleFact  PHistory GHist   AxiSym    AxiSym=1 turn off axisymmetric shear inetraction
#
=2 turn off bending shear interaction
#
=3 turn off both
ELPROP tenslayer1        shearhelix  tube       1.784e-3  0.001e-3  0.0785e-6    0.0        3.81
300        400       10 d d d d
ELPROP tenslayer2        shearhelix  tube       1.784e-3  0.001e-3  0.0785e-6    0.0        4.06
300        400       10 d d d d
#       EleGroupName  EleType        Gap0   TuneTime   AUTOMNPC   AutoSearch
ELPROP contlayer1     layercontact  D      D          D          0
ELPROP contlayer2     layercontact  D      D          D          1
#-----------------------------------------------------------------------
# Boundary condition data
#       Type    NodId   DOF
BONCON GLOBAL 1         1
BONCON GLOBAL 1         2 repeat 81 1
BONCON GLOBAL 1         3
BONCON GLOBAL 1         4
BONCON GLOBAL 1         5
BONCON GLOBAL 1         6
BONCON GLOBAL 81        2
#
BONCON GLOBAL 1001      1
repeat         16      81
BONCON GLOBAL 1081      1
repeat         16      81
BONCON GLOBAL 20001     1
repeat         16      81
BONCON GLOBAL 20081     1
repeat         16      81

BONCON GLOBAL 1001      2
repeat         1296     1
BONCON GLOBAL 20001     2
repeat         1296     1
BONCON GLOBAL 1001      4
repeat         1296     1
BONCON GLOBAL 20001     4
```

```
repeat            1296    1
BONCON GLOBAL   1001    5
repeat            1296    1
BONCON GLOBAL 20001    5
repeat            1296    1


BONCON GLOBAL 101     2
repeat            80      1
BONCON GLOBAL 101     3
repeat            80      1


#----------------------------------------------
#
# Constraint input R=1m, theta=1m/R/2, theta=k*L/2, L=0.5m,   0.5*0.1/2=0.025
#         Ctype Pdtype    NodId DOF Dispval HistNo
CONSTR PDISP GLOBAL    81     3     1     100
constr coneq global 1002 3 0.0 1001 3 1.0 repeat 1295 1 0
constr coneq global 20002 3 0.0 20001 3 1.0 repeat 1295 1 0
#----------------------------------------------
#
#Load input data
#         Hist   Dir   NODE Load     no2 r2          n m
#CLOAD   200    1     21    1.056e6
#         Hist    Elnr1 T1    Elnr2 T2
#TLOAD   200    1      23.0 10    23.0
#         Preshist Gravhist
PELOAD 300       400
#         Hist Elnr1 P1    Elnr2   P2
PILOAD   200   1     20 80       20
#---------------------------------------------------------
# History data
#     pdisp
#     NO    T1     FAC1
THIST_R 100   0.0      5.0     rampcos 0.0
            5.0     25.0   rampcos 60.0e-3


#
#     internal pressure
#     NO    T1     FAC1
THIST_R 200    0      5 rampcos 1.0
            5     400 rampcos 1.0
```

```
THIST 300    0      0.0
             400    0.0
THIST 400    0      0.0
             400    0.0
```

```
#----------------------------------------------------------------------
#   Material data
#           Matname         Mtype        Poiss   Density     Talfa  Tecond  Heatc   EM        GM
Etrans
#MATERIAL tendon           elastic   0.3      7850e-6        11.7e-6 50        800     2.1e5     8.076e4
2.1e5
MATERIAL tendon        linear     0.3      11.7e-6   50        800      0     2.1     1.67e-6    1.67e-6
1.28E-06    2.1e5    8.076e4   7850e-6    2.1e5
```

```
#           Matname    Mtype      Poiss    Talfa     Tecond    Heatc    Beta  EA        EIY        EIZ
GIT       EM       GM         Density    Etrans
#MATERIAL CoreMat      linear     0.4      11.7e-6    50        800      0     4.58     8.78e-3    8.78e-3
6.27e-3    300      120    1000e-6        300
MATERIAL CoreMat    elastic     0.45    1000e-6    11.7e-6      50       800   136.7*7.242
```

```
#   Contact :
#         Mname        Type       MuX    MuY    XName     XName   ZName
MATERIAL contmat      contact     0.2    0.2    ax        ax     az   userdefined
MATERIAL contmat1_1 contact       0.2    0.2    bx        bx     bz     userdefined
```

```
MATERIAL ax       hycurve        -1000    -2.0e3*2
                                  1000     2.0e3*2
```

```
MATERIAL az       hycurve        -1000    -5.15e3*2
                                  1000     5.15e3*2
```

```
MATERIAL bx       hycurve        -1000    -41.3e3
                                  1000     41.3e3
```

```
MATERIAL bz       hycurve        -1000    -107.4e3
                                  1000     107.4e3
```

A.3 Umbilical model

Test cable

HEAD Test the hshear353/hcont463/Bitumen feature -   The Chunyu test pipe -final

#--

Control data

#

maxit   ndim   isolvr npoint ipri   conr   gacc   iproc

CONTROL   500   3   2   16   01   1.e-9   9.81   stressfree

#

Matat   Alpha1   Alpha2   Alpha

DYNCONT   2   0.0   0.09   -0.05

TIMECO   50.0   0.5   0.5   10.0   static   auto   NONE   all   150   5   1e-5

#--

#

Nocoor input

#

no   x   y   z

Nocoor Coordinates

            1   0.0   0.0   0.0

            24   0.905   0.0   0.0

            178   6.931   0.0   0.0

            201   7.811   0.0   0.0

internal tube   no   x   y   z

Nocoor Coordinates

            1001   0.905   0.0   0.0

            1154   6.931   0.0   0.0

outersheath   no   x   y   z

Nocoor Coordinates

            4001   0.905   0.0   0.0

            4154   6.931   0.0   0.0

#

tensile-1

no   x0   y0   z0   b1   b2   b3   R node   xcor   theta

Nocoor Polar   0.0   0.0   0.0   0.0   0.0   0.0   0.0937

40001   0.905   3.1416

40155   6.931   16.811

N   Nodeinc   Xinc   Thetainc

Repeat 16   155   0.0   0.392

#

```
#
#
Visres  Integration  1  sigma-xx     Sigma-xx-ax  sigma-xx-my  sigma-xx-mz  Sigma-yy  Vconfor-z  Vconfor-x
VCONDIS-X


#----------------------------------------------------------------------
# Elcon    input
#
#
# Structural layers
#
#          group       elty        material      no      n1     n2   n3    n4
Elcon   pipe          pipe31       pipemat
501   1     2
502   2     3
503   3     4
504   4     5
505   5     6
506   6     7
507   7     8
508   8     9
509   9     10
510   10    11
511   11    12
512   12    13
513   13    14
514   14    15
515   15    16
516   16    17
517   17    18
518   18    19
519   19    20
520   20    21
521   21    22
522   22    23
523   23    24
524   178   179
525   179   180
526   180   181
527   181   182
528   182   183
```

```
529   183   184
530   184   185
531   185   186
532   186   187
533   187   188
534   188   189
535   189   190
536   190   191
537   191   192
538   192   193
539   193   194
540   194   195
541   195   196
542   196   197
543   197   198
544   198   199
545   199   200
546   200   201
Elcon   tube7            hshear363   tubemat      1      24       25     1001 repeat 154 1 1
Elcon   outersheath14   hshear363   sheathmat   3001   24       25     4001 repeat 154 1 1
Elcon   tensile11        hshear353   steelmat    40001 24       25     40001 40002
                                                 40016 24       25     42326 42327 repeat 154 16 1
#
# Contact layers
#
Elcon   tube7tensile11             hcont463   contmat     70001   1001      40001      40002
                                              70016   1001      42326      42327 repeat
154 16 1
Elcon   tensile11outersheath14     hcont463   contmat     80001   40001     40002     4001
                                              80016   42326     42327     4001 repeat
154 16 1
#
#------------------------------------------------------------------------
# Orient input
#
# structural els
#                       no       x  y       z
Elorient Coordinates   501     0   1e3     0
                       546     0   1e3     0
Elorient Coordinates   1       0   1e3     0
                       154     0   1e3     0
```

Elorient Coordinates   3001   0   1e3   0

                            3154   0   1e3   0

Elorient Coordinates   40001   0   1e3   0

                            42464   0   1e3   0

#

contact

elorient eulerangle 70001 0.0 0.0 0.0

                    72464 0.0 0.0 0.0

elorient eulerangle 80001 0.0 0.0 0.0

                    82464 0.0 0.0 0.0

#---

#

#

groupn   mname   sname   is1   isn   istx   isty   istz   gt1   gt2

#

CONTINT tube7tensile11   tube7   tensile11   1   3   0.0   0.0

0.0   60   2

CONTINT tensile11outersheath14 tensile11 outersheath14   1   3   0.0   0.0   0.0

60   2

#

#

Element property input

#

b   t   md   ms   scale   thims thimd

iop

ELPROP tube7   shearhelix tube   0.0867   0.01   60.8 60.8   1.0   200   200   0

ELPROP outersheath14   shearhelix tube   0.0962   0.001   2.0   2.0   1.0   200   200   0

ELPROP tensile11   shearhelix tube   0.002   0.00001 0.0986 0.0986 8.75   200   200   10

gap0 tunetime AUTOMNPC autosearch scalefac

ELPROP tube7tensile11   layercontact D D   D 0 8.75

ELPROP tensile11outersheath14   layercontact D D   D 0 8.75

#

#---

Material data

#

#

name   type   poiss   dens   talfa   tecond   heatc em

ELPROP PIPE   pipe 0.12 0.001   0.8   0.1   2.0   0.2   0.0 0.0   0.004   0.004 0.5

MATERIAL pipemat   linear   0.3   11.7e-6   2.0   50   800   1e9 1e7   1e7   1e7

2.00E11   0.8e11   8E3 2.00E11

MATERIAL tubemat   elastic   0.45   8e3   11.7e-6   50   800   8.33e8

MATERIAL sheathmat   elastic   0.45   8e3   11.7e-6   50   800   8.33e8

MATERIAL steelmat   linear   0.3   11.7e-6   2.0   50   800   2.63e6   2.51   2.51

1.93   2.07e11   0.8e11   8E3   2.07e11

\#

\#

\#   name   type   rmyx   xmat   zmat

MATERIAL contmat contact   0.0 0.0   bellx   belly   bellz userdefined

\#   name   type   alfa   eps   sig

MATERIAL bellx   epcurve   1   0   0

8.333e-5*1.2   1.0e3*1.2

1000   2.5e3

\#

MATERIAL belly   hycurve   -1000   0.0

1000   0.0

\#

MATERIAL bellz   hycurve   -1000   -3.3e11

1000   3.3e11

\#

\#--

\# Boundary condition data

\#   Loc   node   dir

BONCON GLOBAL 1   1

BONCON GLOBAL 1   2

BONCON GLOBAL 1   3

BONCON GLOBAL 1   4

BONCON GLOBAL 1   6

BONCON GLOBAL 201   2

BONCON GLOBAL 201   3

BONCON GLOBAL 201   4

BONCON GLOBAL 201   6

\# fix the relative disp at ends

\#

\#

BONCON gLObAL 40001   1 repeat 16 155

BONCON gLObAL 40001   2 repeat 2480 1

BONCON gLObAL 40001   5 repeat 2480 1

BONCON gLObAL 40001   4 repeat 2480 1

BONCON gLObAL 40155   1 repeat 16 155

\#

\#

```
BONCON gLObAL 1001          2 repeat 154 1
BONCON gLObAL 1001          3 repeat 154 1
BONCON gLObAL 4001          2 repeat 154 1
BONCON gLObAL 4001          3 repeat 154 1
#---------------------------------------------
#
# Constraint input R=1m, theta=1m/R/2, theta=k*L/2, L=0.5m,   0.5*0.1/2=0.025       0.01745 rad=1 degree
CONSTR PDISP GLOBAL         1 5     0.01745     100
CONSTR PDISP GLOBAL         201 5   -0.01745    100
#
#-------------------------------------------
# Cload input
#
#       hist   dir   no1 r1   no2 r2            n m
#
CLOAD   400     1    201   1.0e3
#-------------------------------------------
#TLOAD   200      1 23.0 10 23.0
#PELOAD 200 200
#PILOAD   200 1     -159e6 200 -159e6
#INISTR   200 1     501   0.15   700 0.15
#TIMECO      2.1   0.10   0.1    10.0   STATIC   auto       none      disp      300     5        1E-3
#TIMECO      50.00  1.0   1.0    1000.0  dynamic  auto       none      disp      30      5        1E-6
#---------------------------------------------------------
# History data
#
#    pdisp
THIST_R 100   0.0              5.0 rampcos 0.0
            5.0              50.0 rampcos 45.0
#          20.0             30.0 rampcos 45.0


#    peload
THIST 200   0     0.0
            10.1 0.0001
            200    1.0


#    cload
#
THIST_R 400   0.0              5.0 rampcos 20.0
```

```
        5.0            300.0 rampcos 20.0
#       20.0            30.0 rampcos 20.0
```

Appendix B. Material data

B.1 Polymer material

Table B-1 Young's modulus of typical polymer material [20]

		E (GPa)		
Polymers [1]				
Elastomer	Butyl Rubber	0.001	-	0.002
	EVA	0.01	-	0.04
	Isoprene (IR)	0.0014	-	0.004
	Natural Rubber (NR)	0.0015	-	0.0025
	Neoprene (CR)	0.0007	-	0.002
	Polyurethane Elastomers (elPU)	0.002	-	0.003
	Silicone Elastomers	0.005	-	0.02
Thermoplastic	ABS	1.1	-	2.9
	Cellulose Polymers (CA)	1.6	-	2
	Ionomer (I)	0.2	-	0.424
	Nylons (PA)	2.62	-	3.2
	Polycarbonate (PC)	2	-	2.44
	PEEK	3.5	-	4.2
	Polyethylene (PE)	0.621	-	0.896
	PET	2.76	-	4.14
	Acrylic (PMMA)	2.24	-	3.8
	Acetal (POM)	2.5	-	5
	Polypropylene (PP)	0.896	-	1.55
	Polystyrene (PS)	2.28	-	3.34
	Polyurethane Thermoplastics (tpPU)	1.31	-	2.07
	PVC	2.14	-	4.14
	Teflon (PTFE)	0.4	-	0.552
Thermoset	Epoxies	2.35	-	3.075
	Phenolics	2.76	-	4.83
	Polyester	2.07	-	4.41
Polymer Foams				
	Flexible Polymer Foam (VLD)	0.0003	-	0.001
	Flexible Polymer Foam (LD)	0.001	-	0.003
	Flexible Polymer Foam (MD)	0.004	-	0.012
	Rigid Polymer Foam (LD)	0.023	-	0.08
	Rigid Polymer Foam (MD)	0.08	-	0.2
	Rigid Polymer Foam (HD)	0.2	-	0.48

Table B-2 yield stress and tensile strength of typical polymer material [20]

		σ_y (MPa)			σ_{ts} (MPa)		
Polymers [1]							
Elastomer	Butyl Rubber	2	-	3	5	-	10
	EVA	12	-	18	16	-	20
	Isoprene (IR)	20	-	25	20	-	25
	Natural Rubber (NR)	20	-	30	22	-	32
	Neoprene (CR)	3.4	-	24	3.4	-	24
	Polyurethane Elastomers (elPU)	25	-	51	25	-	51
	Silicone Elastomers	2.4	-	5.5	2.4	-	5.5
Thermoplastic	ABS	18.5	-	51	27.6	-	55.2
	Cellulose Polymers (CA)	25	-	45	25	-	50
	Ionomer (I)	8.3	-	15.9	17.2	-	37.2
	Nylons (PA)	50	-	94.8	90	-	165
	Polycarbonate (PC)	59	-	70	60	-	72.4
	PEEK	65	-	95	70	-	103
	Polyethylene (PE)	17.9	-	29	20.7	-	44.8
	PET	56.5	-	62.3	48.3	-	72.4
	Acrylic (PMMA)	53.8	-	72.4	48.3	-	79.6
	Acetal (POM)	48.6	-	72.4	60	-	89.6
	Polypropylene (PP)	20.7	-	37.2	27.6	-	41.4
	Polystyrene (PS)	28.7	-	56.2	35.9	-	56.5
	Polyurethane Thermoplastics (tpPU)	40	-	53.8	31	-	62
	PVC	35.4	-	52.1	40.7	-	65.1
	Teflon (PTFE)	15	-	25	20	-	30
Thermoset	Epoxies	36	-	71.7	45	-	89.6
	Phenolics	27.6	-	49.7	34.5	-	62.1
	Polyester	33	-	40	41.4	-	89.6
Polymer Foams							
	Flexible Polymer Foam (VLD)	0.01	-	0.12	0.24	-	0.85
	Flexible Polymer Foam (LD)	0.02	-	0.3	0.24	-	2.35
	Flexible Polymer Foam (MD)	0.05	-	0.7	0.43	-	2.95
	Rigid Polymer Foam (LD)	0.3	-	1.7	0.45	-	2.25
	Rigid Polymer Foam (MD)	0.4	-	3.5	0.65	-	5.1
	Rigid Polymer Foam (HD)	0.8	-	12	1.2	-	12.4

B.2 Most important elastomers used in bonded hoses

Table B-3 Most important elastomers used in bonded hoses [21]

	General properties
Butyl rubber	Excellent weather resistance, low air and gas permeability, good acid and caustic resistance, good physical properties, good heat and cold resistance, no resistance to mineral-oil-derived liquids
Chlorbutyl rubber	Variant of butyl rubber
Chlorinated polyethylene(CPE)	Excellent resistance to ozone and weather, medium resistance to oil and aromatic compounds, excellent flame resistance
Ethylene propylene rubber (EPDM)	Excellent ozone, chemical, and ageing properties, low resistance to oil-derived liquids, very good steam resistance, good cold and heat resistance (-40°C to $+175^{\circ}$C), good resistance to brake fluid based on glycol
Hydrogenated nitrile rubber (HNBR)	Good resistance to mineral oil-based fluids, vegetable and animal fats, aliphatic hydrocarbons, diesel fuels, ozone, acid gas, diluted acids and caustics, suitable for high temperatures
Chlorosulfonated polyethylene	Excellent weather, ozone, and acid resistance, limited resistance to mineral-oil-derived liquids
Natural rubber	Excellent physical properties, high elasticity, flexibility, very good abrasion resistance, limited resistance to acids, not resistant to oil
Polychloroprene (Neoprene)	Excellent weather resistance, flame-retardant, medium oil resistance, good physical properties, good abrasion resistance
Acrylo-nitrile rubber (Nitril, NBR)	Excellent oil resistance, limited resistance to aromatic compounds, the resistance to fuel and flexibility to cold depends on ACN content
NVC (NBR/PVC)	Excellent oil and weather resistance for both lining and cover, not particularly resistant to cold
Acrylate rubber	Excellent oil and tar resistance at high temperatures
Styrene-butadiene rubber (SBR)	Good physical properties, good abrasion resistance, low resistance to mineral-oil-derived liquids
Silicone rubber	Very good hot-air resistance approximately up to $+250^{\circ}$C for short periods of time, good low temperature behaviour, ozone and weather resistance, limited oil resistance, not resistant to petrol and acids
Fluorinated rubber (Viton)	Excellent high-temperature resistance up to $+225^{\circ}$C and up to $+350^{\circ}$C for short periods of time especially in water and oil, very good chemical resistance

B.3 Compression of solid rubber rings
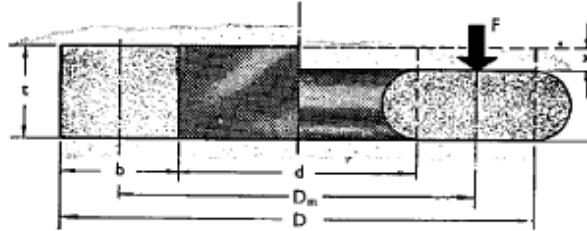
$$K = \frac{F}{x} = \frac{4}{3} \frac{E_0\pi(D^2-d^2)}{4t} \left\{1 + k\left(\frac{D-d}{4t}\right)^2\right\}$$

$$= \frac{4}{3} E_0\pi D_m \frac{b}{t} \left\{1 + \frac{kb^2}{4t^2}\right\}$$

K = stiffness
F = load
x = deflexion
E_0 = Young's modulus (Table 3)
k = a numerical factor (Table 3)

D = external diameter
d = internal diameter
D_m = mean diameter $= \frac{1}{2}(D+d)$
b = radial width of section $= \frac{1}{2}(D-d)$
t = thickness
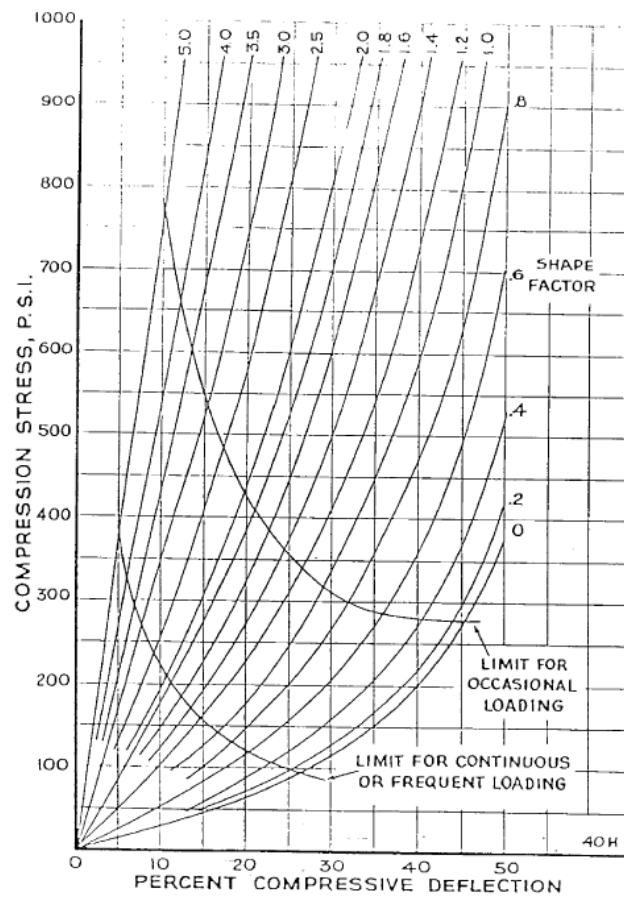
Figure B-4 Compression of solid rubber rings

Appendix C. Numerical result of the bending stiffness of middle section of umbilical pipe

Table C-1 Numerical result of the bending stiffness of middle section of umbilical pipe by time steps

Phase	Curvature (m^{-1})	Bending Stiffness(kNm^2)	Average(kNm^2)
1	1.18E-03	1000.75	1000.78
	1.85E-03	1000.77	
	2.66E-03	1000.78	
	3.62E-03	1000.79	
	4.71E-03	1000.81	
2	5.96E-03	980.43	191.8
	7.31E-03	675.9	
	8.51E-03	422.12	
	9.42E-03	253.18	
	1.02E-02	190.42	
	1.08E-02	134.22	
	1.14E-02	102.61	
	1.21E-02	86.39	
	1.27E-02	66.18	
	1.33E-02	46.02	
	1.41E-02	31.16	
	1.50E-02	23.17	
	1.61E-02	18.2	
	1.73E-02	14.98	
	1.86E-02	12.89	
	1.99E-02	10.96	
3	2.13E-02	9.99	9.02
	2.28E-02	9.54	
	2.43E-02	8.8	
	2.59E-02	8.68	
	2.75E-02	8.62	
	2.92E-02	8.42	
	3.09E-02	8.19	

3.26E-02	8.26	
3.43E-02	8.21	
3.60E-02	8.08	
3.77E-02	8.15	
3.95E-02	8.23	
4.12E-02	8.22	
4.29E-02	8.4	
4.46E-02	8.47	
4.64E-02	8.36	
4.81E-02	8.24	
4.98E-02	8.34	
5.15E-02	8.63	
5.32E-02	8.94	
5.49E-02	8.92	
5.66E-02	8.9	
5.83E-02	8.94	
5.99E-02	9.02	
6.15E-02	9.32	
6.31E-02	9.46	
6.47E-02	9.51	
6.62E-02	9.58	
6.77E-02	9.59	
6.92E-02	9.43	
7.07E-02	9.73	
7.21E-02	9.72	
7.36E-02	9.94	
7.50E-02	9.91	
7.63E-02	9.98	
7.76E-02	9.67	
7.89E-02	9.67	
8.02E-02	9.83	
8.14E-02	9.57	
8.26E-02	9.53	
8.38E-02	9.58	
8.49E-02	9.36	
8.60E-02	9.21	
8.71E-02	9.09	
8.81E-02	8.84	
8.90E-02	8.59	
8.99E-02	8.39	

	9.08E-02	7.71
	9.17E-02	7.11
	9.25E-02	6.7
	9.32E-02	5.7
	9.39E-02	4.88
	9.46E-02	3.79
	9.53E-02	2.88
	9.58E-02	1.09
	9.64E-02	-0.4
4	9.69E-02	-2.4
	9.74E-02	-5.59
	9.78E-02	-9.05
	9.81E-02	-13.21
	9.85E-02	-18.76
	9.87E-02	-27.98
	9.90E-02	-41.9
	9.91E-02	-63.4
	9.93E-02	-110.46
	9.93E-02	-110.46